UNIWERSYTET ŚLĄSKI
W KATOWICACH

Instytut Fizyki
im. Augusta Chełkowskiego

ZAKŁAD BIOFIZYKI I FIZYKI MOLEKULARNEJ

PRACA DOKTORSKA:

BADANIE DYNAMIKI I KINETYKI KRYSTALIZACJI CIECZY FORMUJĄCYCH STAN SZKLISTY W RÓŻNYCH WARUNKACH TERMODYNAMICZNYCH

mgr Grzegorz Szklarz

promotor pracy:
dr hab. Karolina Adrjanowicz

Chorzów 2018

Temat niniejszej rozprawy doktorskiej był realizowany w ramach projektu OPUS Narodowego Centrum Nauki pt. „Indukowana ciśnieniem separacja składowych kinetycznej i termodynamicznej jako nowa metoda badań nad procesem krystalizacji" na podstawie umowy UMO-2014/15/B/ST3/00364

SPIS TREŚCI

STRESZCZENIE

Niniejsza praca doktorska zawiera wyniki systematycznych badań, których głównym celem było lepsze zrozumienie wpływu zmiennych warunków termodynamicznych na dynamikę przejścia szklistego i kinetykę krystalizacji nisko-molekularnych substancji formujących stan szklisty. Przez zmienne warunki termodynamiczne rozumiano tutaj modyfikację parametrów termodynamicznych układu wskutek kompresji a także zastosowania ograniczeń przestrzennych o rozmiarach rzędu „nano". Warto tutaj zaznaczyć, że zarówno w jednym jak i w drugim przypadku należy oczekiwać istotnych zmian gęstości upakowania molekuł, a także zmian charakteru oddziaływań molekularnych, co z kolei, w istotny sposób (choć niekoniecznie identyczny) może mieć przełożenie się na własności dynamiczne badanych materiałów w pobliżu przejścia szklistego, jak również ich zachowania krystalizacyjne. Efekty związane z fluktuacjami gęstości są tuż obok efektów temperaturowych kluczem do zrozumienia procesów zeszklenia i krystalizacji, tak jak diagram fazowy każdej substancji jest dwu- a nie jednowymiarowy (T, ρ). *A* więc, zastosowanie właśnie takiego podejścia do prowadzonych badań umożliwiło spojrzenie na wiele zagadnień związanych z dynamiką przejścia szklistego i sposobów kontrolowania/modyfikowania tendencji do krystalizacji badanych materiałów w zupełnie nowy, bardziej syntetyczny sposób.

Praca ta ma charakter eksperymentalny i opiera się o wyniki badań uzyskanych przede wszystkim przy wykorzystaniu techniki spektroskopii dielektrycznej, która stanowi idealne narzędzie do badań ruchliwości molekularnej cieczy i szkieł w szerokim zakresie czasów relaksacji, jak również monitorowania kinetyki krystalizacji czy też detekcji przejść fazowych. Jednak w kontekście prowadzonych badań jej główną zaletą była stosunkowa łatwość zaadoptowania do badań prowadzonych zarówno w warunkach podwyższonego ciśnienia sięgającego nawet 1.5 GPa (!), jak również ograniczonej do skali „nano" geometrii (ciecz uwięziona w matrycach nanoporowatych o rozmiarach porów rzędu kilkunastu, czy też kilkudziesięciu nanometrów).

W pracy zaprezentowano w jaki sposób podwyższone ciśnienie wpływa na dynamikę procesu zeszklenia i krystalizację dwóch modelowych „glass-formerów" *(i)* węglanu propylenu oraz *(ii)* fenofibratu. Wśród najważniejszych wyników jakie udało się uzyskać należy wymienić *(i)* wykazanie, w analogii do pomiarów temperaturowych prowadzonych w ciśnieniu atmosferycznym, istotnej roli tempa kompresji/dekompresji na tendencję do formowania stanu

szklistego/krystalizacji w warunkach izotermicznych, oraz pokazanie że *(ii)* poprzez umiejętne sterowanie parametrami takimi jak temperatura i ciśnienie, czy też wybór odpowiedniej ścieżki termodynamicznej można wpływać na przebieg procesu krystalizacji i uzyskiwany produkt. Zagadnie to, okazało się być szczególnie ważne zwłaszcza w kontekście fenofibratu należącego do grupy substancji leczniczych obniżających poziom cholesterolu, a wykazującego dość bogaty polimorfizm, który może mieć istotne przełożenie na efekt terapeutyczny leku. W takim przypadku faworyzowanie tylko jednej, wybranej formy polimorficznej bądź też w ogólności kontrolowanie zachowań krystalizacyjnych materiałów formujących stan szklisty z wykorzystaniem techniki kompresji może mieć ważne znacznie aplikacyjne.

Równie ciekawych wyników eksperymentalnych dostarczyły badania prowadzone w ograniczonej geometrii. Przede wszystkim potwierdziły one najnowsze doniesienia naukowe sugerujące, że dynamika związana z przejściem szklistym w ośrodku nanoporowatym podlegać może tym samym regułom co makroskopowe ciecze przechłodzone. Chodzi tutaj zwłaszcza o idee skalowania gęstościowego i izochronicznej superpozycji. Wyniki badań jakie udało się uzyskać w ramach niniejszej pracy doktorskiej poddają jednak w wątpliwość utarte w literaturze przekonanie, że spełnienie jednej z powyższych reguł oznacza również spełnienie tej drugiej. Z kolei, badania kinetyki krystalizacji prowadzone dla cieczy uwięzionej w matrycach nanoporowatych wykazały, że wraz ze zmniejszeniem rozmiaru porów obserwujemy wiele istotnych zmian dotyczących samego przebiegu procesu krystalizacji m.in. kształt krzywej krystalizacji zmienia się z sigmoidalnego na eksponencjalny, stała szybkości krystalizacji i wartości parametru Avramiego maleją, a maksimum krystalizacji przesuwa się w stronę niższych temperatur/wyższych stopni przechłodzenia. A więc, efekty typu „confined" mogą pełnić równie ważną rolę co efekty ciśnieniowe jeśli chodzi o możliwość lepszego i bardziej świadomego kontrolowania tendencji do krystalizacji materiałów formujących stan szklisty.

Uzyskane wyniki niosą za sobą bardzo duży walor poznawczy, zwłaszcza z uwagi na fakt, że w literaturze cały czas brak jest tak systematycznych badań poświęconych zachowaniu materiałów formujących stan szklisty w różnych warunkach termodynamicznych. Świadczyć może o tym choćby fakt, iż część z nich dotyczących wpływu ograniczeń przestrzennych na przebieg procesu krystalizacji została mocno zaakcentowana w najnowszej pracy przeglądowej poświęconej krystalizacji materiałów amorficznych autorstwa prof. Descampsa z Francji (Int. J. Pharm. 542 (2018) 186-195). Badania prowadzone w ramach niniejszej rozprawy doktorskiej

pozwalają spojrzeć na procesy zeszklenia i krystalizacji przez pryzmat zmian nie tylko temperatury/energii termicznej, ale również gęstości upakowania molekuł (generowanych z wykorzystaniem dwóch alternatywnych strategii, dwuwymiarowych ograniczeń przestrzennych rzędu „nano" oraz podwyższonego ciśnienia). Warto zaznaczyć, że poprzez takie połączenie możliwe jest uzyskanie spójnego i kompletnego opisu obu rozpatrywanych procesów, a także sposobów kontrolowania/modyfikowania zachowań krystalizacyjnych materiałów w zależności od potrzeb aplikacyjnych lub przyszłych zastosowań.

1. CEL BADAŃ I WYKAZ PUBLIKACJI STANOWIĄCYCH PODSTAWĘ ROZPRAWY DOKTORSKIEJ

Celem niniejszej pracy doktorskiej pt. „Badanie dynamiki i kinetyki krystalizacji cieczy formujących stan szklisty w różnych warunkach termodynamicznych" było:

1. określenie wpływu szybkości chłodzenia/grzania oraz kompresji/dekompresji na tendencję do krystalizacji modelowej substancji formującej stan szklisty, węglanu propylenu (PC)
2. zbadanie wpływu podwyższonego ciśnienia na dynamikę relaksacyjną fenofibratu w fazie cieczy przechłodzonej i szklistej
3. scharakteryzowanie zachowań krystalizacyjnych fenofibratu w obszarze przechłodzonej cieczy w ciśnieniu atmosferycznym oraz w warunkach podwyższonego ciśnienia.
4. określenie wpływu ograniczonej geometrii na dynamikę przejścia szklistego i krystalizację fenofibratu umieszczonego w matrycy nanoporowatej.

Niniejsza rozprawa doktorska stanowi zbiór czterech artykułów naukowych opublikowanych w recenzowanych czasopismach, znajdujących się na liście filadelfijskiej (A1-A4):

Lp.	Publikacja	Impact Factor czasopisma (rok publikacji)	Liczna punktów czasopisma wg. listy MNiSW (2016)
A1.	**Szklarz G.**;, Adrjanowicz, K.; Dulski, M.; Knapik, J.; Paluch, M. Dielectric Relaxation Study at Ambient and Elevated Pressure of the Modeled Lipophilic Drug Fenofibrate, *The Journal of Physical Chemistry B,* **2016**, *120(43)*, 11298–11306	3.187	30
A2.	**Szklarz, G.**; Adrjanowicz, K.; Knapik, J.; Jurkiewicz, K.; Paluch, M. Crystallization of Supercooled Fenofibrate Studied at Ambient and Elevated Pressures, *Physical Chemistry Chemical Physic,* **2017**, *19(15)*, 9879–9888	4.449	40

A3.	**Szklarz, G.**; Adrjanowicz, K.; Tarnacka, M.; Pionteck, J.; Paluch, M. Confinement-Induced Changes in the Glassy Dynamics and Crystallization Behavior of Supercooled Fenofibrate, *The Journal of Physical Chemistry C*, **2018**, *122(2)*, 1384–1395	4.536	35
A4.	**Szklarz, G.**; Adrjanowicz, K.; Paluch, M. Cooling-Rate Versus Compression-Rate Dependence of the Crystallization in the Glass-Forming Liquid, Propylene Carbonate, *Crystal Growth & Design,* **2018**, *18(4)*, 2538–2544	4.055	35

Treść wyżej wymienionych publikacji wraz z oświadczeniami współautorów można zaleźć w Rozdziale 4. Poza publikacjami stanowiącymi podstawę niniejszej pracy doktorskiej pozostają jeszcze 3 współautorskie artykuły naukowe z tej tematyki, które nie zostały włączone do rozprawy, ale świadczą o mojej aktywności naukowej w ciągu ostatnich trzech lat studiów doktoranckich

B1. Adrjanowicz, K.; Koperwas, K.; **Szklarz**, **G.**; Tarnacka, M.; Paluch, M. Exploring the Crystallization Tendency of Glass-Forming Liquid Indomethacin in the T–p Plane by Finding Different Iso-Invariant Points*, Crystal Growth & Design*, **2016**, *16(12)*, 7000–7010; IF(2015)=4.425, MNiSW(2016)=35.

B2. Adrjanowicz, K.; Kaminski, K. Tarnacka, M.; **Szklarz**,**G.**; Paluch, M. Predicting Nanoscale Dynamics of a Glass-Forming Liquid From Its Macroscopic Bulk Behavior and Vice Versa, *The Journal of Physical Chemistry Letters*, **2017**, *8(3)*, 696–702; IF(2015)=8.539, MNiSW(2016)=45.

B3. Adrjanowicz, K.; **Szklarz**, **G.**; Koperwas, K;. Paluch, M. Comparison of High Pressure and Nanoscale Confinement Effects on Crystallization of Molecular Glass-Forming Liquid, Dimethyl Phthalate, *Physical Chemistry Chemical Physics,* **2017**, *19(22)*, 14366–14375; IF(2015)=4.449, MNiSW(2016)=40.

Rezultaty moich badań prezentowane były na wymienionych poniżej międzynarodowych konferencjach naukowych:

- *9th International Conference on Broadband Dielectric Spectroscopy and its Applications* Piza, Włochy (11.09-16.09.2016)
- *8th International Discussion Meeting on Relaxations in Complex Systems*, Wisła, Polska (23.07-28.07.2017)

Wyniki badań eksperymentalnych, które stanowią podstawę niniejszej pracy doktorskiej były realizowane w ramach projektu OPUS Narodowego Centrum Nauki pt. „Indukowana ciśnieniem separacja składowych kinetycznej i termodynamicznej jako nowa metoda badań nad procesem krystalizacji" na podstawie umowy UMO-2014/15/B/ST3/00364

2. WSTĘP TEORETYCZNY

2a. Przejście szkliste

Według definicji Międzynarodowej Unii Chemii Czystej i Stosowanej (IUPAC) przejście szkliste jest to przejście fazowe drugiego typu (przejście ciągłe), w którym przechłodzona ciecz podczas chłodzenia przyjmuje strukturę szkła.[1] Ta bardzo prosta i przystępna dla każdego definicja, nie opisuje jednak poprawnie natury fizycznej tego procesu, która notabene od lat budzi naprawdę sporo kontrowersji.[2,3,4,5] Na samym początku należy wspomnieć, że nie tylko chłodzenie powoduje przejścia szkliste, lecz również kompresja.[6,7,8] A samo zaklasyfikowanie przejścia szklistego jako przejścia fazowego drugiego typu[9] jest szeroko dyskutowane w środowisku naukowym zajmującym się tym fenomenem. Otóż mimo tego, że podczas przejścia szklistego pierwsza pochodna energii swobodnej Gibbsa - G (według klasyfikacji Landaua-Ginzburga) lub potencjału chemicznego - μ (według klasyfikacji Ehrenfesta) jest ciągła to samo przejście szkliste jest różnorodnie klasyfikowane. Istnieją prace, w których przejście szkliste jest zaklasyfikowane jako przejście fazowe innego stopnia niż drugi,[10,11] lecz przez sporą grupę badaczy jest ono uznawane wyłącznie jako proces kinetyczny, a nie przejście fazowe. Spowodowane jest to kilkoma właściwościami procesu zeszklenia. Po pierwsze, obserwowana temperatura przejścia szklistego jest zależna od tempa chłodzenia, co stanowi istotny problem w analizie przejścia szklistego jako przejścia fazowego (obserwowane przejścia fazowe mają z reguły dobrze zdefiniowaną temperaturę). Ponadto w zależności od szybkości z jaką obniżana jest temperatura otrzymuje się szkła o różnej gęstości i upakowaniu,[6,9,12] mimo tego, że różnice pomiędzy obserwowanymi temperaturami przejść szklistych są nieznaczne i wynoszą do 5 K. Po drugie, ciecz w trakcie procesu zeszklenia nie przyjmuje swojej minimalnej wartości energii swobodnej Gibbsa. Dopiero podczas procesu starzenia, gdzie następuje rearanżacja i zwiększenie upakowania molekuł, szkło zmniejsza powoli swoją energię swobodną Gibbsa aż do jej zrównania się z teoretyczną wartością równą wartości G dla cieczy przechłodzonej.[13] Trzecim argumentem przemawiającym za tym, że przejście szkliste jest wyłącznie efektem kinetycznym, a nie prawdziwym przejściem fazowym jest występowanie tzw. paradoksu Kauzmanna (energia swobodna szkła stałaby się poniżej pewnej temperatury, określanej mianem temperatury Kauzmanna, mniejsza od wartości G dla kryształu).[14,15,16] Dlatego też, z przyczyn wymienionych powyżej, często używane są w literaturze definicje przejścia szklistego T_g powiązane wyłącznie z parametrami eksperymentalnymi. Wśród

stosowanych najczęściej definicji używane są te łączące przejście szkliste z *(i)* lepkością (T_g=T w której lepkość osiąga wartość 10^{12} Pa×s), *(ii)* zmianą ciepła właściwego (charakterystyczny „schodek" obserwowany na termogramach podczas grzania próbki z szkła do cieczy przechłodzonej), czy też *(iii)* czasem relaksacji/współczynnikiem dyfuzji translacyjnej (T_g=T w której czas relaksacji osiąga wartość 100 sekund, a współczynnik samodyfuzji jest rzędu 10^{-15}-10^{-16} cm^2s^{-1}). Ponadto, aby scharakteryzować przejście szkliste bada się również wpływ historii termicznej.[17]

Najprostszą, i jedną z najstarszych, metod otrzymywania szkieł i w ogólności materiałów amorficznych (czyli tych nieposiadających struktury krystalicznej lecz posiadających własności mechaniczne ciał stałych) jest proces witryfikacji/zeszklenia. Metodą tą otrzymuje się m.in. ceramiki, rożnego typu szkła krzemionkowe, a nawet amorficzne leki.[17,18,19] Jest to metoda polegająca na szybkim schłodzeniu substancji ze stanu ciekłego znacznie poniżej temperatury krzepnięcia z uniknięciem procesu krystalizacji.[9,14,20,21] Witryfikacja, oprócz tworzenia substancji amorficznych, znalazła też inne zastosowania, np. w krionice (za opracowanie metody mikroskopii krioelektronowej przyznano w 2017 roku Nagrodę Nobla z chemii),[22] przemyśle spożywczym a nawet w neutralizacji odpadów radioaktywnych. Mimo swoich niewątpliwych zalet jakimi są prostota tego procesu oraz możliwość uzyskania dużych ilości substancji amorficznej witryfikacja ma również swoje ograniczenia. Głównym z nich są trudności w osiąganiu wystarczającego tempa chłodzenie tak by uniknąć krystalizacji (wymaga to niekiedy chłodzenia z tempem kilku czy też kilkudziesięciu tysięcy stopni na sekundę!)[23,24] oraz możliwość rozkładu substancji amorfizowanej w temperaturze topnienia. Z tego powodu zostało opracowanych wiele innych alternatywnych metod amorfizacji ciał stałych, np. mielenie, suszenie rozpyłowe czy też liofilizacja.[25,26]

Materiały szkliste (innymi słowy te które są zdolne do formowania stanu szklistego) są praktycznie niemal wszędzie wokół nas, począwszy od szyb okiennych, kauczuku, gumy, biżuterii wykonanej z minerałów naturalnych, butelek plastikowych, czy też znacznie bardziej wyszukanych zastosowań w przemyśle i medycynie (np. leki o ulepszonej biodostępności, produkcja sztucznych organów, super-materiały na potrzeby nowoczesnej elektroniki, lotnictwa i wojska[27,28]). Niestety, w chwili obecnej ten ogromny potencjał jaki oferują nam materiały formujące stan szklisty nie jest w 100% wykorzystany, a przyczyną tego jest głównie fizyczna i chemiczna niestabilność stanu amorficznego. Mimo wielu lat intensywnych badań nie do końca zrozumiałe jest dlaczego niektóre substancje z łatwością formują stan szklisty (utrzymując tempa

chłodzenia rzędu 1 K/h !), są stabilne przez lata, a z kolei inne, niezwykle trudno przechłodzić a uniknięcie procesu nawet częściowej krystalizacji/rekrystalizacji podczas przechładzania i tak jest niemożliwe. Receptą na ten stan rzeczy wydaje się być spojrzenie na proces zeszklenia przez pryzmat jego nierozerwalnego/ukrytego związku z procesem krystalizacji.[29,30] Obydwa procesy są bowiem jak dwie strony tego samego medalu, a więc niemożliwe jest dogłębne zrozumienie zjawiska zeszklenia przy jednoczesnym odcięciu się od procesu krystalizacji i vice versa. Wśród szeregu strategii umożliwiających modyfikowanie tendencji do zeszklenia/krystalizacji zarówno materiałów organicznych jak i nieorganicznych warto wymienić (*i*) wykorzystanie podwyższonego ciśnienia, (*ii*) silnego pola elektrycznego,[31,32] oraz (*iii*) efekty nanoograniczeń (np. cienkie filmy).[33]

Na sam koniec warto wspomnieć, że aby w pełni scharakteryzować zwłaszcza dynamiczne aspekty przejścia szklistego bardzo często wprowadza się ciśnienie jako drugą (oprócz temperatury) kontrolowaną zmienną termodynamiczną.[6,34] Dotyczy to zarówno badań teoretycznych jak i eksperymentalnych. Wzrost ciśnienia w stałej temperaturze, podobnie jak obniżanie temperatury w stałym ciśnieniu prowadzi do spowolnienia kooperatywnych ruchów molekularnych cieczy i procesu zeszklenia. Jednak należy podkreślić, że obydwa parametry (T i p) wpływają na własności materii w nieco odmienny sposób. Zmiana temperatury modyfikuje bowiem głównie energię termiczną molekuł, a z kolei kompresja upakowanie molekuł/odległości pomiędzy molekułami. Dane literaturowe wskazują, że rola efektów temperaturowych i gęstościowych na własności dynamiczne cieczy przechłodzonych i szkieł może być zupełnie różna.[8,34,35,36] Dlatego też, badania ciśnieniowe stanowią nieocenione uzupełnienie i dopełnienie wiedzy na temat dynamiki materiałów formujących stan szklisty jakie uzyskujemy w przypadku standardowych pomiarów prowadzonych w ciśnieniu atmosferycznym, a więc gdy operujemy jedynie jedną zmienną termodynamiczną, temperaturą.

2b. Krystalizacja

Krystalizacja jest jednym z najbardziej rozpowszechnionych przejść fazowych na świecie. Proces ten zachodzi w warunkach poniżej temperatury krzepnięcia danej substancji i jest procesem samorzutnym. Polega na utworzeniu periodycznej struktury krystalicznej z układu jej nieposiadającej. W praktyce krystalizację można osiągnąć poprzez wiele różnorodnych metod m.in. schładzania cieczy, sublimacji par, odparowaniu rozpuszczalnika bądź reakcji strącania.[1]

Ponadto, w zależności od wybranej metody krystalizacji i parametrów procesu uzyskać można różne odmiany polimorficzne danej substancji,[37] które niejednokrotnie różnią się wieloma właściwościami fizykochemicznymi, a nawet biologicznymi. Należy zwrócić uwagę na to, że mimo tego, że krystalizacja jest procesem samorzutnym to entropia (parametr nieporządku) krystalizowanej substancji maleje, co wydaje się w niezgodzie z II zasadą termodynamiki. Jednakże, układ związany z krystalizacją nie jest układem izolowanym lecz układem zamkniętym - może on wymieniać pracę z otoczeniem. Z tego powodu poprawnym parametrem mówiącym o samorzutności reakcji krystalizacji jest *G*. Otóż, wartość *G* dla zamkniętego systemu związanego z krystalizacją maleje, aż do osiągnięcia minimalnej wartości dla próbki w pełni skrystalizowanej. Jest to następstwem tego, że zysk energetyczny z powodu zmniejszenia się energii wewnętrznej skrystalizowanego układu (praca wykonana przez krystalizowany układ) jest znacznie wyższy od strat spowodowanych zwiększeniem entropii układu.

W trakcie krystalizacji rozróżniamy dwa etapy: proces nukleacji oraz wzrostu kryształu. Procesy te mają zupełnie inne charaktery i przebiegają od siebie niezależnie, ale ich następstwo z zachowaniem odpowiedniej kolejności ma ogromne znaczenie w przebiegu krystalizacji. Nie ma wzrostu kryształu bez wcześniejszej nukleacji (zarodkowania). Podobnie, zarodek krystalizacji o rozmiarach sięgających niekiedy jedynie kilku nanometrów nie utworzy makroskopowego kryształu bez etapu wzrostu. Proces nukleacji jest procesem całkowicie stochastycznym podczas, którego molekuły substancji na wskutek fluktuacji tworzą mniejsze bądź większe klastry. W momencie gdy promień klastra przekroczy wielkość zwaną promieniem krytycznym, klaster formuje zarodek krystalizacji.[38,39] Co więcej, podczas tworzenia zarodka niezbędne jest dostarczenie układowi energii do wytworzenie nowej powierzchni pomiędzy fazą krystaliczną a cieczą. Implikuje to istnienie bariery energetycznej dla procesu nukleacji, a jej wysokość jest pośrednio związana z kinetyką procesu krystalizacji (im wyższa bariera tym proces nukleacji zachodzi wolniej). Bariera ta powoduje, że tylko te klastry, dla których energia termiczna fluktuacji ma większą wartość od bariery energetycznej mogą stać się zarodkami. Ponadto, ze względu na mechanizm powstawania rozróżnia się nukleację homogeniczną i heterogeniczną. O nukleacji homogenicznej mówi się gdy zarodek powstaje otoczeniu wyłącznie molekuł substancji krystalizowanej (nie posiada innych oddziaływań niż z substancją rodzimą) niebędących w fazie krystalicznej. Nukleacja heterogeniczna występuje wtedy gdy tworzący się zarodek oprócz oddziaływań z substancją rodzimą oddziałuje także z innymi substancjami, np. powierzchnią

naczynia, kryształami, zanieczyszczeniami. Wzrost kryształu w odróżnieniu od nukleacji jest procesem deterministycznym, który powoduje zmniejszanie się energii układu oraz *G*. W przypadku tego procesu jego tempo w głównej mierze determinowane przez mobilność molekuł i tempo ich dołączania do istniejącej już struktury krystalicznej. Warto zauważyć, że w ostatnich latach coraz więcej doniesień naukowych wskazuje na to, że wbrew założeniom klasycznej teorii nukleacji, proces ten nie jest jednoetapowy, struktura i dynamika cieczy w trakcie obniżania temperatury staje się coraz bardziej heterogeniczna, a prawdopodobieństwo utworzenia zarodka w obszarze tzw. klastrów cieczopodobnych zdecydowanie większe niż w pozostałych regionach próbki.[40,41]

Jak powszechnie wiadomo, proces krystalizacji jest napędzany przez dwa bardzo ważne czynniki, termodynamiczny i kinetyczny (ruchliwość molekularna). Ich wpływ na przebieg krystalizacji jest nieco odmienny, bowiem wraz ze spadkiem temperatury lepkość układu zwiększa się, a co za tym idzie mobilność molekuł spada (wkład od członu kinetycznego maleje) i proces dołączania kolejnych molekuł do struktury kryształu spowalnia. Jednocześnie towarzyszy temu zmniejszanie się bariery energetycznej dla procesu nukleacji/wzrost termodynamicznej siły napędowej procesu krystalizacji co sprawia, że utworzenie się zarodka i jego późniejszy wzrost są znacznie bardziej ułatwione. Konsekwencją współzawodnictwa między składową kinetyczną i termodynamiczną jest dzwonowaty kształt zależności szybkości zarodkowania oraz wzrostu kryształu. Maksima tempa nukleacji i wzrostu kryształu zlokalizowane są poniżej temperatury topnienia, choć niejednokrotnie w różnych odległościach od siebie. Lokalizacja i stopień nałożenia obu maksimów decyduje tak naprawdę o tendencji do krystalizacji/zeszklenia badanej substancji. Warto tutaj jednak zaznaczyć, że maksimum nukleacji jest zawsze zlokalizowane w niższej temperaturze niż maksimum wzrostu kryształu, dlatego też pomiędzy T_m i T_g występuje strefa gdzie pomimo tego, że występuje wzrost kryształów to układ nie krystalizuje, z powodu braku zarodków.

Tak jak diagram fazowy każdej substancji jest dwuwymiarowy, tak sam proces krystalizacji można rozpatrywać w dwuwymiarowej przestrzeni *T*-*p*, lub w bardziej ogólnym pojęciu *T*-ρ. Należy tutaj zwrócić uwagę na to, że wpływ podwyższonego ciśnienia na tendencję do krystalizacji materiałów formujących stan szklisty jest zdecydowanie słabiej poznany niż efekty temperaturowe.[42,43,44,45] Przede wszystkim nie do końca wiadome jest czy ciśnienie faworyzuje czy hamuje krystalizację, a co za tym idzie w jaki sposób wpływa na lokalizację i wzajemne

nakrycie krzywych nukleacji i wzrostu kryształu, w porównaniu z tym co obserwujemy w ciśnieniu atmosferycznym. Niektóre doniesienia naukowe wskazują również, że modyfikacja gęstości układu poprzez kompresję, czy też zastosowanie ograniczeń przestrzennych rzędu „nano" prowadzić może do uzyskiwania w sposób czasami wręcz selektywny różnych odmian polimorficznych tej samej substancji, niekiedy niemożliwych do uzyskania w żaden inny sposób.[46,47] Wydaje się więc wielce uzasadnione zrozumienie jaką rolę odgrywać mogą nie tylko efekty temperaturowe, ale także gęstościowe na zachowania krystalizacyjne materiałów formujących stan szklisty, tak aby w przyszłości móc wykorzystać tą wiedzę do projektowania i otrzymywania materiałów o pożądanych parametrach oraz własnościach.

2c. Metody badań dynamiki przejścia szklistego i kinetyki krystalizacji

Dynamikę materiałów formujących stan szklisty, a także kinetykę krystalizacji można analizować z wykorzystaniem wielu różnych technik eksperymentalnych takich jak spektroskopia mechaniczna (DMA), spektroskopia dielektryczna (DS), dynamiczne rozpraszanie światła (DLS), różnicowa kalorymetria skaningowa (DSC), spektroskopia w podczerwieni (IR) czy też spektroskopia magnetycznego rezonansu jądrowego (NMR). Każda z powyżej wspomnianych technik eksperymentalnych umożliwia uzyskanie iście swoistych informacji na temat własności dynamicznych badanych układów, koncentrując się na nieco innych aspektach związanych z ruchliwością molekularną i wielkościach/parametrach fizycznych które wykorzystuje się do opisu obserwowanych zjawisk i procesów. Dla przykładu informację na temat ruchów translacyjnych/rotacyjnych można uzyskać z wykorzystaniem techniki NMR, która bazuje na obserwacji zachowania spinów jądrowych w zewnętrznym polu magnetycznym, a przy pomocy DS (która oparta jest na oddziaływaniu przyłożonego pola elektrycznego z próbką posiadającą moment dipolowy) analizować kooperatywne ruchy reorientacyjne molekuł w fazie cieczy przechłodzonej. Z kolei IR idealnie nadaje się do identyfikacji ruchów molekularnych poszczególnych grup funkcyjnych czy fragmentów molekuły. Wzajemne zestawienie wyników otrzymanych z poszczególnych metod umożliwia więc uzyskanie kompletnego zestawu danych na temat dynamiki i własności badanych materiałów.

Niemniej jednak, spośród wszystkich wspomnianych powyżej technik eksperymentalnych tylko jedna z nich, tj. spektroskopia dielektryczna, daje nam tak szerokie spektrum możliwości które obejmuje prowadzenie badań w szerokim zakresie charakterystycznych czasów relaksacji

(obejmującym nawet 10 dekad), temperatury (od -160°C do 400°C), w warunkach podwyższonego ciśnienia (nawet powyżej 1 GPa) a nawet skali „nano" (np. cienkie filmy polimerowe czy też ciecze uwięzione w ośrodku nanoporowatym). Warto zaznaczyć, że ze względu na ograniczenia aparaturowe i trudności eksperymentalne przystosowanie wspomnianych powyżej technik (DMA, DLS, DSC, IR, NMR) do badań własności materiałów formujących stan szklisty zarówno w skali makro jak też nanoskopowej może okazać się zadaniem niełatwym. Natomiast, DS zyskuje tutaj dzięki temu, że pojemność kondensatora wypełnionego dielektrykiem rośnie wraz ze zmniejszeniem się odległości między okładkami kondensatora (im mniejsza grubość próbki/filmu tym lepiej). Sugeruje to więc, że może ona stanowić idealne narzędzie do badań dynamiki nanomateriałów.[48] Oczywiście DS ma też swoje ograniczenia, o których także warto pamiętać. Przede wszystkim badana substancja musi dysponować trwałym momentem dipolowym. DS pozwala nam na (i) detekcję procesów relaksacyjnych w cieczy przechłodzonych i stanie szklistym, jednak nie dostarcza bezpośrednio informacji na temat ich pochodzenia molekularnego, (ii) monitorowanie kinetyki krystalizacji i przebiegu reakcji chemicznych, chociaż analiza poszczególnych etapów procesów jest w oparciu o uzyskane wyniki dość skomplikowana. W przypadku badań kinetyki krystalizacji, DS korzysta z faktu, że w trakcie procesu krystalizacji molekuły cieczy przechłodzonej są zamrażane w fazie krystalicznej, co powoduje, że liczba aktywnie reorientujących molekuł/dipoli maleje. Tym samym implikuje to zmniejszenie się odpowiedzi dielektrycznej wraz z wzrostem stopnia krystaliczności próbki. Wysycenie obserwowane na widmach dielektrycznych będzie tutaj oznaczać zakończenie procesu krystalizacji. Jednakże, takie stwierdzenie będzie prawdziwe jedynie w przypadku gdy odpowiedź dielektryczną badanej substancji możemy utożsamić z odpowiedzią całej molekuły, a nie tylko jej fragmentem (jak może to mieć miejsce na przykład w przypadku polimerów). Najprostszą metodą aby to sprawdzić jest skonfrontowanie stopnia krystaliczności próbki wyznaczonego w oparciu o analizę zmian stałej dielektrycznej zachodzącej w trakcie procesu krystalizacji z wynikami badań strukturalnych.

3. OMÓWIENIE WYNIKÓW

W celu badania wpływu podwyższonego ciśnienia i ograniczonej geometrii na dynamikę przejścia szklistego i kinetykę krystalizacji do badań wybrano dwie modelowe substancje, węglan propylenu i fenofibrat. Podstawowe informacje na ich temat zebrano w Tabeli 1.

Nazwa związku	**Wzór chemiczny**	**Masa molowa [g/mol]**	**Wzór strukturalny**
Węglan propylenu (ang. propylene carbonate)	$C_4H_6O_3$	102,09	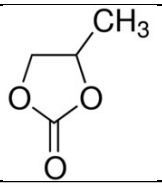
Fenofibrat (ang. fenofibrate)	$C_{20}H_{21}ClO_4$	360,83	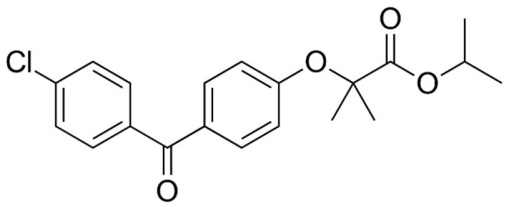

Tabela 1. Charakterystyka badanych substancji.

Wybór obu substancji do badań nie był tutaj w żadnym stopniu kwestią przypadku. Jeśli chodzi o przeprowadzenie pionierskich eksperymentów w trakcie których analogicznie do zmian tempa chłodzenia/grzania w warunkach izobarycznych, starano się kontrolować szybkość kompresji i dekompresji w warunkach izotermicznych, wybór odpowiedniej substancji miał niebagatelne znaczenie. Przede wszystkim, specyfika pomiarów wysokociśnieniowych stawia szereg wyzwań i ograniczeń aparaturowych, z którymi trzeba się mierzyć zarówno w trakcie planowania jak też realizacji poszczególnych etapów badań. W odróżnieniu od symulacji komputerowych w „prawdziwym" eksperymencie mamy znacznie bardziej ograniczone możliwości jeśli chodzi o regulację temperatury i ciśnienia, a stabilizacja nowych warunków (T, p) niejednokrotnie zajmuje minuty, a nie ułamki sekund. Ponadto, temperatury zeszklenia wielu „rzeczywistych" układów niejednokrotnie mogą zupełnie nie komponować się z zakresem temperatur i ciśnień jakie jesteśmy w stanie osiągać z wykorzystaniem dostępnej aparatury. Oprócz tego, należy także wziąć pod uwagę fakt, iż wrażliwość substancji formujących stan

szklisty na efekty ciśnieniowe może być zupełnie różna. Niekiedy bowiem wzrost ciśnienia o 1 GPa przesuwa przejście szkliste aż o 300 K, a innym razem jedynie o 30 K.[8,34] W tym ostatnim przypadku, okazać się więc może, że próba zrozumienia wpływu szybkości kompresji/dekompresji na tendencję do zeszklenia/krystalizacji będzie niemożliwa, a efekty ciśnieniowe praktycznie niezauważalne. Inną problematyczną kwestią może okazać się sama tendencja do krystalizacji badanej substancji w trakcie kompresji/dekompresji. Niemożność zeszklenia badanej substancji z wykorzystaniem dostępnych temp kompresji oczywiście może zrujnować cały eksperyment. Z powodów opisanych powyżej, związkiem, który najlepiej wpisuje się w ideę badań prowadzonych z zastosowaniem różnych temp kompresji/dekompresji okazał się być węglan propylenu (*ang. propylene carbonate*). Dzięki swojej niskiej temperaturze zeszklenia (T_g=159 K w 0.1 MPa) i umiarkowanej wrażliwości na ciśnienie (dT_g/dp > 7 K/ 100 MPa)[36] PC idealnie wkomponował się w dostępne w naszym laboratorium zakresy zmian *T* i *p.* Ponadto, jest to substancja dość dobrze przebadana, (niekiedy określana nawet w literaturze terminem 'kanoniczny glass-former') w przypadku której nie jest koniecznie zastosowanie jakiś niezwykle wymagających szybkości chłodzenia/kompresji tak aby można było ją zeszklić z całkowitym ominięciem procesu krystalizacji.[49]

Z kolei jeśli chodzi o fenofibrat jest to substancja z grupy leków obniżających poziom cholesterolu. Fenofibrat w postaci krystalicznej charakteryzuje się bardzo słabą rozpuszczalnością i biodostępnością.[50] Jedną ze strategii poprawy tych parametrów jest jego amorfizacja.[51] Niestety, fenofibrat w stanie przechłodzonej cieczy jak również stanie szklistym (T_g=254 K) jest fizycznie niestabilny i wykazuje tendencję do rekrystalizacji.[52,53] W takim zrekrystalizowanym materiale zanotować można obecność dwóch odmian polimorficznych fenofibratu: stabilnej formy I która odpowiedzialna jest za efekt terapeutyczny leku (T_m = 353 K) oraz metastabilnej formy II (T_m = 347 K). Co ciekawe, próby stabilizacji fenofibratu np. z dodatkiem talku skutkują pojawieniem się jeszcze jednej metastabilnej formy III (T_m = 323 K).[54] Właśnie z powodu pojawienia się tych „niechcianych" odmian polimorficznych, fenofibrat stał się jedną z modelowych substancji leczniczych do badań poświęconych zrozumieniu zachowań krystalizacyjnych materiałów formujących stan oraz projektowaniu/opracowaniu strategii umożliwiających stabilizację tylko jednej, pożądanej formy polimorficznej z eliminacją pozostałych.

3a. Wpływ szybkości chłodzenia/grzania oraz kompresji/dekompresji na tendencję do krystalizacji modelowej substancji formującej stan szklisty, węglanu propylenu (PC)

Badanie wpływu szybkości chłodzenia/grzania oraz kompresji/dekompresji na tendencję do krystalizacji węglanu propylenu stanowiło treść artykułu A4 opublikowanego w czasopiśmie *Crystal Growth & Design*. W pracy porównano jaki wpływ na tendencję do formowania stanu szklistego/krystalizacji odgrywa obniżanie temperatury w warunkach izobarycznych i wzrost ciśnienia w warunkach izotermicznych. W jednym jak i drugim przypadku kluczowym parametrem okazuje się być szybkość chłodzenia/kompresji. W celu zbadania tendencji do krystalizacji PC zarówno w ciśnieniu atmosferycznym jak również podwyższonym wykorzystano spektroskopię dielektryczną. Monitorowano zmiany rzeczywistej składowej przenikalności dielektrycznej (ε') mierzonej dla częstotliwości f= 1 MHz. Obniżanie temperatury, tak jak i wzrost ciśnienia, może doprowadzić do procesu zeszklenia, o czym świadczą krzywe dyspersji zaprezentowane w funkcji temperatury i ciśnienia odpowiednio na Rys. 1a i 2a. Z kolei, zarówno w trakcie grzania jak i dekompresji ze stanu szklistego zaobserwować można charakterystyczny spadek wartości ε' co świadczy o procesie rekrystalizacji (Rys. 1b i 2b). Krystalizacja w trakcie podnoszenia temperatury/obniżania ciśnienia może być całkowita bądź też tylko częściowa. Z reguły, im wolniejsze tempo grzania czy też dekompresji, tym większa szansa na to, że badana próbka zdąży całkowicie skrystalizować. Gwałtowny wzrost wartości ε' w trakcie dalszego ogrzewania/dekompresji jest oznaką osiągnięcia temperatury (czy też ciśnienia) topnienia kryształu. Warto zauważyć, że uniknięcie procesu krystalizacji w trakcie grzania próbki w warunkach izobarycznych jest zdecydowania trudniejsze niż w trakcie jej chłodzenia. Dla przykładu, tempo chłodzenia 2 K/min jest wystarczające by udało się bez problemu zeszklić badaną substancję. Z kolei, podczas ogrzewania PC ze stanu szklistego z szybkością 2 K/min nie pozwoli nam uniknąć procesu rekrystalizacji. Do analogicznego wniosku może doprowadzić porównanie zachowania PC w trakcie kompresji/dekompresji choćby z tempem ~30 MPa/min. Wyniki te sugerują, że maksimum nukleacji musi być zlokalizowane w pobliżu przejścia szklistego, natomiast maksimum wzrostu kryształu w regionie nieco wyższych temperaturach/niższych ciśnień.

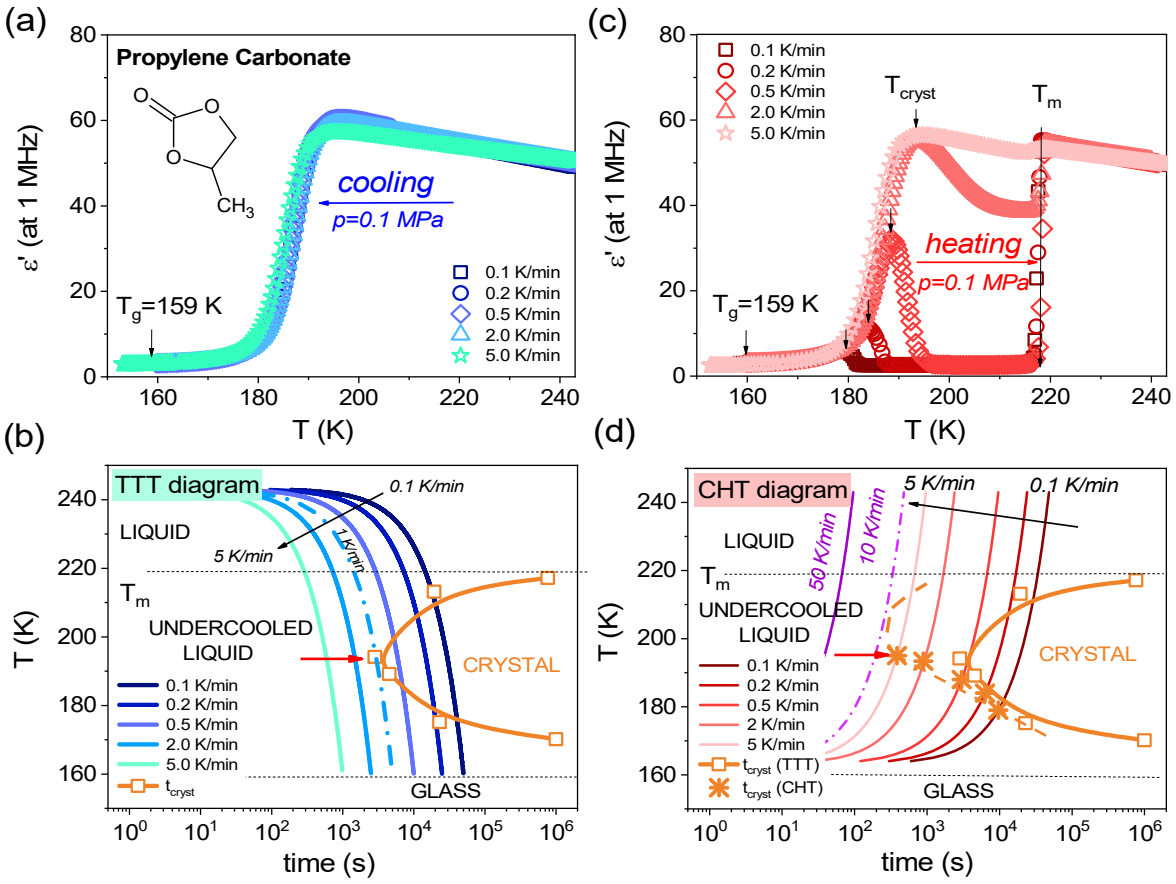

Rysunek 1. Zmiany przenikalności dielektrycznej (przy częstotliwości 1MHz) w funkcji temperatury dla PC w trakcie (a) chłodzenia i (b) grzania z tempem od 0.1 K/min do 5 K/min. Diagramy (c) TTT (ang. Time–Temperature–Transformation diagram) i (d) CHT (ang. Continuous–Heating–Transofrmation diagram) przygotowane dla PC w oparciu o badania dielektryczne prowadzone w ciśnieniu 0.1 MPa.

Aby zobrazować tendencję do krystalizacji PC w różnych warunkach termodynamicznych przygotowano diagramy Time-Temperature-Transformation/Continious-Heating-Transformation dla krzywych chłodzenia/grzania (Rys. 1c, 1d), oraz ich ciśnieniowe odpowiedniki, Time–Pressure-Transformation/Time-Decompression-Transformation (Rys. 2c i 2d). W oparciu o dostępną wiedzę literaturową można stwierdzić, że zaproponowane diagramy TPT i TDT dla PC są pierwszymi tego typu diagramami skonstruowanymi dla cieczy molekularnej formującej stan szklisty poddawanej kompresji/dekompresji. Skonstruowane pary diagramów TTT/CHT i TPT/TDT obrazują w bardzo prosty i spójny sposób minimalne tempo zmian temperatury i ciśnienia jakie są konieczne by zeszklić badaną substancję/ewentualnie uniknąć rekrystalizacji w trakcie wychodzenia ze stanu szklistego. Co ciekawe, maksymalne czasy krystalizacji zanotowane

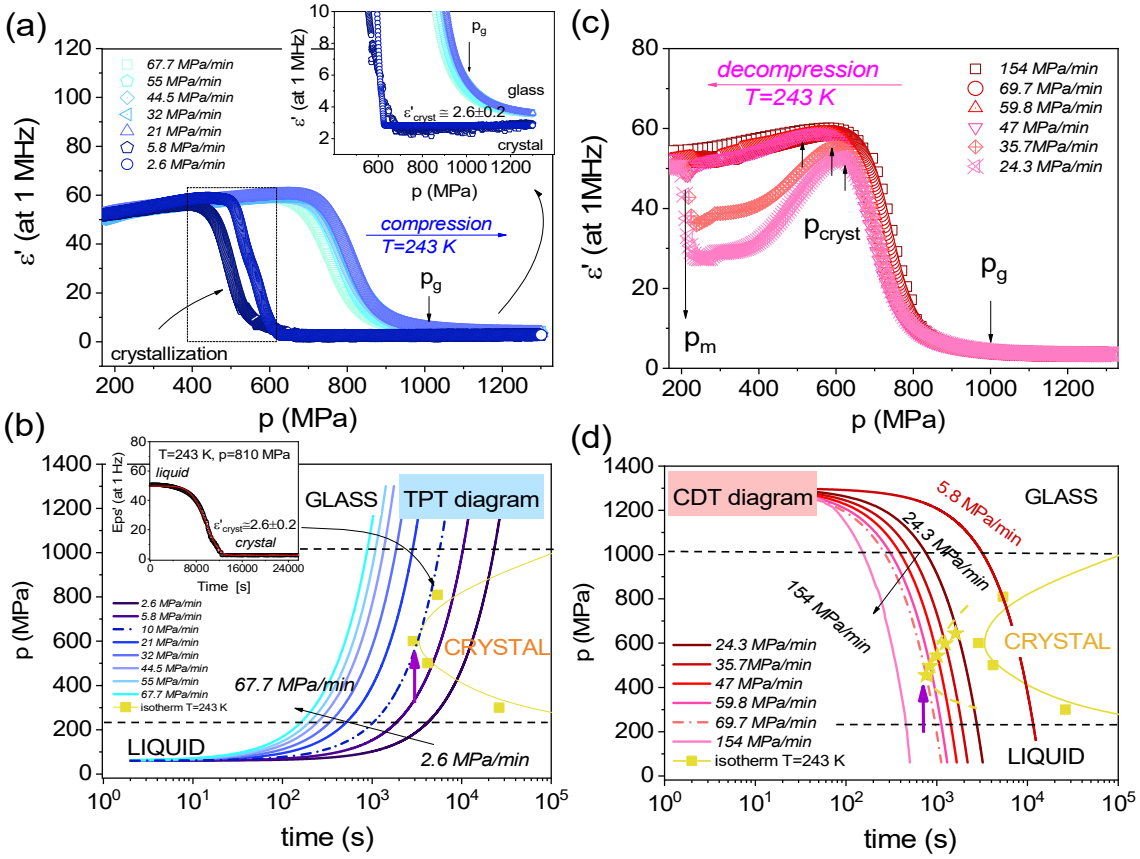

Rysunek 2. Zmiany przenikalności dielektrycznej (przy częstotliwości 1MHz) w funkcji ciśnienia dla PC w trakcie (a) kompresji i (b) dekompresji z tempem w zakresie od 2.6 MPa/min do nawet 154 MPa/min. Diagramy (c) TPT (ang. Time–Pressure–Transformation diagram) i (d) CDT (ang. Continuous–Decompression–Transofrmation diagram) przygotowane dla PC w oparciu o badania dielektryczne prowadzone w stałej temperaturze, T=243 K.

w trakcie podnoszenia temperatury/obniżania ciśnienia dla próbki wcześniej zeszklonej są zdecydowanie krótsze w porównaniu w wartościami zanotowanymi w trakcie chłodzenia/kompresji cieczy. Potwierdza to tylko wcześniejsze przypuszczenia na temat lokalizacji maksimum nukleacji w okolicach przejścia szklistego. Oczywistym jest więc, że dla takiej próbki czasy krystalizacji w obszarze wyższych temperaturach/niższych ciśnieniach będą po prostu krótsze (choćby dlatego iż liczba zarodków krystalizacji będzie większa).

Dalsze wyniki prowadzonych badań doprowadziły do bardzo ciekawych i zaskakujących wyników dotyczących ewolucji czasów krystalizacji i wartości parametrów Avramiego (mówiącym o mechanizmie nukleacji i wymiarowości rosnących kryształów) dla PC krystalizowanego w warunkach izobarycznych (p=0.1 MPa) jak i izotermicznych (T=243 K,

T=253 K). Okazało się bowiem, że wartość parametru Avramiego jest praktycznie stała i oscyluje wokół wartości 3, niezależnie od tego czy rozważamy dane izobaryczne czy izotermiczne. Z kolei jeśli chodzi o zależność czasu krystalizacji w funkcji temperatury (dla p=0.1 MPa) i ciśnienia (dla T=243 K, czy też =253 K) to są one niemalże identyczne. Wyniki przedstawione w pracy A4 sugerują więc, że bez względu na to której zmiennej termodynamicznej, temperatury czy też ciśnienia, użyjemy w celu modyfikowania tendencji do zeszklenia/krystalizacji badanej substancji, nie będzie to mieć znaczącego wpływu na pewien ogólny obraz dotyczący zachowań krystalizacyjnych w różnych warunkach (T, p) który uzyskamy. A więc, w pewnym sensie obie zmienne mogą być wykorzystywane zamiennie w celu sterowania procesami zeszklenia i krystalizacji.

3b. Wpływ podwyższonego ciśnienia na dynamikę relaksacyjną fenofibratu w fazie przechłodzonej cieczy i szklistej

Kolejny etap prowadzonych badań dotyczył wpływu podwyższonego ciśnienia na dynamikę relaksacyjną fenofibratu w cieczy przechłodzonej i fazie szklistej. Zagadnienia z tej tematyki stanowią podstawę publikacji A1 zamieszczonej na łamach czasopisma *The Journal of Physical Chemistry B*. W pracy tej, z wykorzystaniem spektroskopii dielektrycznej, scharakteryzowano dynamikę przejścia szklistego fenofibratu w zakresie temperatur od 255 K do 363 K i ciśnień sięgających nawet 0.5 GPa. Wymagało to przeprowadzenia serii pomiarów dielektrycznych w warunkach izobarycznych (0.1 MPa, 110 MPa, 230 MPa, 305 MPa, 380 MPa, 480 MPa, 530 MPa) i izotermicznych (273 K, 297 K, 324 K, 339 K, 351 K). Na podstawie uzyskanych wyników i w oparciu o model teoretyczny zaproponowany przez Avramova[55] możliwe stało się opisanie zachowania czasów relaksacji strukturalnej dla przechłodzonego fenofibratu w dwuwymiarowej przestrzeni T-p (Rys. 3).

W dalszej kolejności pozwoliło to na wyznaczenie podstawowych parametrów charakteryzujących dynamikę przejścia szklistego fenofibratu. Jednym z takich parametrów jest współczynnik dT_g/dp, który informuje o tym jak dynamika przejścia szklistego jest wrażliwa na zmiany ciśnienia (Rys. 4a). Wartość dT_g/dp=0.225 K/MPa, którą uzyskano dla fenofibratu sugeruje, że związek ten można sklasyfikować jako substancję dość wrażliwą na efekty ciśnieniowe, podobnie zresztą jak ma to miejsce w przypadku większości układów van der waalsowskich. Dla porównania, dT_g/dp dla substancji wykazujących tendencję do tworzenia

silnych wiązań wodorowych są zdecydowanie niższe (np. gliceryna 0.040 K/MPa). Z kolei, w przypadku niektórych polimerów wartość współczynnika ciśnieniowego temperatury przejścia szklistego, dT_g/dp, może osiągnąć nawet 0.500 K/MPa (!). Zgodnie z najnowszymi wynikami badań,[56] wrażliwość dynamiki strukturalnej na efekty ciśnieniowe pozwala, w pierwszym przybliżeniu, uzyskać informacje na temat tego czy badany związek będzie również wrażliwy na fluktuacje gęstości i efekty nanoograniczeń 1D i 2D. Prawidłowość ta zostanie zweryfikowana w dalszej części niniejszej pracy doktorskiej, gdzie przedstawione zostaną wyniki badań dla fenofibratu umieszczonego w matrycy nanoporowatej.

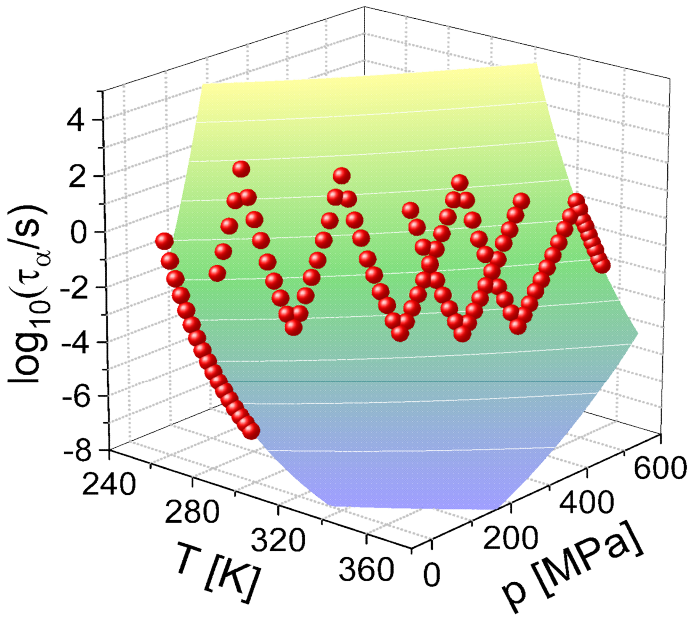

Rysunek 3. Zależność czasów relaksacji strukturalnej w funkcji temperatury i ciśnienia dla fenofibrate sparametryzowana z wykorzystaniem równania Avramova.

Analiza wyników badań dielektrycznych dla fenofibratu wykazała również, że w obszarze przechłodzonej cieczy spełnia on zasadę izochronicznej superpozycji. Jak pokazano na Rys. 4b, przy zachowaniu stałego czasu relaksacji kształt procesu pozostaje niezmienny mimo różnych kombinacji (T, p). Ponadto, wraz ze wzrostem ciśnienia parametr kruchości izobarycznej maleje (Rys. 4c), co z kolei świadczy o tym, że wraz ze wzrostem ciśnienia proces α staje się coraz mniej wrażliwy na zmiany T. Innymi słowy, wraz ze wzrostem ciśnienia zależność czasów relaksacji strukturalnej $\tau_\alpha(T)$ dla fenofibratu ma coraz bardziej charakter arrheniousowski. Warto jednak zauważyć, że w odróżnieniu od typowych cieczy van der waalsowskich spadek kruchości dla

fenofibratu w zakresie ciśnień od 0.1 MPa do 530 MPa jest bardzo niewielki, jedynie w zakresie 4-7 jednostek.

W pracy A4 pokazano także, że wykorzystując kompresję można odseparować od siebie drugorzędowe procesy o charakterze inter- i intramolekularnym. Dodatkowy proces relaksacyjny (β-relaksacja) widoczny jako dobrze odseparowany pik na widmach dielektrycznych zeszklonego fenofibratu w ciśnieniu p=480 MPa okazał się mieć ponad dwukrotnie wyższą wartość energii aktywacji niż szybszy proces γ (E_a=28 kJ/mol) i być praktycznie niewrażliwy na zmiany gęstości próbki. Co ciekawe, w warunkach ciśnienia atmosferycznego β-relaksacja jest zupełnie niewidoczna na widmach dielektrycznych fenofibratu, zarówno powyżej jak i poniżej T_g. Jest to spowodowane przede wszystkim niską amplitudą tego procesu i jego bliską lokalizacją w stosunku do procesu α-relaksacji. Obecności β-relaksacji o międzycząsteczkowym pochodzeniu (typu Johari-Goldstein) należało jednak oczekiwać choćby w oparciu o przewidywania modelu sprzężeniowego Ngai'a (*ang. coupling model*).[57]

Dysponując odpowiednią liczbą danych eksperymentalnych analizie poddano również związek pomiędzy relaksacją strukturalną opisującą reorientację molekuł dipolowych i przewodnictwem stałoprądowym, które związane jest z translacyjnym ruchem nośników ładunku. Okazało się, że w warunkach podwyższonego ciśnienia obserwuje się zjawisko rozprzężenia (*ang. decoupling*) pomiędzy reorientacją molekuł i ruchami translacyjnymi jakie mają miejsce w obrębie badanego materiału. Odzwierciedleniem tego jest ewidentna zmiana wykładnika *s* z równania Debyea-Stokesa-Einsteina (DSE). W ciśnieniu atmosferycznym *s=1*, co świadczy o tym, że temperaturowe zależności czasów relaksacji strukturalnej i przewodnictwa stałoprądowego podążają za sobą, a więc omawiane tu ruchy są ze sobą w pewien sposób skorelowane (Rys. 4d). Natomiast wraz ze wzrostem ciśnienia wykładnik *s* systematycznie maleje i w ciśnieniu 530 MPa osiąga wartość *s*=0.3. Oznacza to więc, że zachodzi pewnego rodzaju wzmocnienie ruchów translacyjnych cząstek posiadających ładunek elektryczny nad ruchami reorientacyjnymi molekuł. Warto tutaj podkreślić, że zgodnie z posiadaną wiedzą tak dramatyczny spadek wartości wykładnika „s" w funkcji ciśnienia nie był do tej pory obserwowany w przypadku materiałów formujących stan szklisty. Próby interpretacji tego niezwykle interesującego wyniku obejmować mogą zagadnienia związane z pojęciem mikrolepkości i nieco innym rozmiarem dwóch rodzajów cząsteczek obecnych w badanym materiale (molekuły dipolowe i cząstki obdarzone ładunkiem, np. jony). W takim „zatłoczonym" środowisku za jakie można uważać ciecz przechłodzoną w

pobliżu przejścia szklistego może to mieć istotny wpływ na spowolnienie jednego typu ruchów względem innego. Inna koncepcja, która mogłaby wyjaśnić zmianę relacji pomiędzy σ i τ dla fenofibratu w warunkach podwyższonego ciśnienia wiąże się ze zmianami w transferze protonu wzdłuż sieci wiązań wodorowych. Jak pokazały bowiem wyniki badań z wykorzystaniem spektroskopii w podczerwieni fenofibrat wykazuje tendencję do tworzenia wewnątrz i międzymolekularych wiązań wodorowych. Zagadnienie to wymaga jednak przeprowadzenia bardziej szczegółowych badań i analiz w przyszłości.

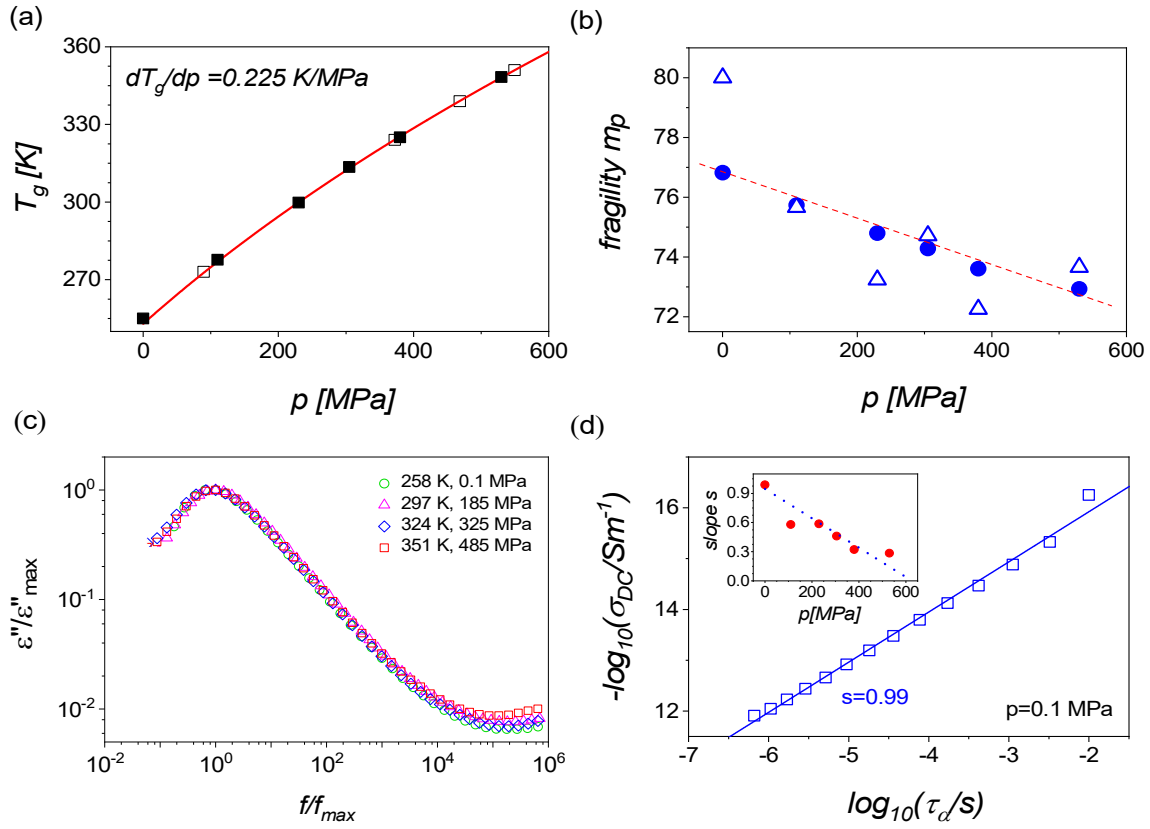

Rysunek 4.(a) Zależność temperatury zeszklenia od ciśnienia dla fenofibratu sparametryzowana z wykorzystaniem równania Andersson'a-Andersson'a. (b) Zachowanie parametru kruchości izobarycznej w funkcji ciśnienia, (c) Porównanie widm dielektrycznych zarejestrowanych w różnych warunkach temperatury i ciśnienia jednak przy zachowaniu tego samego czasu relaksacji ($\tau_\alpha \approx 0.16$ s). W celu ułatwienia testowania zasady izochronicznej superpozycji widma dielektryczne zostały znormalizowane względem ε''_{max} i f_{max} (d) Relacja pomiędzy przewodnictwem stałoprądowym i czasem relaksacji strukturalnej przedstawiona w skali podwójnie logarytmicznej dla ciśnienia atmosferycznego. Wstawka obrazuje zmianę współczynnika „s" z równania DSE w funkcji ciśnienia.

3c. Badanie zachowań krystalizacyjnych fenofibratu w obszarze przechłodzonej cieczy w ciśnieniu atmosferycznym oraz w warunkach podwyższonego ciśnienia.

Po zbadaniu wpływu podwyższonego ciśnienia na dynamikę relaksacyjną fenofibratu, kolejny etap badań dotyczył wpływu temperatury oraz ciśnienia na proces krystalizacji z fazy przechłodzonej cieczy dla tego związku. Tematyka ta stanowiła treść publikacji A2 opublikowanej w czasopiśmie *Physical Chemistry Chemical Physics*. W niniejszej pracy proces krystalizacji fenofibratu z fazy przechłodzonej cieczy został zbadany z użyciem trzech różnych metod pomiarowych: spektroskopii dielektrycznej, skaningowej kalorymetrii różnicowej oraz rentgenografii proszkowej. Ponadto, by rozseparować nukleację i wzrost kryształów przeprowadzono pomiary wzrostu kryształów z wykorzystaniem mikroskopu światła spolaryzowanego. By otrzymać pełny obraz dotyczący przebiegu procesu krystalizacji w stanie przechłodzonej cieczy przeprowadzono pomiary przy pomocy spektroskopii dielektrycznej w zakresie temperatur od 275 K do 350 K. Uzyskane wyniki zostały następnie przeanalizowane przy pomocy modelu JMAK. Umożliwiło to wyznaczenie wartości oraz zachowania w zależności od stopnia przechłodzenia parametrów charakterystycznych dla procesu krystalizacji takich jak stałej krystalizacji (k) oraz parametru Avramiego (n). O ile, niezależnie od stopnia przechłodzenia, wartość parametru n fluktuowała wokół 3 (co świadczyło o tym, że mechanizm krystalizacji jest nieczuły na temperaturę), to parametr k wykazał silną zależność wartości od temperatury, co zostało pokazane na Rys. 5a. Najmniejsze wartość k zaobserwowano w pobliżu temperatury zeszklenia oraz w pobliżu temperatury topnienia. Zauważono także, że proces izotermicznej krystalizacji wraz z zmniejszaniem stopnia przechłodzenia przyśpiesza monotonicznie aż do osiągnięcia maksimum w temperaturze około 330 K, by następnie gwałtownie spowolnić. Na podstawie wyników pomiarów dielektrycznych z publikacji A1 odczytano, że dla temperatury 330 K czas relaksacji strukturalnej wynosił w przybliżeniu 10^{-8} s. Jest to ważna obserwacja ze względu na to, że dla tego czasu relaksacji następuje zmiana w obserwowanym mechanizmie dynamiki molekularnej (*ang. dynamic crossover*). Wynika z tego, że mechanizm oddziaływania pomiędzy molekułami ma znaczący wpływ na proces krystalizacji.

W dalszym toku badań przeprowadzono pomiary wzrostu kryształów pod mikroskopem optycznym w zakresie temperatur od 293 K do 343 K. Otrzymane wyniki zestawiono z wartościami k (Rys. 5a), w wyniku czego stwierdzono, że dla fenofibratu proces krystalizacji w

zakresie niskich temperatur jest determinowany w głównej mierze poprzez nukleację, a wysokich temperaturach decydujący jest wzrost kryształów. Zostało to potwierdzone poprzez obserwacje morfologii kryształów pod mikroskopem optycznym. Dla próbek skrystalizowanych w niższych temperaturach otrzymano wiele, bardzo drobnych kryształów, za to dla próbek skrystalizowanych w pobliżu temperatury topnienia otrzymano kilka dużych kryształów. Ze względu na to, że spektroskopia dielektryczna nie jest metodą ściśle dedykowaną do badania polimorfizmu substancji, w celu zbadania do jakiej odmiany polimorficznej krystalizuje fenofibrat w zależności od temperatury przeprowadzono badania kinetyki krystalizacji przy użyciu skaningowej kalorymetrii różnicowej jak również proszkowej dyfrakcji rentgenowskiej. Pomiary te wykazały, że podczas krystalizacji w wyższych temperaturach fenofibrat krystalizuje wyłącznie do formy I. Natomiast, w niższych temperaturach zaobserwowano równoczesną krystalizację (tzw. co-krystalizację) formy I i II fenofibratu (Rys. 5b i 5c) co okazuje się być w zgodzie z danymi literaturowymi.[58] Szczegółowa analiza uzyskanych wyników pozwoliła oszacować także, że podczas procesu co-krystalizacji około 25% fenofibratu krystalizuje do metastabilnej formy II.

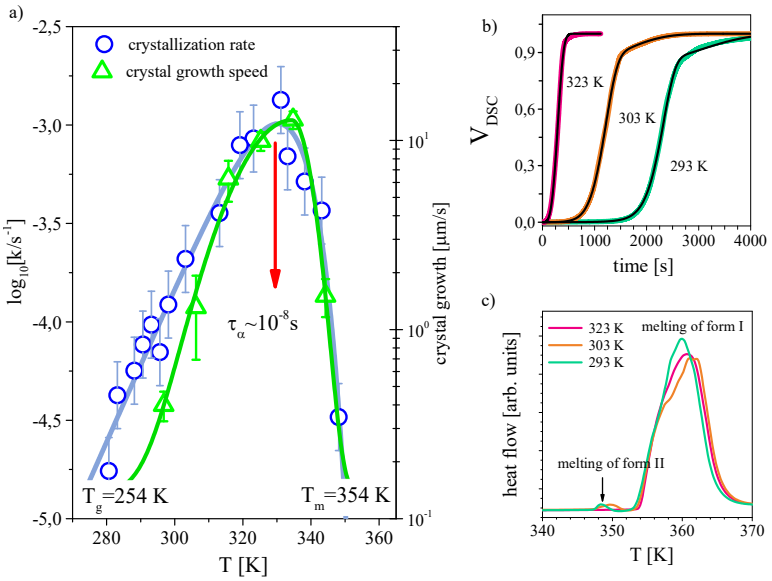

Rysunek 5. Wykresy zależności a) stałej krystalizacji (oś lewa) w oparciu o badania dielektryczne oraz tempa wzrostu kryształów (oś prawa) od temperatury krystalizacji b) stopnia krystaliczności od czasu dla izotermicznych krystalizacji przy pomocy DSC, czarne linie przedstawiają fity uzyskane poprzez modelu JMAK dla dwóch faz c) krzywe kalorymetryczne uzyskane podczas grzaniu skrystalizowanego fenofibratu w 293 K (zielona krzywa), 303 K (pomarańczowa krzywa), 323 K (magentowa krzywa).

W dalszej części badań sprawdzono wpływ podwyższonego ciśnienia na kinetykę krystalizacji przechłodzonego fenofibratu z użyciem spektroskopii dielektrycznej. W pomiarach tych wykorzystano ciśnienia rzędu 362 MPa przy temperaturze 358 K, a otrzymane wyniki porównano danymi uzyskanymi podczas krystalizacji w temperaturze 280.6 K i ciśnieniu atmosferycznym (temperatura została tak dobrana by czas relaksacji strukturalnej w obydwóch przypadkach był identyczny). Analiza otrzymanych wyników udowodniła, że przy zachowaniu mniej więcej tego samego wkładu pochodzącego od składowej związanej z ruchliwością molekularną krystalizacja fenofibratu spowalnia w warunkach podwyższonego ciśnienia (Rys. 6). Należy jednak zauważyć, że pomimo zastosowania tak znacznych wartości ciśnienia zmiana tempa krystalizacji jest niewielka, dla porównania taką samą zmianę wartości k w ciśnieniu atmosferycznym powodowała zmiana temperatury krystalizacji o około 10 K.

Pionierskim etapem opisywanych dalej badań było zrozumienie wpływu ścieżki termodynamicznej na proces krystalizacji (górny panel na Rys. 6). W tym celu przeprowadzono dwa niezależne pomiary kinetyki krystalizacji w tych samych finalnych warunkach (T_c, p_c), jednak osiągniętych z wykorzystaniem dwóch nieco odmiennych ścieżek. W pierwszym przypadku wystartowano z ciśnienia atmosferycznego podnosząc najpierw temperaturę badanego układu z T=354 K do T_c=358 K (grzanie w warunkach izobarycznych). A potem, po osiągnięciu zadanej temperatury rozpoczęto izotermiczną kompresję do p_c=362 MPa. Druga ścieżka obejmowała natomiast izobaryczne chłodzenie w p=580 MPa z temperatury T=368 K do T_c=358 K, a następnie izotermiczną dekompresję (580 MPa do 362 MPa). Podczas porównania wyników okazało się, że gdy warunki końcowe uzyskane są poprzez dekompresję z większego stopnia przechłodzenia to proces krystalizacji jest wolniejszy niż gdy stosujemy kompresję stopionej substancji z temperatury powyżej T_m. Otrzymany rezultat świadczy o tym, że można manipulować/sterować tempem procesu krystalizacji/tendencją do krystalizacji materiałów formujących stan szklisty nie tylko modyfikując wartości temperatury i ciśnienia wzdłuż izochrony, a więc krzywej łączącej pary (T, p) o jednakowym czasie relaksacji, ale również zmieniając historię termodynamiczną próbki.

Na sam koniec aby sprawdzić w jaki sposób ciśnienie wpływa na skład polimorficzny skrystalizowanej próbki przeprowadzono badania kalorymetryczne materiału uzyskanego po krystalizacji w podwyższonym ciśnieniu (dolny panel Rys. 6). W wyniku badań stwierdzono, że przyłożone ciśnienie powoduje krystalizacje fenofibratu do I formy polimorficznej, pomimo, że

na podstawie wyników badań przeprowadzonych pod ciśnieniem atmosferycznym spodziewano się obecności obydwóch form. Jest to również zaskakujące, ze względu na to, że zgodnie z zasadą stopni Ostwalda (*ang. Ostwald step rule*), podczas krystalizacji pod zwiększonym ciśnieniem powinna być faworyzowana odmiana polimorficzna posiadająca większą gęstość, a dla fenofibratu jest to forma II.

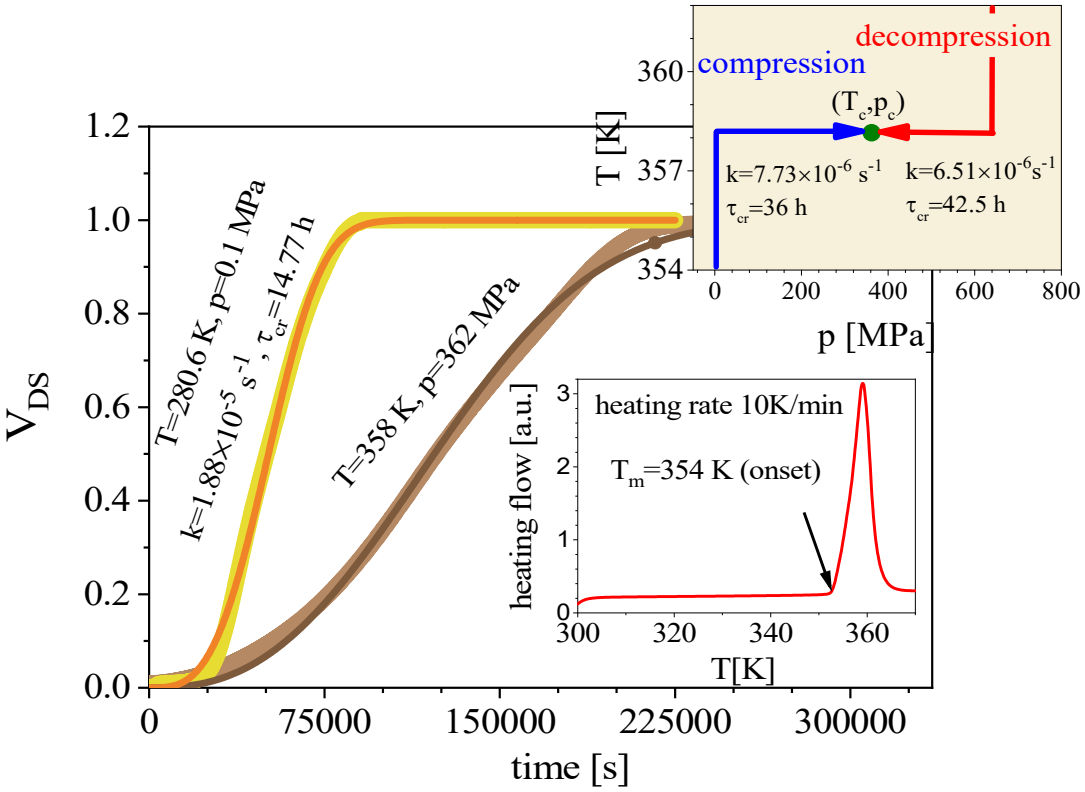

Rysunek 6. Główny panel: Wykres zależności stopnia krystaliczności od czasu dla pomiaru dla krystalizacji przeprowadzonych pod ciśnieniem atmosferycznym oraz pod podwyższonym ciśnieniem. Górny panel: Porównanie ścieżek termodynamicznych pod ciśnieniem na otrzymane wyniki procesu krystalizacji Dolny panel: krzywa kalorymetryczna otrzymana dla próbki skrystalizowanej pod ciśnieniem.

3d. Wpływ ograniczonej geometrii na dynamikę przejścia szklistego i krystalizację fenofibratu umieszczonego w matrycy nanoporowatej.

Ostatni etap pracy poświęcony był zrozumieniu wpływu ograniczonej geometrii na dynamikę przejścia szklistego i zachowania krystalizacyjne fenofibratu. Wyniki badań z tej

tematyki zamieszczono w artykule A4 opublikowanym na łamach czasopisma *The Journal of Physical Chemistry C*. Należy tutaj zaznaczyć, że „twarde" ograniczenia przestrzenne (*ang. hard confinement*) o rozmiarach rzędu „nano" podobnie zresztą jak kompresja mogą w istotny sposób wpływać na własności dynamiczne i tendencję do krystalizacji substancji formujących stan szklisty. Ponadto, wbrew pozorom, efekty nanoograniczeń i wysokociśnieniowe mają ze sobą wiele wspólnego, bowiem w obydwóch przypadkach istotną rolę na obserwowane zjawiska odgrywają fluktuacje gęstości.[8,59] W związku z powyższym, informacje na temat dynamiki i krystalizacji fenofibratu uwięzionego w matrycach nanoporowatych stanowiły tutaj istotne dopełnienie wyników badań uzyskanych w warunkach podwyższonego ciśnienia dla materiału litego. W badaniach tych wykorzystano komercyjnie dostępne matryce nanoporowate wykonane z dwutlenku aluminium, zbudowane z prostych i niełączących się ze sobą kanałów o średnicach od 150 nm aż do 18 nm. Szczegółowe informacje na temat zastosowanej strategii napełniania porów badaną substancją można znaleźć w pracy A4, w sekcji 'Experimental Methods'.

W pierwszej kolejności przeprowadzone zostały badania dielektryczne i kalorymetryczne których celem była analiza dynamiki przejścia szklistego w obecności nanoograniczeń. Jednym z charakterystycznych efektów 'confined' obserwowanych dla (większości) cieczy molekularnych uwięzionych w ośrodku nanoporowatym jest odejście temperaturowych zależności czasów relaksacji strukturalnej od zachowania obserwowanego dla materiału litego. Jak można zauważyć na Rys. 7a, wraz ze zmniejszeniem średnicy użytych porów efekt ten staje się w przypadku fenofibratu coraz bardziej widoczny. Co więcej, w zależności od historii termicznej próbki zmiana zależności $\tau_\alpha(T)$ może nastąpić w nieco wyższej czy też niższej temperaturze (wstawka Rys. 7a). Wykorzystując wyniki badań kalorymetrycznych można wykazać, że temperatura w której obserwuje się to charakterystyczne odejście zależności $\tau_\alpha(T)$ jest związana z zamrożeniem (zeszkleniem) warstwy molekuł znajdujących się w bezpośrednim sąsiedztwie ścianek porów ($T_{g\_interface}$). W trakcie dalszego chłodzenia molekuły znajdujące się w środku kanałów również podlegają procesowi zeszklenia (T_{g_core}). Jednakże, jak wskazują na to najnowsze wyniki badań,[56] proces ten zachodzi w warunkach quasi-izochorycznych, a więc przy 'zamrożeniu' objętości układu. W takim przypadku, wykorzystując dane ciśnieniowe dla materiału litego można nawet opisać zależności $\tau_\alpha(T)$ w obszarze temperatur pomiędzy T_{g_core} i $T_{g\_interface}$. A więc, podobnie jak w przypadku kompresji, efekty związane z fluktuacjami gęstości pełnią istotną rolę w zrozumieniu zachowania materiałów formujących stan szklisty w ograniczonej do skali nano geometrii.

Rozpatrując dynamikę materiałów formujących stan szklisty uwięzionych w ośrodku nanoporowatym, kwestią istotną z fundamentalnego punktu widzenia wydaje się być znalezienie odpowiedzi na pytanie *czy może ona również podlegać tym samym regułom co materiał lity?* Podążając za najnowszymi wynikami badań,[60] których jestem również współautorem, w artykule A4 pokazano, że dynamika związana z przejściem szklistym dla fenofibratu podlega idei skalowania gęstościowego zarówno w warunkach podwyższonego ciśnienia jak również ograniczonej do skali nano geometrii (w obszarze temperatur pomiędzy T_{g_core} a $T_{g\_interface}$). Jak pokazano na Rys. 7b, oznacza to więc możliwość zeskalowania na jedną krzywą czasów relaksacji strukturalnej uzyskanych w różnych warunkach termodynamicznych z użyciem pojedynczego wykładnika skalującego γ wynoszącego dla fenofibratu 4.3. Wynik ten jest niezwykle istotny z kilku powodów: *(i)* dowodzi że charakter oddziaływań międzymolekularnych pozostaje niezmienny zarówno w warunkach podwyższonego ciśnienia jak również w obecności nanoograniczeń (γ można powiązać ze składową odpychającą potencjału oddziaływań międzymolekularnych), *(ii)* umożliwia przewidywanie zachowania czasów relaksacji w warunkach nanoograniczeń w oparciu o dane ciśnieniowe i vice versa, *(iii)* pokazuje, że w przypadku materiałów formujących stan szklisty idea skalowania gęstościowego stanowić może uniwersalny łącznik pomiędzy światem makro- a nanoskopowym.

Słuszność idei skalowania gęstościowego sugerować by mogła, że w obecności nanoograniczeń, podobnie zresztą jak w warunkach podwyższonego ciśnienia, powinna obowiązywać również zasada izochronicznej superpozycji. W literaturze poświęconej dynamice materiałów formujących stan szklisty utarło się bowiem takie przekonanie, że spełnienie jednej z powyższych reguł, oznacza niejako spełnienie tej drugiej.[61]Aby to zweryfikować, w pracy A4 przeanalizowano kształt procesu relaksacji strukturalnej dla fenofibratu umieszczonego w matrycy nanoporowatej o różnej średnicy kanalików. Analizy porównawczej dokonano dla dwóch izochron $\log_{10}(\tau_\alpha/\mathrm{s})$=-4.2 i $\log_{10}(\tau_\alpha/\mathrm{s})$=-0.2 zlokalizowanych odpowiednio w obszarze powyżej jak i poniżej temperatur zeszklenia molekuł przyściankowych. Uzyskane dla fenofibratu wyniki wskazują na spełnienie zasady izochronicznej superpozycji w obszarze $T>T_{g\_interface}$, i jej brak w obszarze temperatur pomiędzy $T_{g\_core}<T<T_{g\_interface}$, tj. w obszarze gdzie obowiązuje skalowanie gęstościowe (Rys. 7c). A więc, że wbrew powszechnej opinii te dwie obserwacje eksperymentalne niekoniecznie muszą być ze sobą w jakikolwiek sposób powiązane. Taka konkluzja wymaga jednak dalszych badań, prowadzonych zarówno na podłożu teoretycznym jak i eksperymentalnym.

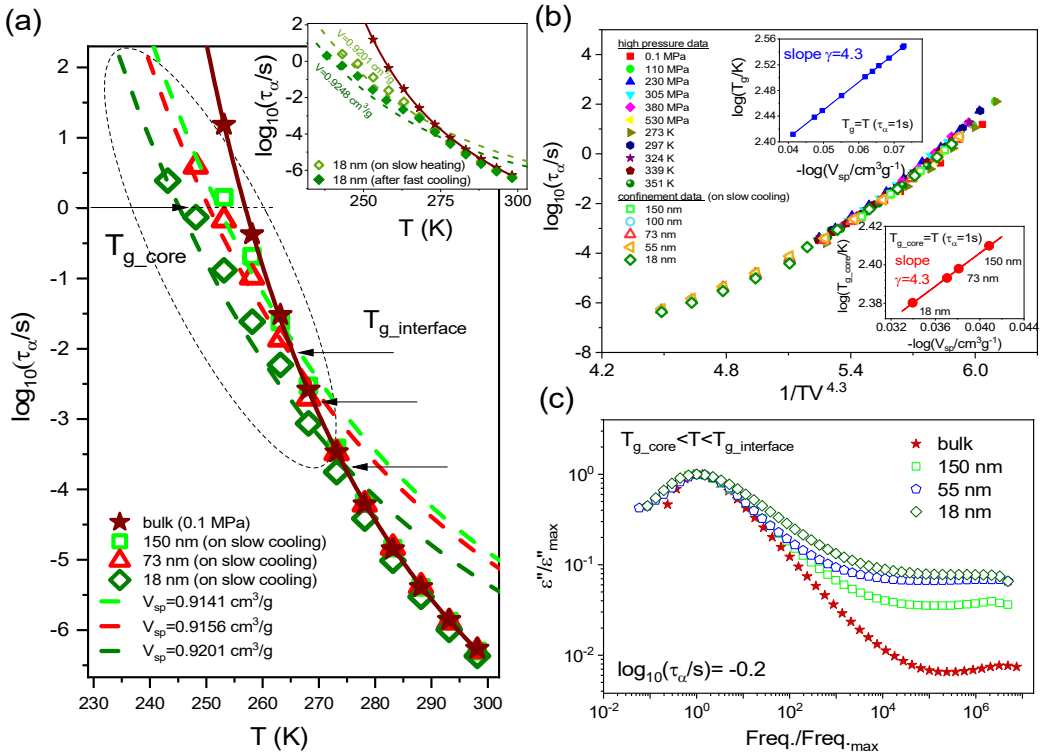

Rysunek 7. (a) Temperaturowe zależności czasów α-relaksacji obrazujące dynamikę molekuł w środkowej części pora dla fenofibratu umieszczonego w matrycach nanoporowatych o różnej średnicy porów. Zachowanie czasów α-relaksacji poniżej $T_{g\_interface}$ opisują odpowiednie izochory. Wstawka demonstruje wpływ historii termicznej na zachowanie $\tau_\alpha(T)$ w obszarze poniżej $T_{g\_interface}$. (b)Weryfikacja idei skalowania gęstościowego dla fenofibratu obejmująca wyniki badań uzyskane w warunkach podwyższonego ciśnienia jak i ograniczonej geometrii (2D). Wstawki prezentują zależności T_g vs V_g (przejście szkliste zdefiniowane dla 1s) w skali podwójnie logarytmicznej. Zarówno w przypadku danych wysokociśnieniowych (górna wstawka) jak i tych uzyskanych w ośrodku nanoporowatym (dolna wstawka) parametr γ wyznaczono z nachylenia prostej.(c)Porównanie widm dielektrycznych zarejestrowanych dla fenofibratu umieszczonego w nanoporach o różniej średnicy kanalików w obszarze temperatur poniżej $T_{g\_interface}$ ale przy zachowaniu tej samej skali czasowej procesu α-relaksacji.

W następnej kolejności zbadano wpływ ograniczenia przestrzennego na proces izotermicznej krystalizacji fenofibratu. W tym celu przeprowadzono pomiary procesu krystalizacji wybranych matryc nanoporowatych (średnica porów 100 nm, 55 nm oraz 18 nm) w szerokim zakresie temperatur ($T_{g\_interface}<T_c<T_m$) przy użyciu spektroskopii dielektrycznej. Pierwszym zaobserwowanym efektem ograniczenia przestrzennego na proces krystalizacji była zmiana kształtu krzywych krystalizacji uzyskanych w tej samej temperaturze dla różnych porów (Rys. 8a).

Analiza tego zjawiska wykazała, że wraz z zmniejszaniem się średnicy porów odchylenie krzywej krystalizacyjnej od sigmoidalnego charakteru było coraz większe. Korelowało się to także z zmniejszeniem wartości parametrów krystalizacji *k* oraz *n*. Powyższe wyniki zostały wykorzystane w pracy Marca Descampsa, z 2018 roku o krystalizacji w układach o ograniczonym rozmiarze jako potwierdzenie eksperymentalne przeprowadzonych rozważań teoretycznych.[62] Dalsza analiza przeprowadzonych pomiarów wykazała, że oprócz spowolnienia procesu krystalizacji (Rys. 8b) oraz zmniejszenie wartości parametru *n* (Rys. 8c) wraz z zmniejszeniem średnicy porów obserwuje się również przesunięcie maksimum krystalizacji w stronę wyższych stopni przechłodzenia. Świadczy to o tym, że wraz z zmniejszeniem się średnicy porów nukleacja zmienia charakter z nukleacji heterogenicznej (dominującą w niższych stopniach przechłodzenia) w nukleację homogeniczną. Znaczne zmniejszenie wartości parametru *n* w porównaniu do materiału litego (z 3 do 1 dla 18 nm) świadczy, oprócz zmiany charakteru nukleacji, również o zmianie wymiarowości wzrostu kryształów i całego procesu krystalizacji.

Na samo zakończenie zbadano wpływ ograniczenia przestrzennego na proces topnienia fenofibratu. Jak pokazano na Rys. 8e, temperatura topnienia fenofibratu maleje praktycznie liniowo z odwrotnością średnicy porów. Z kolei, analiza danych kalorymetrycznych dla w pełni skrystalizowanych próbek wykazała obniżenie temperatury topnienia wraz z zmniejszeniem się rozmiaru porów(Rys. 8f). Spowodowane jest to działaniem sił kapilarnych (im mniejsza jest średnica porów tym są silniejsze), które to powodują przesunięcie równowagi termodynamicznej pomiędzy cieczą a kryształem w niższe temperatury. Oprócz tego na krzywych kalorymetrycznych zaobserwowano poszerzenie piku topnienia wraz z wzrostem ograniczenia przestrzennego. Świadczy to o wzroście heterogeniczność procesu topnienia wraz z zmniejszeniem średnicy porów. Do całkiem zaskakujących rezultatów doprowadziło wyznaczenie entalpii procesów topnienia (wstawka na Rys. 8f). O ile sama zmiana entalpii topnienia w zależności od średnicy porów nie jest zaskakująca to jednak jej liniowa zależność od odwrotności średnicy porów (pomimo że temperatura topnienia nie spełnia tej zależności) jest niezwykle cennym i intrygującym rezultatem. Z jednej strony może to być wytłumaczone tym, że liczba molekuł biorących udział w procesie topnienia maleje wraz z wzrostem ograniczenia przestrzennego, a z drugiej działaniem sił kapilarnych i związanych z nimi zmianami energii oddziaływań pomiędzy fazami ciekłą, stałą a podłożem. Aby rozstrzygnąć co ma wpływ na takie zachowanie entalpii

topnienia dla fenofibratu pod ograniczeniem przestrzennym niezbędne jest przeprowadzenie w przyszłości kolejnych, bardziej ukierunkowanych na ten problem eksperymentów.

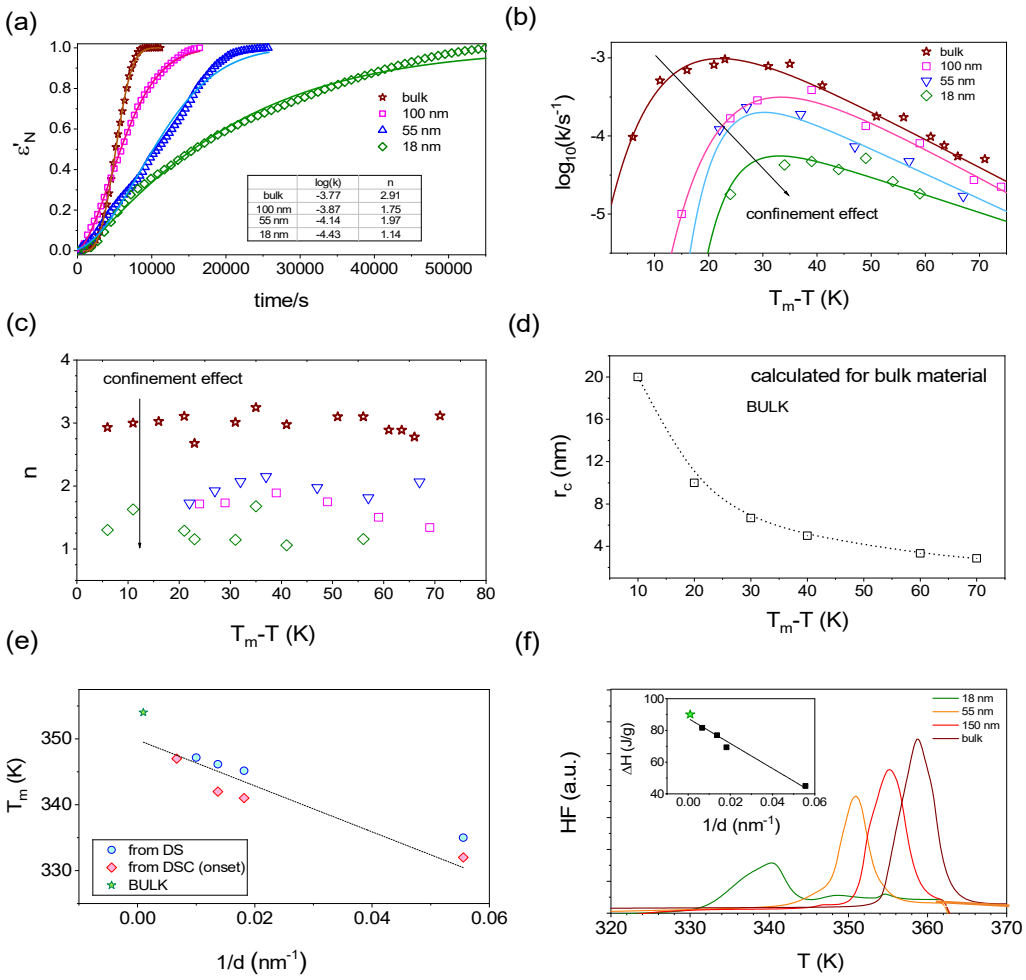

Rysunek 8. a) Porównanie czasowej zależność stopnia krystaliczności podczas izotermicznej krystalizacji fenofibratu w fazie litej (bordowe gwiazdki) oraz uwięzionego w ośrodku nanoporowatym w temperaturze T=298 K. Linie pokazują dopasowania modelu JMAK do wyników eksperymentalnych b) Zależność wartości stałej krystalizacji c) parametru Avramiego od różnicy temperatury topnienia i temperatury krystalizacji. Strzałka wskazuje kierunek zmian obserwowanych w obecności nanoograniczeń d) Wykres zależności promienia krytycznego nukleacji od stopnia przechłodzenia dla materiału litego e) Wykres zależności temperatury topnienia fenofibratu od odwrotności średnicy porów. Przerywana linia reprezentuje spodziewaną linię trendu zachowania temperatury topnienia zgodnie z równaniem Gibbsa-Thomsona f) Krzywe kalorymetryczne otrzymane podczas grzania skrystalizowanego fenofibratu w matrycach nanoporowatych o różnej średnicy. Wstawka pokazuje zależność entalpii topnienia od odwrotności średnicy porów.

4. TREŚCI ARTYKUŁÓW STANOWIĄCYCH PODSTAWĘ ROZPRAWY DOKTORSKIEJ WRAZ Z OŚWIADCZENIAMI WSPÓŁAUTORÓW

A1. Dielectric relaxation study at ambient and elevated pressure of the modeled lipophilic drug fenofibrate

Autorzy: G. Szklarz, K. Adrjanowicz, M. Dulski, J. Knapik, M. Paluch
Referencja: J. Phys. Chem. B 2016, 120, 11298–11306
DOI: 10.1021/acs.jpcb.6b08511
Impact Factor czasopisma z roku opublikowania pracy: **3.187**
Liczba punktów ministerialnych MNiSW czasopisma (2016): **30**

Mój udział w poniższym artykule polegał na wykonaniu większości pomiarów dielektrycznych, analizie i opracowaniu wyników pomiarów oraz przygotowaniu manuskryptu. Wkład pozostałych współautorów zamieszczono w formie oświadczeń.

THE JOURNAL OF PHYSICAL CHEMISTRY B

Article

pubs.acs.org/JPCB

Dielectric Relaxation Study at Ambient and Elevated Pressure of the Modeled Lipophilic Drug Fenofibrate

Grzegorz Szklarz,[†,‡] Karolina Adrjanowicz,[*,†,‡] Mateusz Dulski,[§,‡] Justyna Knapik,[†,‡] and Marian Paluch[†,‡]

[†]Institute of Physics, University of Silesia, ulica Uniwersytecka 4, 40-007 Katowice, Poland

[‡]Silesian Center for Education and Interdisciplinary Research, ulica 75 Pulku Piechoty 1a, 41-500 Chorzow, Poland

[§]Institute of Material Science, Univeristy of Silesia, ulica 75 Pulku Piechoty 1a, 41-500 Chorzow, Poland

S *Supporting Information*

ABSTRACT: We have investigated the molecular dynamics in supercooled liquid and glassy state of the pharmaceutical agent fenofibrate. To do that, dielectric relaxation studies at ambient and elevated pressure were performed. Data collected at atmospheric pressure were found to be in good agreement with that already reported in the literature. High-pressure studies enable us to distinguish the secondary relaxation processes of the different molecular origin. This includes (i) pressure insensitive γ-relaxation of the activation energy E_a = 28 kJ/mol and (ii) β-relaxation that senses the density increase and originates most probably from the intermolecular movements (E_a = 77 kJ/mol at 480 MPa). The results of high-pressure studies have also revealed the validity of isochronal superposition and decoupling between α-relaxation and translational motions of charged species reflected by dc conductivity. The latter one was found to intensify with increasing pressure. Finally, we also show that the presence of quite complex inter- and intramolecular hydrogen bonds might still exert some subtle effect on the molecular dynamics of supercooled fenofibrate.

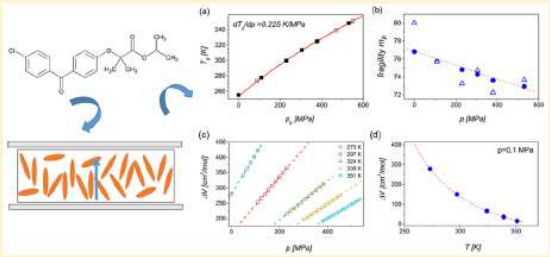

■ INTRODUCTION

Fenofibrate is a BCS class II lipid modifying agent used in the treatment of cardiovascular diseases, hypercholesterolemia, and hypertriglyceridemia. Its main action is to reduce the high level of cholesterol and triglycerides in the blood. Fenofibrate is highly lipophilic and water-insoluble drug (0.3 μg/mL).[1] Therefore, various strategies were employed to improve its restricted solubility and oral bioavailability. This includes manipulating with the formulation via micronization,[1,2] formulation of microemulsion,[3,4] electrospray deposition,[5] thin film freezing,[6] hot-melt extrusion,[7] loading into microcapsules[8] and mesopores,[9] or synthesis of the nanocrystals.[10] Some of these methods are based on changing a crystalline form of the drug to an amorphous form which is, by its nature, better soluble in aqueous media. In the amorphous state, the molecules are mutually disordered, which is in contrast to the crystalline state characterized by the long-range arrangement of the molecules. Higher than for the crystalline state, Gibbs free energy is responsible for improved reactivity and water solubility of the amorphous state. This can result in better oral bioavailability and therapeutic properties of the drugs.[11−16] On the other hand, it is also responsible for chemical and physical instability of the amorphous solids.[17−20] For amorphous fenofibrate obtained by quenching of the melt (so-called "glass"), recrystallization from the amorphous state is detected just after 2 days of storage at room temperature.[21] Recrystallization is an unwanted process limiting its potential usage in the pharmaceutical formulation and processing. Surprisingly, upon regular DSC scans, fenofibrate fails to crystallize both (i) when cooling from the melt and (ii) reheating from the glassy state.[22−24] On the basis of these features, Baird et al. have classified it as a molecular system with high glass-forming ability on cooling and high glass stability upon reheating.[22]

Finding an effective strategy allowing to improve the physical stability of amorphous drugs requires a better understanding of the most critical parameters that determine crystallization/glass-forming tendencies. Except for the apparent thermodynamic aspect, physical instability of amorphous solids also relates to the mobility factor.[17,25−30] The molecular movements change by many orders of magnitude when cooling liquid from the melting point down to the glassy state. Such a broad range of dynamics and appearance of the relaxation processes of the different origin might be challenging from an experimental point of view. Nevertheless, we can still probe the molecular mobility in supercooled liquid and glassy state by utilizing dielectric spectroscopy (DS).[31,32] Dielectric spectroscopy is an impedance technique which principal idea relies on the interactions of the molecular dipoles with an external electric field. Also, DS is a nondestructive for measured samples, requires a small quantity of the substance, and enables to follow the dynamic features of the studied samples in the real time of

Received: August 23, 2016
Revised: October 11, 2016
Published: October 17, 2016

DOI: 10.1021/acs.jpcb.6b08511
J. Phys. Chem. B 2016, 120, 11298−11306

the experiment. The dielectric relaxation process represents a particular type of molecular movement such as cooperative reorientation of molecules (α-relaxation) or single-particle motion of either inter- or intramolecular origin (labeled in the order of the decreasing time scale as β-relaxation, γ-relaxation, and so on). By following their evolution with the temperature, it is possible to not only characterize the molecular movements potentially responsible for the recrystallization process of glassy substances but also understand better the glass-formation phenomenon considered still as a fundamental problem of the condensed matter physics.[33−36]

Typically the molecular dynamics of glass-forming liquids is probed by changing the temperature at atmospheric pressure. However, such a strategy is not enough to provide a complete understanding of the glassy phenomenon, particularly quantifying the relative importance of the thermal energy and density effects in slowing down the molecular dynamics in the vicinity of the glass transition. For that reason, we often introduce pressure as an additional thermodynamic variable to control upon the dielectric relaxation studies.[37−39] The decrease of temperature at fixed pressure and the increase of pressure at constant temperature slows down the molecular movements. However, compression may exert a bit distinct effect on the molecular dynamics close to the glass transition than does the temperature. The most pronounced differences were reported for systems with strong intermolecular forces such as ionic or hydrogen bonding interactions.[40−44] High-pressure studies can be used to distinguish secondary relaxations of the different nature based on the sensitivity to density changes and their connection to the α-relaxation (i.e., the process which is directly involved in the glass transition event).[45,46]

In this paper, we present high-pressure dielectric relaxation studies of fenofibrate. Our results cover a broad range of temperatures (255−363 K) and pressures (up to 530 MPa). Except for the pharmaceutical significance, the sample selected for the present study poses many physicochemical properties that make it an attractive system to study. Molecular dynamics of amorphous fenofibrate at ambient pressure has been already reported in the literature. From that we know that investigated sample is a fragile glass-forming liquid (fragility index m = 94[23,24]) with nonexponential character of the α-relaxation (β_{KWW} = 0.7,[23] β_{KWW} = 0.635[24]) and well-pronounced γ-relaxation of the activation energy approximately 32 kJ/mol.[23] The reported glass transition temperature of fenofibrate is T_g = 251.4 K[24] (T_g = 254 K[22,23] from calorimetric studies). As pointed out by Tipduangta and co-workers,[47] the fenofibrate molecule is composed of the two main parts: aromatic rings linked by ketone group and the flexible aliphatic tail with ester moieties (see Figure 1). In addition to that, fenofibrate has four acceptors groups of the hydrogen bonds but none of the hydrogen-bond-donating groups such as −OH or $-NH_2$. In consequence, it should lack strong intermolecular hydrogen bonds[48] and behaves like typical van der Waals liquids. In contrast to that the hydrogen bonding propensity of fenofibrate was reported by Sailaja and co-workers.[23] Apart from that

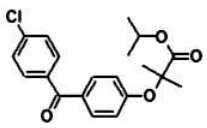

Figure 1. Molecular structure of fenofibrate.

Fenofibrate is known to possess three polymorphic forms among which form I (T_m = 353 K) is the most stable one and used in the pharmaceutical formulations. The metastable form II (T_m = 347 K) accompanies form I upon recrystallization of the quenched cooled sample, while form III (T_m = 323 K) is obtained when recrystallizing in the presence of the small amounts of pharmaceutical excipient talc.[21,47] The molecules in the crystalline form of fenofibrate are aligned in layers stabilized by C−H···O interactions, being naturally weak hydrogen bonds.[49,50] Pressure-dependent dielectric measurements can validate the importance of such interactions on the relaxation dynamics in the supercooled liquid state. Increased pressure may affect the size and the population of the hydrogen bonds. This effect immediately leads to significant changes in the relaxation behavior in the vicinity of the glass transition.[51,52]

EXPERIMENTAL SECTION

Material. Fenofibrate ($C_{20}H_{21}ClO_4$, M_w = 360.83 g/mol) with purity >99% was purchased from Sigma-Aldrich as a white crystalline powder. Chemical structure of fenofibrate is shown in Figure 1. We obtain amorphous fenofibrate by fast cooling of the melted sample. For that purpose, we have heated up the crystalline powder above the melting point (form I, T_m = 352−354.8 K[21−24]) and then rapidly cool it to the room temperature.

Dielectric Measurements. Dielectric measurements at atmospheric pressure were performed using a Novocontrol dielectric spectrometer. Complex dielectric permittivity ($\epsilon^*(f) = \epsilon'(f) + i\epsilon''(f)$) was recorded in the frequency range 5.6×10^{-2}−1.8×10^6 Hz. The temperature was controlled by the Novo-Control Quattro system using a nitrogen gas cryostat with the stability better than 0.1 K. Measurements were performed by placing a crystalline material on a stainless steel electrode (20 mm diameter) and heating above the melting temperature of the polymorph I. After complete melting, the liquid was covered with another electrode of the same diameter to yield a layer of ca. 50 μm thickness provided by Kapton spacer and cooled to room temperature on a chilled brass block. Then, we have mounted the capacitor inside a cryostat. Dielectric spectra were collected on reheating the glassy sample from 163 to 313 K with different temperature steps: in the temperature range 163−223 K data were gathered every 5 K, while in temperature range 223.15−313.15 K in a step of 2.5 K. To ensure that the unwanted crystallization event does not spoil the dielectric signal, the sample placed inside the cryostat was heated again above the melting temperature and then rapidly cooled to 163 K (15 K/min).

For dielectric studies at elevated pressure, we have utilized the high-pressure system with MP5 micropump (Unipress, Institute of High-Pressure Physics, Warsaw, Poland). The pressure was exerted by using silicon oil transmitted to the pressure chamber by a system of the capillary tubes (Nova Swiss). The real and imaginary parts of the complex permittivity were measured within the same frequency range using impedance Alpha-A analyzer (Novocontrol GmbH, Montabaur, Germany). The temperature was controlled by thermal bath with stability better than 0.1 K. We have used a homemade capacitor placed inside a Teflon capsule to separate it from the pressurizing fluid. We have collected dielectric relaxation spectra along isobars 110, 230, 305, 380, 480, and 530 MPa and isotherms 273, 297, 324, 339, and 351 K. Isobar p = 480 MPa was measured to evaluate the effect of pressure on the secondary relaxations. In the supercooled liquid regime, the

DOI: 10.1021/acs.jpcb.6b08511

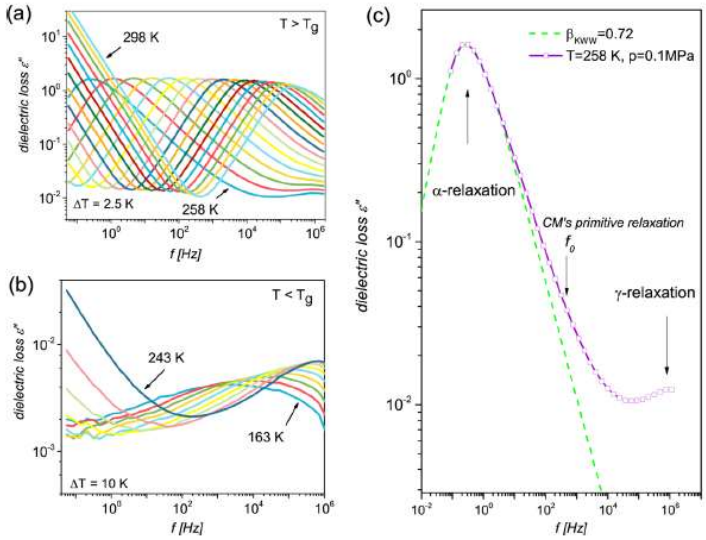

Figure 2. Dielectric loss spectra of fenofibrate as measured at atmospheric pressure (a) above and (b) below glass transition temperature. Data were collected on reheating the glassy sample. (c) Dielectric loss spectrum collected at temperature 258 K with KWW fit $\beta_{KWW} = 0.72$; arrow indicates the position of the primitive frequency f_0 calculated from the coupling model.

frequency at the maximum of the structural relaxation loss peak was kept below 1000 Hz to avoid crystallization.

■ RESULTS AND DISCUSSION

Dielectric Relaxation Study at Ambient Pressure. Dielectric loss (ϵ'') spectra measured in the supercooled liquid and glassy state of fenofibrate are shown in Figure 2. Analysis of the collected spectra agrees fairly well with the results reported by Sailaja[23] and Tu.[24] The presence of the multiple relaxation processes indicates the existence of the different molecular motions in the studied sample. Highly intense and well-pronounced relaxation peak detected in the supercooled liquid state comes from the α-relaxation that reflects cooperative movements of molecules closely related to the glass formation. Its characteristic time can be determined as an inverse of the frequency corresponding to the peak maximum ($\tau_\alpha = 1/2\pi f_{max}$). From the dielectric measurements we can identify the glass transition temperature T_g as a temperature at which the α-relaxation time, τ_α, is equaled 100 s. However, in many cases (e.g., to avoid considerable uncertainty as due to data extrapolation) T_g is defined as the temperature at which τ_α is equal to 10 s. We use the same procedure also in the present study. As a result of that we obtained $T_g = 253.6$ K. This value is slightly higher than that reported in the literature from the dielectric method. Such discrepancy comes from the difference in definition of T_g. The growth of the dielectric signal on the left side of the α-relaxation (see Figure 2a) is due to dc conductivity which reflects translational movements of the charged species present in the sample, e.g., small amount of the ionic impurities still present in the sample after synthesis.

Once the α-relaxation shifts out of the experimentally accessible frequency range, we enter the glassy state (see Figure 2b). In this temperature range, we have observed secondary relaxation, less intense, and much faster than the previously described α-relaxation. In agreement with Sailaja and co-workers,[23] we have labeled it as the γ-process. This relaxation involves local movements of only some part of the molecule (this could be possibly as due to molecular fluctuations of the methyl group[23]). For fenofibrate, the β-process origates most probably from the intermolecular motion (called Johari–Goldstein) and cannot be detected at atmospheric pressure as a separated peak neither above nor below the glass transition temperature. This is because its maximum is located too close to the α-peak. In consequence, it becomes submerged under the α-peak and appears only as a slight broadening of the high-frequency side of the α-relaxation. Nevertheless, we can still provide some signatures of its presence, e.g., by using the coupling model (CM).[53] CM predicts that the primitive relaxation time (τ_0) describing the one-body relaxation possess similar features as the relaxation involving internal degree of freedom (Johari–Goldstein β-relaxation[54]) which is connected to the cooperative many-body dynamics via the relation[53,55]

$$\tau_0 = t_c^{1-\beta_{KWW}} \tau_\alpha^{\beta_{KWW}}, \quad \tau_0 \cong \tau_{\beta\text{-JG}} \tag{1}$$

where $t_c = 2 \times 10^{-12}$ s for small molecular glass-formers and β_{KWW} is the stretching parameter from the Kohlrausch–Williams–Watts (KWW) function[56,57] that describes the width of the relaxation process. In Figure 2c, we present dielectric loss spectrum collected at 258 K together with the fits of the α-peak to the one-sided Fourier transform of the KWW function. For the α-relaxation time corresponding to this temperature (τ_α = 0.55 s) we obtain that the primitive frequency $f_{0\text{-JG}} \approx 782$ Hz is located in the halfway between the α- and γ- relaxations. On the basis of this result, we suppose that there should an additional relaxation covered by the prominent α-process. To detect the JG motions and distinguish them from the non-JG ones, we can use incresed pressure because relaxation process of inter- and intramolecular origin have different pressure sensitivity. We will demonstrate that in the further part of this paper.

Dielectric Relaxation Study at Elevated Pressure. To characterize the glassy dynamics of the investigated sample in $T-p$ space temperature and pressure dependent measurements were performed. We present the representative dielectric loss

DOI: 10.1021/acs.jpcb.6b08511
J. Phys. Chem. B 2016, 120, 11298–11306

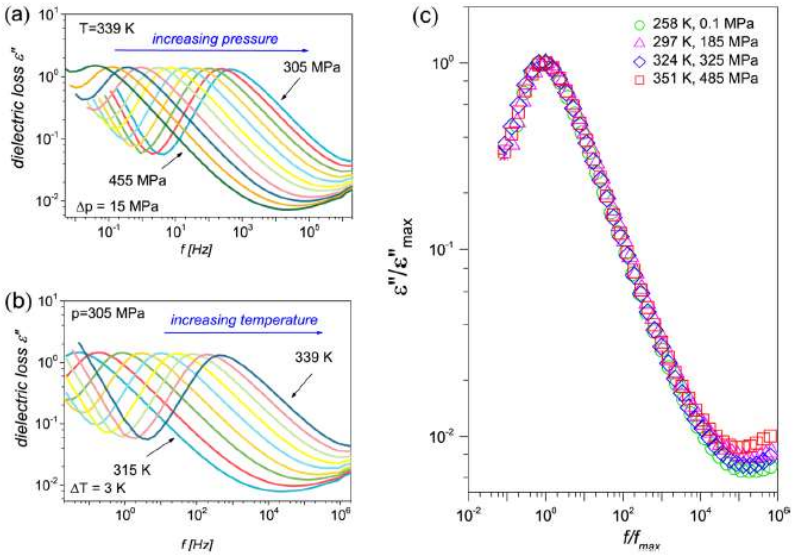

Figure 3. Representative dielectric loss spectra of fenofibrate collected under (a) isothermal conditions at 339 K in the pressure range from 305 to 455 MPa and (b) isobaric conditions at 305 MPa in the temperature range from 315 to 339 K. (c) Isochronal superposition of the dielectric loss spectra obtained for fenofibrate at different conditions (T, p). All chosen spectra have approximately the same time of the structural relaxation (τ_α) and were normalized to facilitate the comparison.

spectra collected during isothermal and isobaric measurements in Figure 3a,b. Both, increasing pressure and decreasing temperature shift the position of the α-peak to lower frequencies and slow down the relaxation dynamics. We have also noticed that the dc-conductivity contribution increases with pressure in the vicinity of the glass transition. This effect signifies decoupling between translational motions of charged species and reorientational movements of the molecules. We will study this effect in more details in the further part of this paper. In Figure 3c we show the superposition of the dielectric loss spectra measured at different combinations of (T, p) but with the same τ_α. For this purpose spectra collected at various conditions with the maximum of the α-peak located approximately at frequency f = 1 Hz were normalized. As can be seen, for a given (fixed) time scale, the shape of the α-process is invariant to temperature and pressure changes. So, fenofibrate as many other molecular glass-formers lacking strong intermolecular bonding confirms the isochronal superposition rule.

Except for the shape of the α peak describing the distribution of the characteristic relaxation time for molecular reorientation, its evolution with T and p is crucial to characterize the glassy behavior of the investigated sample. From the analysis of the dielectric relaxation spectra obtained at different thermodynamic conditions, we have determined the α-relaxation times. Figure 4 shows the evolution of α-relaxation time for fenofibrate in the T−p space. In the Supporting Information (see Figure S3) we have plotted separately isobaric and isothermal data. Since the α-relaxation time depends on both temperature and pressure, we have used Avramov equation to described experimentally obtained dependences for investigated material.[58,59]

$$\log \tau_\alpha = \log \tau_\infty + \log \frac{\tau_g}{\tau_\infty}\left(\frac{T_g(p_0)}{T}\right)^{\alpha}\left(1+\frac{p}{\Pi}\right)^{\beta} \quad (2)$$

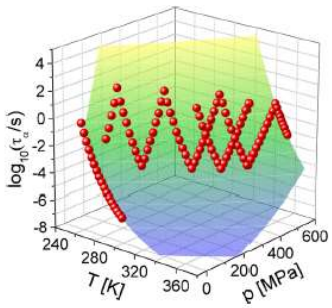

Figure 4. α-Relaxation time of fenofibrate plotted in the T−p space. The wire surface was obtained by fitting experimental data to the Avramov equation.

with parameter α defined as

$$\alpha = \alpha_0\left(1-\frac{C_p}{C_{p0}}\ln\left(1+\frac{p}{\Pi}\right)\right) \quad (3)$$

In eq 2, τ_∞ is time of the relaxation in extremely high temperature, τ_g is equilibrium time of glass transition, T_g is glass transition temperature obtained from measurements at ambient pressure (for fenofibrate we use 255 K), T is temperature, α is pressure depend fragility parameter, p is pressure, Π is fit parameter (the value of pressure at which the isothermal bulk modulus increases 2 times with respect to the reference value of the isothermal bulk modulus at ambient pressure), β is dimensionless fit parameter lineary dependent on the thermal expansion coefficient, α_0 is fragility parameter at ambient pressure, C_p is pressure depend heat capacity, and C_{p0} is heat capacity at ambient pressure. From the fitting we have obtained the following set of parameters: $\log \tau_\infty = -9.18 \pm 0.15$ log(s), $\Pi = 381 \pm 15$ MPa, $\beta = 2.6 \pm 0.1$, $C_p/C_{p0} = 0.05 \pm 0.01$, and α_0

DOI: 10.1021/acs.jpcb.6b08511
J. Phys. Chem. B 2016, 120, 11298−11306

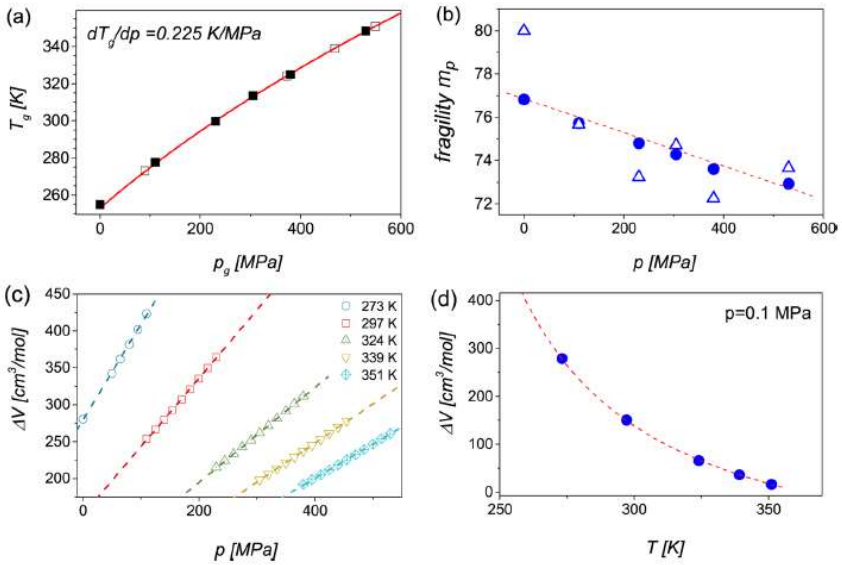

Figure 5. (a) Pressure dependence of the glass transition temperature (defined for τ_α = 10 s). The open and filled symbols come from isothermal and isobaric measurements, respectively. The solid line represents the fit of the experimental data to eq 4. (b) Pressure dependence of the isobaric fragility m_p (calculated assuming that $T_g = T$ at which τ_α = 10 s). Open symbols denote fragility values determined from τ_α dependencies described by using the VFT equation, while filled circles from the Avramov model. (c) Dependence of the activation volume ΔV plotted for isothermal data as a function of pressure. Dashed lines are linear fits. (d) Apparent activation volume for fenofibrate calculated at atmospheric pressure and different temperature conditions.

= 7.53 ± 0.17. We have made an assumption that τ_g = 1, which corresponds to the glass transition temperature T_g = 253.6 K at atmospheric pressure. As can be seen, the $\tau_\alpha(T,p)$ dependences form a two-dimensional surface that can be described quite well with the use of eq 2. In Figure S3, we show fitted curves separately for isobaric and isothermal data.

Having the τ_α dependence in $T-p$ space described by Avramov surface, we can use it to analyze some other relevant parameters related to the glassy dynamics of the investigated sample. Temperature (and pressure) at which τ_α = 10 s were taken from the fitted $\tau_\alpha(T,p)$ curves and used to determine T_g and p_g values. In Figure 5a we present obtained results. The increase of T_g (and glass transition pressure p_g) with increasing pressure (temperature) can be explained by recalling intermolecular motions. With increasing pressure molecules have less free space around each other. Moreover, the distances between molecules are smaller. In consequence, the intermolecular motions are hindered, and molecules must have higher energy to have that same mobility as the system at lower pressure.

To describe the nonlinear trend of the $T_g(p)$ dependence, we have employed an empirical equation proposed by Andersson and Andersson[60]

$$T_g = k_1\left(1 + \frac{k_2}{k_3}p_g\right)^{1/k_2} \tag{4}$$

where k_1, k_2, and k_3 are fitting parameters. Also, the ratio k_1/k_3 provides an estimate of the value of the pressure coefficient of the glass transition temperature (dT_g/dp) at zero pressure limit. This coefficient informs about the pressure sensitivity of the α-relaxation time—large values correspond to the higher sensitivity of the glassy dynamics to the pressure changes. For fenofibrate, we obtain 0.225 K/MPa, which is a rather typical value for molecular glass-formers, e.g., polyphenyl ether 0.220 K/MPa and *o*-terphenyl 0.260 K/MPa.[61] In contrast, for systems with strong hydrogen bonding interactions dT_g/dp is reported to be much lower, e.g., glycerol 0.040 K/MPa and benzyl alcohol 0.090 K/MPa.[61]

One of the most fundamental parameters describing the temperature dependence of the α-relaxation in various glass-forming liquids is Angell's fragility parameter[62,63]

$$m_p = \left.\frac{\partial \log(\tau_\alpha)}{\partial(T_g/T)}\right|_{p=\text{const},T=T_g} \tag{5}$$

Fragility informs about the deviation of the temperature dependency of the viscosity (or τ_α) from the Arrhenius behavior.[62] The value of isobaric fragility m_p classifies the glass-forming materials as "fragile" or "strong". For clarity, "strong" liquids have m_p values below 40 and are characterized by Arrhenius-like behavior, whereas "fragile" liquids show non-Arrhenius behavior and values of m_p that can reach at most 200. For fenofibrate at atmospheric pressure, we obtain m_p = 77, which confirms its fragile nature. Previous studies have reported slightly higher fragility value, $m_p \cong 94$.[23,24] Such difference arises from the fact that we have defined the glass transition temperature for much shorter relaxation time (10 s instead of 100 s) to avoid extrapolation of the fitted curves. From DSC measurements, the reported values of fragility for fenofibrate are m_p = 76[22] and m_p = 84.[64]

It is well-known that the fragility parameter depends on pressure. To probe this feature for the investigated sample, we have determined values of m_p for isobaric data and then plot them as a function of p. We have used $\tau_\alpha(T)$ dependences parametrized with the use of the Avramov equation (eq 1) but

DOI: 10.1021/acs.jpcb.6b08511
J. Phys. Chem. B 2016, 120, 11298−11306

also more widespread Vogel–Fulcher–Tamman (VFT) equation ($\tau_\alpha = \tau_0 \exp(DT_0/T - T_0)$).[65−67] As demonstrated in Figure 5b, m_p decreases with increasing pressure, which the most typical behavior reported for glass-forming liquids lacking strong intermolecular bonding. For associated liquids, compression breaks hydrogen bonding associates/networks leading to a dramatic change in the structural dynamics.[68] However, we wish to note that for the investigated sample changes in the fragility parameter with pressure are not very significant (m_p decreases by the value of 4−7 in the pressure range from 0.1 up to 530 MPa). For typical van der Waals liquids (but even also ionic liquids) the drop of the fragility parameter with compression is more pronounced (see for example refs 37−39 and 69). This could be an indication that the hydrogen bonds in fenofibrate might exert some noticeable effect on its glassy dynamics. We have drawn a similar conclusion recently for ketoprofen able to form only hydrogen-bonded dimers.[70]

Another very useful parameter extracted from isothermal measurements is activation volume, ΔV, defined as the difference between the volumes occupied by a molecule in activated and nonactivated states.[71] In practice, the volume of activation can be calculated using the equation[72]

$$\Delta V = RT\left(\frac{\partial \ln \tau_\alpha}{\partial p}\right)_T \tag{6}$$

where R is gas constant. Obtained results for each isotherm are plotted versus pressure as shown in Figure 5c. As can be seen, at fixed temperature the volume of activation increases with increasing pressure. In analogy, it increases with lowering the temperature of constant pressure. Using parametrized by the Avramov equation τ_α dependencies we have also calculated the temperature evolution of ΔV in the limit of the atmospheric pressure. Figure 5d presents obtained results. The activation volume is expected to increase significantly with lowering the temperature from T_m to T_g. This behavior of ΔV is considered as a characteristic feature of the molecular dynamics of the supercooled liquids and linked with increasing cooperativity between molecules in the vicinity of the glass transition.[73]

Next, we wish to consider the relationship between dielectric α-relaxation times and dc-conductivity as described by the Debye–Stokes–Einstein equation

$$\frac{\sigma_{DC}\tau_\alpha T}{c} = \text{constant} \tag{7}$$

where σ_{DC} is conductivity and c is a concentration of charges which we assume to change only slightly with the temperature. Values of τ_α and σ_{DC} can be obtained simultaneously by fitting the dielectric permittivity data to the Havriliak–Negami function[74] with an additional conductivity term $\sigma_{DC}/\omega\epsilon_0$ (where ϵ_0 is the dielectric permittivity of the vacuum). To test the validity of DSE law for fenofibrate, we plot in double logarithmic scale values of σ_{DC} versus τ_α, as presented in Figure 6a. The linear trend with the slope equaled to 0.99 indicates that translational movements of charges and reorientational movements of molecules couple (i.e., their temperature dependences follow each other) at atmospheric pressure. However, on increased pressure, the relationship between both quantities starts to deviate from the DSE equation systematically. The signature of that provides a change in the slope of the $\sigma_{DC}(\tau_\alpha)$ dependence (see the inset in Figure 6a). Therefore, on increased pressure, the temperature evolution of α-relaxation time changes much faster than the dc conductivity.

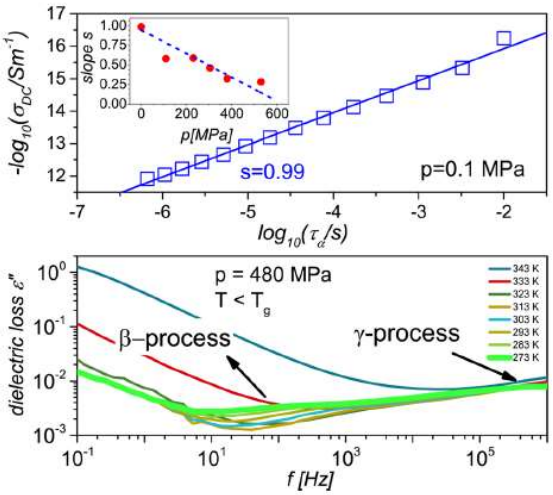

Figure 6. (a) Plot of dc conductivity versus α-relaxation time on the log–log scale. The solid line is linear fit to the data. The inset shows the evolution of the fractional exponent with increasing pressure while the dashed line indicates the trend line. (b) Dielectric loss spectra of fenofibrate obtained at pressure 480 MPa and cooling from 343 to 273 K. The secondary relaxations observed below the glass transition temperature were described with the use of Havriliak–Negami function with the following values of the fitting parameters (at 480 MPa and 273 K): $\alpha_{HN} = 0.7$, $\beta_{HN} = 0.5$, $\tau_{HN} = 0.0025$, $\Delta\epsilon = 0.007$ for β-relaxation and $\alpha_{HN} = 0.3$, $\beta_{HN} = 1$, $\tau_{HN} = 9 \times 10^{-8}$, $\Delta\epsilon = 0.064$ for γ-relaxation. The α-relaxation tail was fitted with the power law 0.55.

In such case the relationship between σ_{DC} and τ_α follows fractional Debye–Stokes–Einstein (fDSE)[75] relation

$$\sigma_{DC}\tau_\alpha{}^s = \text{constant} \tag{8}$$

where s is a fractional exponent equal to 1 or less (for 1 it takes the form of DSE equation). For fenofibrate, we observe a quite remarkable decrease of the fractional exponent from 0.99 at atmospheric pressure to 0.3 at 530 MPa. Such behavior of σ_{DC} with increasing pressure might originate from the microviscosity and its relation to the difference of size of the species probing different types of motions. In such crowded environment as the supercooled liquid state near the glass transition, this can have a strong impact on slowing the various movements to varying extent. We cannot also exclude the effect of proton translocation along the hydrogen bonds. However, this hypothesis needs some further verification in the future.

Finally, we have also made use of the high-pressure dielectric measurements to identify the presence of the β-relaxation in the glassy state of fenofibrate. In the previous part of this paper, we have applied CM to find a possible location of the hidden JG β-process (Figure 2c). This relaxation process is expected to be not only temperature but also pressure sensitive which can be used to separate it from some other secondary modes. In Figure 6b we show isobaric data collected in the glassy state of fenofibrate at 480 MPa and temperature range from 343 to 273 K. As can be seen, with decreasing the temperature an additional relaxation peak emerges between α- and γ- peaks. This additional process becomes more separated from the γ-relaxation when lowering the temperature. By analyzing the temperature dependence of its relaxation time (please see

DOI: 10.1021/acs.jpcb.6b08511
J. Phys. Chem. B 2016, 120, 11298−11306

Figure S4) with the use of Arrhenius equation ($\tau = \tau_0 \exp(E_a/RT)$[76]), we obtain activation energy $E_\beta = 77.0 \pm 7.0$ kJ/mol. This value is more than two times higher than E_a for the γ-process ($E_\gamma = 28.2 \pm 0.5$ kJ/mol). The obtained energy of activation of γ-process corresponds to the value reported in the literature, 32.67 kJ/mol.[23] However, during high-pressure experiments, the γ-process turned out to practically pressure insensitive. In contrast to the β-relaxation, this implies pressure independence of its activation energy. We present the corresponding temperature dependences of both secondary relaxation times in the Supporting Information (Figure S4).

CONCLUSIONS

Fenofibrate is a modeled pharmaceutical glass-former revealing quite complex inter- and intramolecular hydrogen bonding capabilities. We have confirmed that by performing IR studies (please see Supporting Information for results). To probe its glassy dynamics (and verify if it is affected by the presence of the hydrogen bonds), we have performed dielectric relaxation studies at ambient and elevated pressure. The results obtained at atmospheric pressure were found to be in good agreement with the previous reports. As this is not enough to get a complete understanding of the glassy phenomenon in the phase space, the high-pressure dielectric relaxation studies have also been carried out. On the basis of obtained results, we have demonstrated that the α-relaxation dynamics of fenofibrate is quite sensitive to pressure changes ($dT_g/dp = 0.225$ K/MPa) and that the distribution of the α-relaxation time remains constant for a given isochrone. These are the common features reported for molecular van der Waals liquids. It is, however, surprising that the drop in the isobaric fragility in the pressure range from 0.1 up to 530 MPa is very subtle. This is not the typical behavior reported for van der Waals liquids for which we usually observe more noticeable changes. Therefore, possibly, the presence of the hydrogen bonds is still able to exert some effect on the glassy dynamics of fenofibrate. Apart from that we have also demonstrated that on increased pressure the decoupling between translational movements of charged species present in the sample, and the α-relaxation dynamics takes place. This effect can be due to microviscosity and its relation to the difference of size of the species probing different types of motion. The other possible scenario is related to changes in the proton transport along the hydrogen bonds. However, this hypothesis needs to be validated in the further. Lastly, we show that by applying pressure it was possible to distinguish the secondary relaxations of the different molecular origin.

ASSOCIATED CONTENT

Supporting Information

The Supporting Information is available free of charge on the ACS Publications website at DOI: 10.1021/acs.jpcb.6b08511

IR studies on the dynamics of the hydrogen bonds and additional dielectric results (PDF)

AUTHOR INFORMATION

Corresponding Author

*E-mail kadrjano@us.edu.pl; tel +48 32 349 75 70 (K.A.).

Notes

The authors declare no competing financial interest.

ACKNOWLEDGMENTS

Authors are grateful for the financial support from the National Science Centre within the framework of the Opus project (Grant DEC 2014/15/B/ST3/00364).

REFERENCES

(1) Vogt, M.; Kunath, K.; Dressman, J. B. Dissolution Enhancement of Fenofibrate by Micronization, Cogrinding and Spray-Drying: Comparison with Commercial Preparations. *Eur. J. Pharm. Biopharm.* **2008**, *68*, 283−288.

(2) Adkins, J. C.; Faulds, D. Micronised Fenofibrate. *Drugs* **1997**, *54*, 615−633.

(3) Hu, L.; Wu, H.; Niu, F.; Yan, C.; Yang, X.; Jia, Y. Design of Fenofibrate Microemulsion for Improved Bioavailability. *Int. J. Pharm.* **2011**, *420*, 251−255.

(4) Babu, A. M.; Rao, B.; Sudhakar, P. Development and Characterization of Novel Selfmicroemulsion Drug Delivery of Low Solubility Drug Fenofibrate for Improved Oral Bioavailability. *Int. J. Biol. Pharm. Res.* **2012**, *3*, 616−623.

(5) Kawakami, K.; Zhang, S.; Chauhan, R. S.; Ishizuka, N.; Yamamoto, M.; Masaoka, Y.; Kataoka, M.; Yamashita, S.; Sakuma, S. Preparation of Fenofibrate Solid Dispersion Using Electrospray Deposition and Improvement in Oral Absorption by Instantaneous Post-Heating of the Formulation. *Int. J. Pharm.* **2013**, *450*, 123−128.

(6) Zhang, M.; Li, H.; Lang, B.; O'Donnell, K.; Zhang, H.; Wang, Z.; Dong, Y.; Wu, C.; Williams, R. O. Formulation and Delivery of Improved Amorphous Fenofibrate solid Dispersions Prepared by Thin Film Freezing. *Eur. J. Pharm. Biopharm.* **2012**, *82*, 534−544.

(7) He, H.; Yang, R.; Tang, X. In Vitro and In Vivo Evaluation of Fenofibrate. *Drug Dev. Ind. Pharm.* **2010**, *36*, 681−687.

(8) Yousaf, A. M.; Kim, D. W.; Kim, J. K.; Kim, J. O.; Yong, C. S.; Choi, H.-G. Novel Fenofibrate-Loaded Gelatin Microcapsules with Enhanced Solubility and Excellent Flowability: Preparation and Physicochemical Characterization. *Powder Technol.* **2015**, *275*, 257−262.

(9) Niu, X.; Wan, L.; Hou, Z.; Wang, T.; Sun, C.; Sun, J.; Zhao, P.; Jiang, T.; Wang, S. Mesoporous Carbon as a Novel Drug Carrier of Fenofibrate for Enhancement of the Dissolution and oral Bioavailability. *Int. J. Pharm.* **2013**, *452*, 382−389.

(10) Zuo, B.; Sun, Y.; Li, H.; Liu, X.; Zhai, Y.; Sun, J.; He, Z. Preparation and In Vitro/In Vivo Evaluation of Fenofibrate Nanocrystals. *Int. J. Pharm.* **2013**, *455*, 267−275.

(11) Amidon, G. L.; Lennernas, H.; Shah, V. P.; Crison, J. R. A Theoretical Basis for a Biopharmaceutic Drug Classification: The Correlation of in Vitro Drug Product Dissolution and in Vivo Bioavailability. *Pharm. Res.* **1995**, *12*, 413−420.

(12) Hancock, B. C.; Zografi, G. Characteristics and Significance of the Amorphous Pharmaceutical Systems. *J. Pharm. Sci.* **1997**, *86*, 1−12.

(13) Hancock, B. C.; Parks, M. What is the True Solubility Advantage for Amorphous Pharmaceuticals? *Pharm. Res.* **2000**, *17*, 397−404.

(14) Babu, N. J.; Nangia, A. Solubility Advantage of Amorphous Drug and Pharmaceutical Cocrystals. *Cryst. Growth Des.* **2011**, *11*, 2662−2679.

(15) Murdande, S.; Pikal, M.; Shanker, R.; Bogner, R. Solubility Advantage of Amorphous Pharmaceuticals: I A Thermodynamic Analysis. *J. Pharm. Sci.* **2010**, *99*, 1254−1264.

(16) Murdande, S.; Pikal, M.; Shanker, R.; Bogner, R. Solubility Advantage of Amorphous Pharmaceuticals: II Application of Quantitative Thermodynamic Relationship for Prediction of Solubility Enhancement in Structurally Diverse Insoluble Pharmaceuticals. *Pharm. Res.* **2010**, *27*, 2704−2714.

(17) Grzybowska, K.; Paluch, M.; Grzybowski, A.; Wojnarowska, Z.; Hawelek, L.; Kolodziejczyk, K.; Ngai, K. L. Molecular Dynamics and Physical Stability of Amorphous Anti-Inflammatory Drug: Celecoxib. *J. Phys. Chem. B* **2010**, *114*, 12792−12801.

(18) Adrjanowicz, K.; Wojnarowska, Z.; Grzybowska, K.; Hawelek, L.; Kaminski, K.; Paluch, M.; Kasprzycka, A.; Walczak, K. Molecular

Dynamics and Crystallization Phenomenon of Supercooled and Glassy DNA and RNA Nucleosides:β-adenosine, β-thymidine and β-uridine. *Phys. Rev. E* **2011**, *84*, 051507.
(19) Knapik, J.; Wojnarowska, Z.; Grzybowska, K.; Hawelek, L.; Sawicki, W.; Wlodarski, K.; Markowski, J.; Paluch, M. Physical Stability of the Amorphous Anticholesterol Agent (Ezetimibe): The Role of Molecular Mobility. *Mol. Pharmaceutics* **2014**, *11*, 4280−4290.
(20) Adrjanowicz, K.; Paluch, M.; Kaminski, K.; Hawelek, L.; Grzybowska, K.; Zakowiecki, D. Comprehensive Studies on Physical and Chemical Stability in Liquid and Glassy States of Telmisartan (TEL): Solubility Advantages given by Cryomilled and Quenched Material. *Philos. Mag.* **2011**, *91*, 1926−1948.
(21) Martino, D.; Palmieri, P.; Martelli, G. Evidence of a Metastable Form of Fenofibrate. *Chem. Pharm. Bull.* **2000**, *55*, 625−626.
(22) Baird, J. A.; Van Eerdenbrugh, B.; Taylor, L. S. A Classification System to Assess the Crystallization Tendency of Organic Molecules from Undercooled Melts. *J. Pharm. Sci.* **2010**, *99*, 3787−3806.
(23) Sailaja, U.; Thayyil, M. S.; Kumar, N. K.; Govindaraj, G. Molecular Dynamics of Amorphous Pharmaceutical Fenofibrate Studied by Broadband Dielectric Spectroscopy. *J. Pharm. Anal.* **2016**, *6*, 165−170.
(24) Tu, W.; Li, X.; Chen, Z.; Liu, Y. D.; Labardi, M.; Capaccioli, S.; Paluch, M.; Wang, L.-M. Glass Formability in Medium-Sized Molecular Systems/Pharmaceuticals. I. Thermodynamics vs. Kinetics. *J. Chem. Phys.* **2016**, *144*, 174502.
(25) Bhugra, C.; Pikal, M. J. Role of Thermodynamic, Molecular, and Kinetic Factors in Crystallization from the Amorphous State. *J. Pharm. Sci.* **2008**, *97*, 1329−1349.
(26) Zhou, D.; Zhang, G. G. Z.; law, D.; Grant, D. J. W.; Schmitt, E. A. Physical Stability of Amorphous Pharmaceuticals: Importance of Configurational Thermodynamic Quantities and Molecular Mobility. *J. Pharm. Sci.* **2002**, *91*, 1863−1872.
(27) Bhardwaj, S. P.; Arora, K. K.; Kwong, E.; Templeton, A.; Clas, S.-D. Correlation Between Molecular Mobility and Physical Stability of Amorphous Itraconazole. *Mol. Pharmaceutics* **2013**, *10*, 694−700.
(28) Bhardwaj, S. P.; Suryanarayanan, R. Molecular Mobility as an Effective Predictor of the Physical Stability of Amorphous Trehalose. *Mol. Pharmaceutics* **2012**, *9*, 3209−3217.
(29) Adrjanowicz, K.; Wojnarowska, Z.; Wlodarczyk, P.; Kaminski, K.; Paluch, M.; Mazgalski, J. Molecular Mobility in Liquid and Glassy States of Telmisartan (TEL) Studied by Broadband Dielectric Spectroscopy. *Eur. J. Pharm. Sci.* **2009**, *38*, 395.
(30) Descamps, M.; Dudognon, E. Crystallization from the Amorphous State: Nucleation-Growth Decoupling, Polymorphism Interplay, and the Role of Interfaces. *J. Pharm. Sci.* **2014**, *103*, 2615−2628.
(31) Kremer, F.; Schönhals, A. *Broadband Dielectric Spectroscopy*; Springer-Verlag: Berlin, 2003.
(32) Descamps, M., Ed. *Disordered Pharmaceutical Materials*; Wiley-VCH Verlag GmbH & Co.: Weinheim, Germany, 2016.
(33) Anderson, P. W. Through the Glass Lightly. *Science* **1995**, *267*, 1615−1616.
(34) Debenedetti, P.; Stillinger, F. Supercooled Liquids and the Glass Transition. *Nature* **2001**, *410*, 259−267.
(35) Sokolov, A. P. Why the Glass Transition is Still Interesting. *Science* **1996**, *273*, 1675.
(36) Chang, K. The New York Times, July 29, 2008; http://www:nytimes:com/2008/07/29/science/29glass:html?r/1&8dpc.
(37) Wojnarowska, Z.; Adrjanowicz, K.; Wlodarczyk, P.; Kaminska, E.; Grzybowska, K. K.; Wrzalik, K.; Paluch, R.; Ngai, M. K. L. Broadband Dielectric Relaxation Study at Ambient and Elevated Pressure of Molecular Dynamics of Pharmaceutical: Indomethacin. *J. Phys. Chem. B* **2009**, *113*, 12536−12545.
(38) Adrjanowicz, K.; Kaminski, K.; Wojnarowska, Z.; Dulski, M.; Hawelek, L.; Pawlus, S.; Paluch, M. Dielectric Relaxation and Crystallization Kinetics of Ibuprofen at Ambient and Elevated Pressure. *J. Phys. Chem. B* **2010**, *114*, 6579−6593.
(39) Wojnarowska, Z.; Paluch, M.; Grzybowski, A.; Adrjanowicz, K.; Grzybowska, K.; Kaminski, K.; Wlodarczyk, P.; Pionteck, J. Study of Molecular Dynamics of Pharmaceutically Important Protic Ionic Liquid Verapamil Hydrochloride. I. Test of Thermodynamic Scaling. *J. Chem. Phys.* **2009**, *131*, 104505.
(40) Roland, C. M.; Hensel-Bielowka, S.; Paluch, M.; Casalini, R. Supercooled Dynamics of Glass-Forming Liquids and Polymers under Hydrostatic Pressure. *Rep. Prog. Phys.* **2005**, *68*, 1405.
(41) Floudas, G., Paluch, M., Grzybowski, A., Ngai, K., Eds.; *Molecular Dynamics of Glass-Forming Systems: Effects of Pressure*; Springer-Verlag: Berlin, 2011.
(42) Casalini, R.; Roland, C. M. Excess Wing in the Dielectric Loss Spectra of Propylene Glycol Oligomers at Elevated Pressure. *Phys. Rev. B: Condens. Matter Mater. Phys.* **2004**, *69*, 094202.
(43) Grzybowska, K.; Pawlus, S.; Mierzwa, M.; Paluch, M.; Ngai, K. L. Changes of Relaxation Dynamics of a Hydrogen-Bonded Glass Former after Removal of the Hydrogen Bonds. *J. Chem. Phys.* **2006**, *125*, 144507.
(44) Wojnarowska, Z.; Roland, C. M.; Swiety-Pospiech, A.; Grzybowska, K.; Paluch, M. Anomalous Electrical Conductivity Behavior at Elevated Pressure in the Protic Ionic Liquid Procainamide Hydrochloride. *Phys. Rev. Lett.* **2012**, *108*, 015701.
(45) Ngai, K. L.; Paluch, M. Classification of Secondary Relaxation in Glass-Formers Based on Dynamic Properties. *J. Chem. Phys.* **2004**, *120*, 857−873.
(46) Ngai, K. L. *Relaxation and Diffusion in Complex Systems*; Springer: 2012.
(47) Tipduangta, P.; Takieddin, K.; Fábián, L.; Belton, P.; Qi, S. A New Low Melting-Point Polymorph of Fenfibrate Prepared via Talc Induced Heterogeneous Nucleation. *Cryst. Growth Des.* **2015**, *15*, 5011−5020.
(48) Heinz, A.; Gordon, K. C.; McGoverin, C. M.; Rades, T.; Strachan, C. J. Understanding the Solid-State Forms of Fenofibrate - A Spectroscopic and Computational Study. *Eur. J. Pharm. Biopharm.* **2009**, *71*, 100−108.
(49) Desiraju, G. R. The C-H−O Hydrogen Bond: Structural Implications and Supramolecular Design. *Acc. Chem. Res.* **1991**, *24*, 290−296.
(50) Koch, U.; Popelier, P. L. A. Characterization of C-H-0 Hydrogen Bonds on the Basis of the Charge Density. *J. Phys. Chem.* **1995**, *99*, 9747−9754.
(51) Roland, C. M.; Casalini, R.; Bergman, R.; Mattsson, J. Role of Hydrogen Bonds in the Supercooled Dynamics of Glass-Forming Liquids at High Pressures. *Phys. Rev. B: Condens. Matter Mater. Phys.* **2008**, *77*, 012201.
(52) Pawlus, S.; Paluch, M.; Dzida, M. Molecular Dynamics Changes Induced by Hydrostatic Pressure in a Supercooled Primary Alcohol. *J. Phys. Chem. Lett.* **2010**, *1*, 3249−3253.
(53) Ngai, K. L.; Paluch, M. Classification of Secondary Relaxation in Glass-Formers Based on Dynamic Properties. *J. Chem. Phys.* **2004**, *120*, 857−873.
(54) Johari, G. P.; Goldstein, M. Viscous Liquids and the Glass Transition. II. Secondary Relaxations in Glasses of Rigid Molecules. *J. Chem. Phys.* **1970**, *53*, 2372−2388.
(55) Ngai, K. L.; Rendell, R. W. In *Supercooled Liquids, Advances and Novel Applications*; ACS Symposium Series Vol. 676; Fourkas, J. T., Kivelson, D., Mohanty, U., Nelson, K., Eds.; American Chemical Society: Washington, DC, 1997; Chapter 4.
(56) Kohlrausch, R. Theorie des elektrischen Rückstandes in der Leidner Flasche. *Ann. Phys.* **1854**, *167*, 56−82.
(57) Williams, G.; Watts, D. C. Non-Symmetrical Dielectric Relaxation Behaviour Arising from a Simple Empirical Decay Function. *Trans. Faraday Soc.* **1970**, *66*, 80−85.
(58) Avramov, I. Pressure Dependence of Viscosity of Glassforming Melts. *J. Non-Cryst. Solids* **2000**, *262*, 258−263.
(59) Avramov, I.; Grzybowski, A.; Paluch, M. A New Approach to Description of the Pressure Dependence of Viscosity. *J. Non-Cryst. Solids* **2009**, *355*, 733−736.
(60) Andersson, S. P.; Andersson, O. Relaxation Studies of Poly(propylene glycol) under High Pressure. *Macromolecules* **1998**, *31*, 2999−3006.

DOI: 10.1021/acs.jpcb.6b08511
J. Phys. Chem. B 2016, 120, 11298−11306

(61) Atake, T.; Angell, C. A. Pressure Dependence of the Glass Transition Temperature in Molecular Liquids and Plastic Crystals. *J. Phys. Chem.* **1979**, *83*, 3218−3223.
(62) Angell, C. A. Formation of Glasses from Liquids and Biopolymers. *Science* **1995**, *267*, 1924−1935.
(63) Richert, R.; Angell, C. A. Dynamics of Glass-Forming Liquids. V. On the link Between Molecular Dynamics and Configurational Entropy. *J. Chem. Phys.* **1998**, *108*, 9016−9026.
(64) Zhou, D.; Zhang, G. G. Z.; Law, D.; Grant, D. J. W.; Schmitt, E. A. Physical Stability of Amorphous Pharmaceuticals: Importance of Configurational Thermodynamic Quantities and Molecular Mobility. *J. Pharm. Sci.* **2002**, *91*, 1863−1872.
(65) Vogel, H. J. Das Temperaturabhangigkeitgesetz der Viskosität. von Flüssigkeiten. *Phys. Z.* **1921**, *22*, 645−646.
(66) Tammann, G.; Hesse, W. Die Abhängigkeit der Viscosität von der Temperatur bie unterkühlten Flüssigkeiten. *Zeitschrift für anorganische und allgemeine Chemie* **1926**, *156*, 245−257.
(67) Fulcher, G. S. Analysis of Recent Measurements of the Viscosity of Glasses. *J. Am. Ceram. Soc.* **1925**, *8*, 339−355.
(68) Paluch, M.; Casalini, R.; Hensel-Bielowka, S.; Roland, C. M. Effect of Pressure on the Alpha Relaxation in Glycerol and Xylitol. *J. Chem. Phys.* **2002**, *116*, 9839.
(69) Paluch, M.; Masiewicz, E.; Pawlus, A. G. S.; Pionteck, J.; Wojnarowska, Z. General Rules Prospected for the Liquid Fragility in Various Material Groups and Different Thermodynamic Conditions. *J. Chem. Phys.* **2014**, *141*, 134507.
(70) Adrjanowicz, K.; Kaminski, K.; Tarnacka, M.; Szutkowski, K.; Popenda, L.; Bartkowiak, G.; Paluch, M. The Effect of Hydrogen Bonding Propensity and Enantiomeric Composition on the Dynamics of Supercooled Ketoprofen - Dielectric, Rheological and NMR studies. *Phys. Chem. Chem. Phys.* **2016**, *18*, 10585−93.
(71) Glasstone, S.; Laidler, K. J.; Eyring, H. *Theory of Rate Processes*; McGraw-Hill Book Co.: 1941.
(72) Leyser, H.; Schulte, A.; Doster, W.; Petry, W. High-Pressure Specific-Heat Spectroscopy at the Glass Transition in O-terphenyl. *Phys. Rev. E: Stat. Phys., Plasmas, Fluids, Relat. Interdiscip. Top.* **1995**, *51*, 5899−5904.
(73) Hong, L.; Gujrati, P. D.; Novikov, V. N.; Sokolov, A. P. Molecular Cooperativity in the Dynamics of Glass-forming Systems: A New Insight. *J. Chem. Phys.* **2009**, *131*, 194511.
(74) Havriliak, S.; Negami, S. A Complex Plane Analysis of Alpha-Dispersions in Some Polymer Systems. *J. Polym. Sci., Part C: Polym. Symp.* **1966**, *14*, 99−117.
(75) Bielowka, S. H.; Psurek, T.; Ziolo, J.; Paluch, M. Test of the Fractional Debye-Stokes-Einstein Equation in Low-Molecular-Weight Glass-Forming Liquids under Condition of High Compression. *Phys. Rev. E: Stat. Phys., Plasmas, Fluids, Relat. Interdiscip. Top.* **2001**, *63*, 9489−9494.
(76) Arrhenius, S. Über die Dissociationswärme und den Einfluss der Temperatur auf den Dissociationsgrad der Elektrolyte. *Z. Phys. Chem.* **1889**, *IV*, 96−116.

DOI: 10.1021/acs.jpcb.6b08511
J. Phys. Chem. B 2016, 120, 11298−11306

Supporting Information

Dielectric Relaxation Study at Ambient and Elevated Pressure of the Modeled Lipophylic Drug: Fenofibrate

Grzegorz Szklarz,[†,‡] Karolina Adrjanowicz,[*,†,‡] Mateusz Dulski,[¶,‡] Justyna Knapik,[†,‡] and Marian Paluch[†,‡]

†*Institute of Physics, University of Silesia, ulica Uniwersytecka 4, 40-007 Katowice, Poland*

‡*Silesian Center for Education and Interdisciplinary Research, ulica 75 Pulku Piechoty 1a, 41-500 Chorzow, Poland*

¶*Institute of Material Science, Univeristy of Silesia, ulica 75 Pulku Piechoty 1a, 41-500 Chorzow, Poland*

E-mail: kadrjano@us.edu.pl

Infrared spectroscopy

Method

Infrared measurements were performed using an Agilent Cary 640 FTIR spectrometer equipped with a standard source and a DTGS Peltier-cooled detector. The spectra have been collected using GladiATR diamond accessory (Pike Technologies) in the 4000-400 cm^{-1} range. All spectra were accumulated with a spectral resolution of 4 cm^{-1} and recorded by accumulating of 16 scans. The dynamic measurements were performed in the temperature range from 298 K to 373 K both during heating and cooling with temperature ratio 5 K/min and stabilization $\pm$0.5 K. Finally; baseline correction was done as well as water vapor and carbon dioxide were subtracted from each spectrum.

Results

Infrared study of the dynamics of the hydrogen bonds

Motivated by the fact that the presence of the hydrogen bonds might have a significant impact on the relaxation dynamics in the vicinity of the glass transition, we have performed FTIR measurements. Here, our aim is to get better insight into the molecular structure of the investigated sample and its impact on the H-bonding pattern. IR studies have been carried out on the structural data reported for fenofibrate.[1] The inter- and intramolecular H-bonding scheme obtained based on single crystal X-ray diffraction data is presented in Figure S1. Changes in the inter- and intramolecular H–bond patterns and their influence on the molecular conformation have been analyzed by the dynamic measurements during sample annealing and cooling (298 K$\rightarrow$ 373 K$\rightarrow$ 298 K). As a result, the temperature-dependent infrared spectra visualized in the 3600-1000 cm^{-1}region we summarize in Figure S2a whereas the magnified data presented in Figure S2b give a closer look at the molecular dynamic of ketone and ester bands near the melting point in the 1800-1600 cm^{-1} region.

The vibrational frequencies in the regions between 3600-3200 and 1800-1600 cm^{-1} are

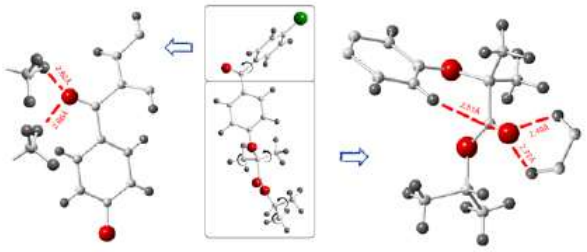

Figure S1: Inter- and intramolecular H-bonding scheme obtained based on the single crystal X-ray diffraction data. CrystalMaker 2.4.1 software visualized the structure. Black arrows indicate possible rotational movements of the molecular fragments at the melting temperature.

typical for the OH stretching vibrations with hydrogen bonds nature typically exhibited as a multiplicity of weak–to–moderate as well as to stretching vibration of ν(C=O) within e.g. ester and ketone groups, respectively. Spectral range between 3200-2800 cm^{-1} results from stretching vibration of CH_3 and CH groups/moieties (see Fig. S2a).[2–6] Thus, the molecular arrangement in the crystalline structure of fenofibrate provides an existence of intramolecular $d_{CH\cdots O}$ bond distance close 2.81 Å at the C–H$\cdots$O angle is equaled to 145^o occurred between an aromatic hydrogen atom and the carbonyl oxygen of the ester. Additionally, one can find intermolecular C–H$\cdots$O interactions occurred between hydrogen atoms from aromatic rings and the ester carbonyl group where $d_{CH\cdots O}$ distances are equaled to 2.49 and 2.77 Å at the C–H$\cdots$O angles close to 128^o and 172^o, respectively. Intermolecular bond interactions between isopropyl methyl groups and ketone carbonyl oxygen atoms imply on the formation of $d_{CH\cdots O}$ distances equaled to 2.66 and 2.82 Å at the C–H$\cdots$O angles close 145^o and 156^o. As a result, fenofibrate molecules form 3D layered molecular system combined by inter- and intramolecular H-bond network which according to Tipduangta et al. characterizes Form III, one of fenofibrate polymorph.[7] Additionally, those data determine band position on infrared spectrum located at 3451 and 3244 cm^{-1} result from weak and moderate H–bond (see Fig. S1).[5] The H–bonding pattern influence the position of bands ascribed to the stretching vibration of the carbonyl group in ketone and ester moieties, located, respectively

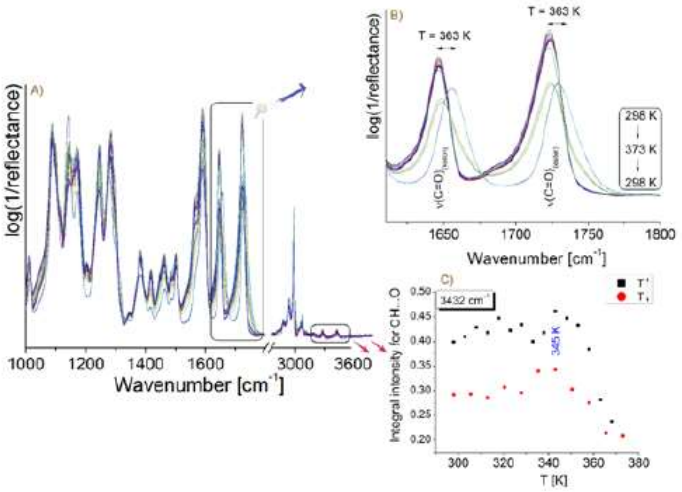

Figure S2: (a) Temperature-dependent infrared spectra in the 3600-1000 cm^{-1} range measured for fenofibrate during heating and cooling runs from 298 K up to 373 K. (b) The magnified temperature-dependent infrared spectra in the 1800-1600 cm^{-1} range with an indication of the vibration of υ(C=O)ketone and υ(C=O)ester. (c) The dynamic of the integral intensity of bands ascribed to the medium hydrogen bonding (3600-3200 cm^{-1}). The kink in H-bond signal accompanies a sample melting.

at 1645 and 1723 cm^{-1} (see Fig. S2B). Temperature-dependent infrared measurements revealed blue-shift band associated with C=O vibration due to disruption of H–molecular bond arrangement influencing a greater molecular mobility as a result of sample melting (T = 353 K). Interestingly, one can observe a greater band shift about six cm^{-1} of ketone band (1645→ 1655 cm^{-1}) on the infrared ester features (1723→ 1729 cm^{-1}). A higher blue-shift band within ketone moieties indicates lower stability of this molecular fragment and greater freedom of rotational movement in case of isopropyl methyl groups at melting temperature (see black arrows in Figure S1).

To follow changes in the populations of hydrogen bonds with the temperature, we have also performed an integrated intensity analysis. We presented the results in Figure S2c. Constant values of the integrated intensity are observed only up to 345 K. Above that temperature we note a gradual decrease of the infrared signal. This effect comes from the weakening of the binding strength and decreasing the number of H-bonds in the system.

Infrared data have also revealed broadening of that bands at T = 363 K suggesting an increase of H–bond distribution with different $d_{CH\cdots O}$ bond distances (see Fig. S2). Those data are also in good agreement with the analysis of carbonyl bands position, mentioned before (see Fig. S2B). It is worth to note that during the slow cooling of the system it is observed a gradual bands shift to their original position (see band position of H-bond in Fig S2A or $\upsilon(\mathrm{C{=}O})_{ketone}$ and $\upsilon(\mathrm{C{=}O})_{ester}$ in Fig. S2B). This indicates molecular ordering and rebuilding of the H-bond network, typical for Form I. However; the integration analysis revealed 25 % reduction of the number of H-bond on the sample before thermal treatment. This effect suggests some slight differences in the molecular arrangement (and/or small changes in the conformation of fenofibrate molecules in the 3D network) for recrystallized sample.

Dielectric spectroscopy

Dielectric relaxation study at elevated pressure - Supporting figures

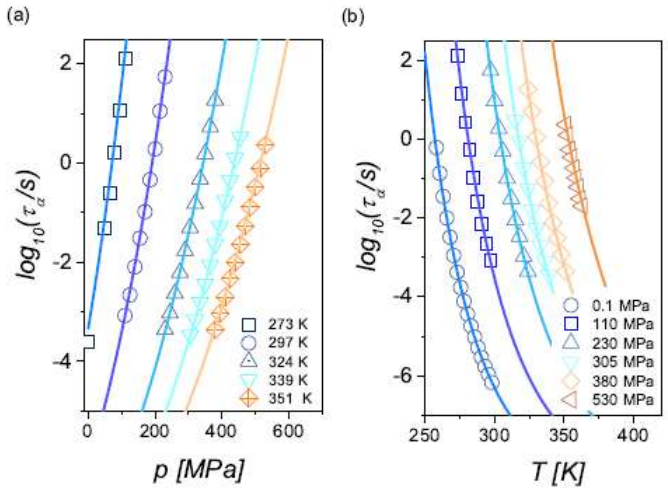

Figure S3: The α-relaxation time of fenofibrate plotted versus (a) pressure and (b) temperature at labelled T (or p) conditions. Solid lines denote fits of the experimental data to the Avramov equation.

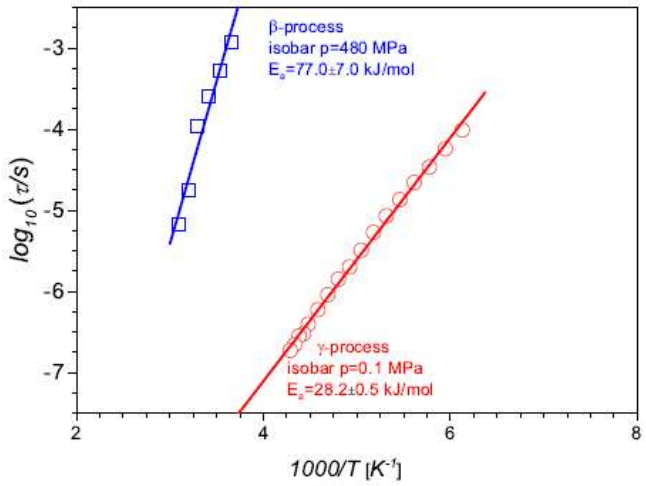

Figure S4: The temperature dependences of the β-relaxation time at 480 MPa and γ-relaxation time at 0.1 MPa. Solid lines represent the fit of the data to Arrhenius equation.

References

(1) Henry, R. F.; Zhang, G. Z.; Gao, Y.; Buckner, I. S. Fenofibrate. *Acta Crystallographica Section E* **2003**, *59*, 699–700.

(2) Hadzi, D. *Theoretical Treatments of Hydrogen Bonding*; Wiley, 1997.

(3) Jeffrey, G. A. *An Introduction to Hydrogen Bonding*; Oxford University Press, 1997.

(4) Schuster, P.; (Eds), W. M. Hydrogen Bond Research. *Monatshefte fur Chemie* **1999**, *130*.

(5) Desiraju, G. R.; Steiner, T. *The Week Hydrogen Bond*; Oxford University Press, 1999.

(6) Coates, J. *Encyclopedia of Analytical Chemistry R.A. Meyers*; John Wiley & Sons Ltd, 2000; pp 10815–10837.

(7) Tipduangta, P.; Takieddin, K.; Fábián, L.; Belton, P.; Qi, S. A New Low Melting-Point Polymorph of Fenfibrate Prepared via Talc Induced Heterogeneous Nucleation. *Cryst. Growth Des.* **2015**, *15*, 5011–5020.

Dr Mateusz Dulski
Wydział Informatyki i Nauki o Materiałach
Uniwersytet Śląski w Katowicach
ul. 75 Pułku Piechoty 1A
41-500 Chorzów

Chorzów, 5.07.2018 r.

OŚWIADCZENIE

Oświadczam, że w pracy:

1. G. Szklarz, K. Adrjanowicz, M. Dulski, J. Knapik, and M. Paluch, *Dielectric relaxation study at ambient and elevated pressure of the modeled lipophilic drug fenofibrate*, J. Phys. Chem. B, 2016, 120 (43), pp 11298–11306, DOI: 10.1021/acs.jpcb.6b08511

mój wkład polegał na wykonaniu pomiarów spektroskopią podczerwoną (IR) oraz analizy i interpretacji otrzymanych wyników pomiarów.

Mateusz Dulski

Dr Justyna Knapik-Kowalczuk
Instytut Fizyki, Uniwersytet Śląski w Katowicach
Zakład Biofizyki i Fizyki Molekularnej
ul. 75 Pułku Piechoty 1A
41-500 Chorzów

Chorzów, 5.07.2018 r.

OŚWIADCZENIE

Oświadczam, że w pracach:

1. G. Szklarz, K. Adrjanowicz, M. Dulski, J. Knapik, and M. Paluch, *Dielectric relaxation study at ambient and elevated pressure of the modeled lipophilic drug fenofibrate*, J. Phys. Chem. B, 2016, 120 (43), pp 11298–11306, DOI: 10.1021/acs.jpcb.6b08511

2. G. Szklarz, K. Adrjanowicz, J. Knapik-Kowalczuk, K. Jurkiewicz and M. Paluch, *Crystallization of supercooled fenofibrate studied at ambient and elevated pressures*, Phys. Chem. Chem. Phys., 2017, 19, 9879–9888, DOI: 10.1039/C7CP00823F

mój wkład polegał na wykonaniu pomiarów skaningowej kalorymetrii różnicowej (DSC).

Dr hab. inż. Karolina Adrjanowicz
Instytut Fizyki, Uniwersytet Śląski w Katowicach
Zakład Biofizyki i Fizyki Molekularnej
ul. 75 Pułku Piechoty 1A
41-500 Chorzów

Chorzów, 5.07.2018 r.

OŚWIADCZENIE

Oświadczam, że w pracach:

1. G. Szklarz, K. Adrjanowicz, M. Dulski, J. Knapik, and M. Paluch, *Dielectric relaxation study at ambient and elevated pressure of the modeled lipophilic drug fenofibrate*, J. Phys. Chem. B, 2016, 120 (43), pp 11298–11306, DOI: 10.1021/acs.jpcb.6b08511

2. G. Szklarz, K. Adrjanowicz, J. Knapik-Kowalczuk, K. Jurkiewicz and M. Paluch, *Crystallization of supercooled fenofibrate studied at ambient and elevated pressures*, Phys. Chem. Chem. Phys., 2017, 19, 9879–9888, DOI: 10.1039/C7CP00823F

3. G. Szklarz, K. Adrjanowicz, M. Tarnacka, J. Pionteck, M. Paluch, *Confinement-induced changes in the glassy dynamics and crystallization behavior of supercooled fenofibrate*, J. Phys. Chem. C, 2018, 122, 1384–1395, DOI: 10.1021/acs.jpcc.7b10946

4. G. Szklarz, K. Adrjanowicz, M. Paluch, *Cooling-rate versus compression-rate dependence of the crystallization in the glass-forming liquid, propylene carbonate*, Cryst. Growth Des., 2018, 18, 2538–2544, DOI: 10.1021/acs.cgd.8b00123

mój wkład polegał na nadzorowaniu przeprowadzonych badań, analiz, dyskusji otrzymanych wyników, korekcie tekstu manuskryptu oraz pomocy przy korespondencji z recenzentami.

Prof. dr hab. Marian Paluch
Instytut Fizyki, Uniwersytet Śląski w Katowicach
Zakład Biofizyki i Fizyki Molekularnej
ul. 75 Pułku Piechoty 1A
41-500 Chorzów

Chorzów, 5.07.2018 r.

OŚWIADCZENIE

Oświadczam, że w pracach:

1. G. Szklarz, K. Adrjanowicz, M. Dulski, J. Knapik, and M. Paluch,*Dielectric relaxation study at ambient and elevated pressure of the modeled lipophilic drug fenofibrate*, J. Phys. Chem. B, 2016, 120 (43), pp 11298–11306, DOI: 10.1021/acs.jpcb.6b08511

2. G. Szklarz, K. Adrjanowicz, J. Knapik-Kowalczuk, K. Jurkiewicz and M. Paluch,*Crystallization of supercooled fenofibrate studied at ambient and elevated pressures*, Phys. Chem. Chem. Phys., 2017, 19, 9879–9888, DOI: 10.1039/C7CP00823F

3. G. Szklarz, K. Adrjanowicz, M. Tarnacka, J. Pionteck, M. Paluch,*Confinement-induced changes in the glassy dynamics and crystallization behavior of supercooled fenofibrate*,J. Phys. Chem. C, 2018, 122, 1384–1395, DOI: 10.1021/acs.jpcc.7b10946

4. G. Szklarz, K. Adrjanowicz, M. Paluch, *Cooling-rate versus compression-rate dependence of the crystallization in the glass-forming liquid, propylene carbonate*, Cryst. Growth Des., 2018, 18, 2538–2544, DOI: 10.1021/acs.cgd.8b00123

mój wkład polegał na dyskusji otrzymanych wyników

A2. Crystallization of supercooled fenofibrate studied at ambient and elevated pressures

Autorzy: G. Szklarz, K. Adrjanowicz, J. Knapik, K. Jurkiewicz, M. Paluch
Referencja: Phys. Chem. Chem. Phys.2017, 19, 9879–9888
DOI: 10.1039/c7cp00823f
Impact Factor czasopisma z roku opublikowania pracy: **4.449**
Liczba punktów ministerialnych MNiSW czasopisma (2016): **40**

Mój udział w poniższym artykule polegał na przeprowadzeniu badań dielektrycznych oraz pomiarów wzrostu kryształów pod mikroskopem optycznym, analizie i interpretacji wyników procesu krystalizacji, a także na przygotowaniu manuskryptu. Wkład pozostałych współautorów zamieszczono w formie oświadczeń.

PCCP

PAPER

View Article Online
View Journal | View Issue

Cite this: *Phys. Chem. Chem. Phys.*, 2017, **19**, 9879

Crystallization of supercooled fenofibrate studied at ambient and elevated pressures

Grzegorz Szklarz,*[ab] Karolina Adrjanowicz,*[ab] Justyna Knapik-Kowalczuk,[ab] Karolina Jurkiewicz[ab] and Marian Paluch[a]

Received 7th February 2017,
Accepted 14th March 2017

DOI: 10.1039/c7cp00823f

rsc.li/pccp

In this work, we have performed a detailed investigation on the crystallization tendency of the modeled glass-forming pharmaceutical compound, fenofibrate. To do this, we have employed four different experimental techniques allowing following of the crystallization process. This has included dielectric spectroscopy, optical microscopy, X-ray diffraction and differential scanning calorimetry. From the crystallization kinetic studies carried out at atmospheric pressure, we have determined the temperature dependence of the crystal growth rate and the overall crystallization rate. It was found that the time scale of the molecular motions responsible for α-relaxation correlates much better with the crystal growth rate than with the overall crystallization rate. Experiments carried out under varying thermodynamic conditions while remaining on the same timescale of α-relaxation have demonstrated that the crystallization tendency of the supercooled fenofibrate significantly slows down with increasing pressure. Lastly, we have also shown that the thermodynamic history of reaching crystallization conditions has a substantial impact on its overall progress.

1 Introduction

Crystallization is one of the most fascinating phenomena that occurs widely in nature and of great importance to industry. It leads to the formation of a solid substance with a long-range ordered structure, built from repeated blocks called primitive cells. Among crystallization methods the most popular are crystallization by (i) cooling, (ii) evaporation of solvent and (iii) precipitation from solution.[1–4] Depending on the chosen method and crystallization conditions the final product can vary in structure and morphology. The diversity of crystal forms and their physical and mechanical properties fascinate scientists around the world and lead to an enormous number of studies devoted to the crystallization phenomenon. However, despite years of studies, a complete understanding and control of this process remain a major challenge.[4–6]

Crystallization is commonly observed when the temperature of a liquid is lowered below its freezing point. In such a case, the liquid phase will have higher Gibbs free energy so that crystallization will be thermodynamically more favorable. However, there is also a large group of substances which do not transform immediately into crystals when cooling from the melt. Instead, it remains in a metastable supercooled liquid state. In such a case, gradual cooling will lead to the formation of a disordered solid, called glass. Glass-forming materials are of great scientific and practical importance, *e.g.* in the pharmaceutical industry or photovoltaic systems.[7–10] More control over the crystallization process is a key to obtain new materials with desired properties. A useful strategy to do this is by introducing pressure. In the case of a viscous liquid, the increase of pressure has a very similar effect on its molecular dynamics with a decrease in temperature.[11,12] However, temperature and pressure are not equivalent thermodynamic variables. While the temperature affects the kinetic energy of materials, the pressure alters their molecular spacing, allowing obtaining a denser and more closely packed structure. Thus, only when operating with both thermodynamic variables, it is possible to unveil the thermodynamic and kinetic contributions and get a complete picture of the crystallization process.[13–15]

Crystallization proceeds *via* nucleation and crystal growth. Both are inseparable and nonexchangeable steps of the crystallization process. It means that without nucleation crystals cannot grow; and, in the opposite way, without the growth of crystals, nuclei would not transform into stable macroscopic crystals. Since a critical nucleus might contain tens of molecules, following the early stages of the crystallization process is an experimental challenge. Typically, such small objects cannot be detected, only after growing to a size large enough to reach the threshold of instrument sensitivity. Directly following the nucleation process succeeded only using *e.g.* a double pulse technique, laser scanning confocal microscopy or real-time

[a] *Institute of Physics, University of Silesia, Ulica Uniwersytecka 4, 40-007 Katowice, Poland. E-mail: gszklarz@us.edu.pl, kadrjano@us.edu.pl*
[b] *Silesian Center for Education and Interdisciplinary Research, 75 Pulku Piechoty 1a, 41-500 Chorzow, Poland*

X-ray absorption.[16–19] Because of the experimental limitations, our knowledge about the crystallization behavior of various materials originates mostly from the analysis of the overall crystallization or crystal growth kinetics. Among various experimental techniques used to investigate the crystallization from the undercooled liquid state the most frequently used are differential scanning calorimetry (DSC), X-ray powder diffraction (XRD), and microscopic (*e.g.* polarized light, atomic-force or transmission electron microscopy) and spectroscopic (*e.g.* infra-red, Raman or dielectric spectroscopy) techniques.[16,20–24] Their applicability in crystallization studies relies on recording the changes in certain physical properties of a given material that accompanies transformation from the liquid to the crystalline state. From this, it is possible to determine the characteristic parameters describing the crystallization process such as the crystallization time scale, the induction period, or the dimensionality and morphology of the growing crystals. Each of these methods has its own limitations, but their proper combination results in a more accurate and complete insight into the crystallization process.

In this paper, we have performed a detailed investigation on the crystallization behavior of the glass-forming liquid, fenofibrate. Fenofibrate is a substance of great pharmaceutical interest which shows high lipophilicity and very low solubility in aqueous media.[25–27] It is a model drug substance to test various strategies aiming to improve its dissolution rate and poor oral bioavailability.[28–33] Amorphous or metastable supercooled liquid forms play an important role in enhanced dissolution ability. Unfortunately, fenofibrate shows very high (or even unpredictable) tendency to crystallize from the supercooled liquid state which significantly curbs its potential usefulness in the pharmaceutical formulations.[23,34–37] Here, we have employed complementary experimental techniques with the aim to provide a better understanding of its crystallization behavior in the supercooled liquid regime. We have also studied the effect of compression on the crystallization process and the relationship between the molecular mobility (as expressed by α-relaxation), overall crystallization and crystal growth rates.

2 Experimental

2.1 Materials

Fenofibrate ($C_{20}H_{21}ClO_4$, molar mass 360.831 g mol^{-1}) of >99% purity was purchased from Sigma-Aldrich as a white crystalline powder and was used without further purification. The chemical structure of fenofibrate is presented in Fig. 1. Amorphous fenofibrate was obtained by supercooling the melted sample.

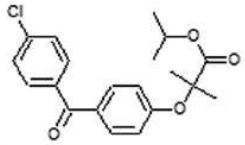

Fig. 1 Structure of fenofibrate.

For this purpose, we heated the powder above the melting point (353–354 K[35,38,39]) and then rapidly cooled it.

2.2 Differential scanning calorimetry

Calorimetric analysis of isothermal crystallization kinetics of fenofibrate was carried out by using a Mettler-Toledo DSC 1 STARe System. The measuring device was equipped with a HSS8 ceramic sensor having 120 thermocouples and a liquid nitrogen cooling station. Temperature and enthalpy calibrations were performed by using indium and zinc standards. Measurements were carried out in aluminum crucibles (40 μL) under nitrogen purge (flow rate 60 mL min^{-1}). First, the crystalline material was heated above the melting temperature and held for 10 minutes to ensure complete melting. After that, it was rapidly cooled (30 K min^{-1}) to the temperature range well below the glass transition temperature (T_g = 254 K). As a next step, the sample was heated up to the crystallization temperature (293 K, 303 K and 323 K) with a heating rate of 10 K min^{-1}. At selected temperatures, we have recorded the changes in the DSC heat flow signal as a function of time. When crystallization was completed, the temperature was increased again to melt the crystalline material.

2.2.1 X-ray diffraction. The X-ray diffraction experiments were performed using a Rigaku-Denki D/MAX RAPID II-R diffractometer (Rigaku Corporation, Tokyo, Japan) with a rotating anode Ag Kα tube (λ = 0.5608 Å), equipped with an incident beam (002) graphite monochromator and an image plate in the Debye–Scherrer geometry. The temperature was controlled by using an Oxford Cryostream Plus and a Compact Cooler with a resolution of 0.1 K. Measurements were performed for the sample filled and empty capillaries, and the intensity for the empty capillary was then subtracted. The beam width of the sample was 0.3 mm. The two-dimensional diffraction patterns were converted into one-dimensional intensity data using suitable software. Isothermal cold crystallization was performed at temperatures: 280 K, 283 K, 288 K, 293 K 303 K, 323 K and 343 K. Prior to this, the crystalline material was placed inside the capillary, melted, and then quenched to the required temperature. Changes in crystallinity were recorded as a function of time.

2.2.2 Polarized light microscopy. To measure the growth rates we have used an Olympus BX51 polarized light microscope equipped with an Olympus SC30 camera and a halogen source light. Optical figures were collected using Olympus Soft Imaging Solutions GmbH 5.1 at UMPlanFI 10× and 0.30 aperture. A Linkam THM 600 thermal stage was used to control the temperature during the experiment. The sample was maintained between two glass covers with no spacers. The experimental protocol involved melting the sample, cooling to room temperature, and heating to and holding at different temperatures. Changes in the radius of the growing crystals were tracked by taking pictures at regular time intervals. Measurements were performed at temperatures 298 K, 308 K, 318 K, 328 K, 338 K and 348 K. Crystal growth rates were measured using seeded crystals, four times at each temperature.

2.2.3 Dielectric measurements. The real and imaginary parts of complex dielectric permittivity were recorded by using

a Novo-Control Alpha dielectric spectrometer over the frequency range of 10^{-2} to 10^{6} Hz. The temperature was controlled by a Quattro system using a nitrogen gas cryostat with stability better than 0.1 K. Isothermal cold crystallization studies of fenofibrate at ambient pressure were performed at different temperatures, ranging from 281 K to 348 K. The sample was placed between two stainless-steel electrodes separated by a spacer (distance ~0.1 mm) and mounted inside a cryostat. Before each measurement, the sample was kept for a while above the melting temperature to ensure complete melting. Next, it was cooled and held at different crystallization temperatures. Then, we have recorded the changes in the dielectric signal of the studied sample with the crystallization process.

Crystallization studies at increased pressure were performed at temperature $T = 358$ K and pressure $p = 362$ MPa. For this, we have utilized a Unipress high-pressure system with an MP5 micropump (Institute of High-Pressure Physics, Warsaw, Poland). The pressure was exerted by transmitting silicon oil to the pressure chamber using a system of capillary tubes (Nova Swiss). The temperature was controlled by the thermal bath (Julabo) with stability better than 0.1 K. We have used a homemade capacitor placed inside a Teflon capsule to separate it from the pressurizing fluid. The real and imaginary parts of complex permittivity were measured within the same frequency range as the atmospheric pressure data using an impedance Alpha-A Analyzer (Novocontrol GmbH, Montabaur, Germany). Crystallization measurements at atmospheric pressure were repeated using a high-pressure cell to eliminate the contribution coming from different sample geometries. Temperature, $T = 280.6$ K, was chosen to obtain the same position of the α-process peak as that obtained during crystallization measurements at increased pressure.

2.2.4 Kinetics of isothermal crystallization. Crystallization kinetics of fenofibrate was analyzed within the Johnson–Mehl–Avrami–Kolmogorov (JMAK) theory.[40–43] The five main postulates of JMAK theory are listed below:[44]

1. At the beginning, in volume – V – exists only the 'parent phase', which is substituted with time by the grain phase.

2. The volume of any formed grain is much smaller than V.

3. The nucleation process is fully random, the probability of new nuclei is independent of the distribution of the existing nuclei.

4. All crystals have a convex shape.

5. The velocity of the growth of crystals is a linear vector which depends only on time and direction.

It is important to mention that JMAK theory can provide a reasonable description of the crystallization data even when all postulates are not satisfied. To describe the crystallization kinetics JMAK theory introduces the 'extended volume' – V^* – defined as the volume occupied by a crystal in relation to the 'parent phase'. V^* is described in the following form:

$$V^* = \frac{4\pi}{3}\int_0^t I(t')\left(\int_{t'}^t G(\tau)\mathrm{d}\tau\right)^3 \mathrm{d}t' \qquad (1)$$

where $I(t) = \mathrm{d}N/\mathrm{d}t$ (N – number of nuclei) is the nucleation rate and $G(t) = \mathrm{d}R/\mathrm{d}t$ (R – average radius of the crystal) is the mean growth rate in three dimensions. After substituting $I(t)$ by $I_0 t^a$ and $G(t)$ by $G_0 t^b$ and integrating, this equation can be rewritten as

$$V^* = \frac{4\pi I_0 G_0^3}{3\ C} t^{a+1+3(b+1)} = Kt^n = (kt)^n \qquad (2)$$

where k is the crystallization rate and n is the Avrami exponent. It can be easily seen that both parameters incorporate information on nucleation and crystal growth. Taking under consideration the statistical geometrical criteria, V^* is connected with the actual transformed volume – V – by the relationship

$$\frac{\mathrm{d}V}{\mathrm{d}V^*} = 1 - V \qquad (3)$$

Integrating with boundary conditions ($V^* = 0$ and $V = 0$) gives

$$V = 1 - \exp(-V^*) \qquad (4)$$

Substituting V^* using eqn (2) leads to the famous Avrami expression allowing description of the crystallization process[40–43]

$$V = 1 - \exp(-(kt)^n) \qquad (5)$$

where V is the crystalline volume fraction and t is the time.

3 Results and discussion

3.1 Thermal analysis of cold-crystallization

Differential scanning calorimetry (DSC) measurements of the 'as received' compound were performed in the temperature range between 200 K and 380 K (Fig. 2a). From this, we have determined the melting temperature to be 354 K (defined as the onset of the melting peak). The obtained value is in good agreement with that reported in the literature for polymorphic form I of fenofibrate.[35,36,38,45] Next, the sample was quenched to 200 K to form a glass. Upon heating the glassy material (10 K min^{-1}), we

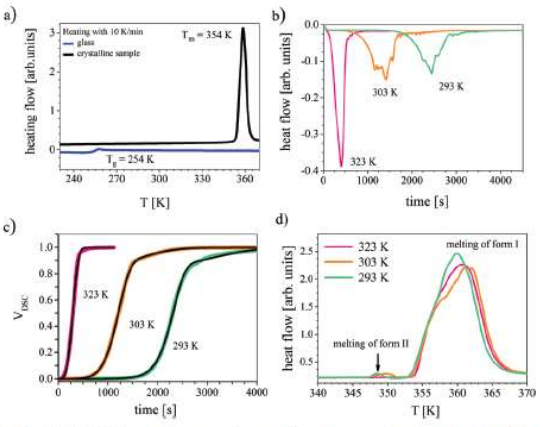

Fig. 2 (a) DSC thermograms of crystalline (as received) and amorphous fenofibrate obtained upon heating with 10 K min^{-1}. (b) Heat flow *versus* time upon isothermal cold-crystallization of fenofibrate at different crystallization temperatures. (c) Evolution of the degree of crystallinity with time. Black lines represent Avrami fits. (d) Thermograms recorded during heating of crystalline fenofibrate obtained at different crystallization temperatures.

have observed the glass transition event (defined as the mid-point of the heat flow increment) at 254 K but no signatures of recrystallization. Afterward, we have performed isothermal cold-crystallization studies at three selected temperatures located in the supercooled liquid regime ($T_g < T < T_m$). The basic idea of the subsequent crystallization using DSC calorimetry relies on recording the changes in the enthalpy (and therefore the internal energy) of the sample as a function of time. As illustrated in Fig. 2b cold-crystallization is observed as an exothermic peak that shifts towards longer times upon lowering the temperature. From this, we were able to calculate the changes in the crystallinity (V) of the measured system using the following formula:

$$V_{DSC} = \frac{\int_{t_0}^{t} \frac{dH}{dt} dt}{\int_{t_0}^{t_\infty} \frac{dH}{dt} dt} = \frac{H_t}{H_\infty} \quad (6)$$

where t_0 and t_∞ represent the time corresponding to the crystallization onset and its termination, respectively. H_t is the enthalpy of crystallization that is released at time t, whereas H_∞ is the enthalpy value reached at the end of the isothermal crystallization process (area under the peak). In Fig. 2c we have displayed the time-dependence of the crystallization degree obtained for the three different temperatures. As can be seen, the curves have a sigmoidal shape, but they are not perfectly symmetric. The rate of crystallization seems to slow down at later times, especially for fenofibrate crystallized at lower temperatures. This effect is frequently associated with a secondary crystallization process. Fenofibrate shows some different polymorphic forms among which form I (T_m = 354 K) is the most stable one. When recrystallizing from the supercooled liquid state, form I is being accompanied by metastable form II (T_m = 347 K).[45,46] Keeping this in mind, we suppose that the presence of trace amounts of the second crystalline form of fenofibrate might impede the final stages of the crystallization process. To verify this supposition, we have performed DSC scans of the crystalline materials obtained from isothermal cold-crystallization studies. The results are illustrated in Fig. 2d. For all three samples we can see melting of form I at 354 K. However, for samples recrystallized at temperatures 293 K and 303 K an additional peak located at 347 K indicates the presence of form II.

To estimate the fraction of form II in the total crystalline material we have applied two methods. In the first method, we have assumed that the entire fenofibrate from form II transforms into form I. And next, we have calculated the enthalpy needed to melt such crystals, as areas below the melting peaks. Using values of the melting enthalpy reported in the literature, we obtained the amount of recrystallised fenofibrate and the content of form II. Due to significant differences between the melting enthalpy of form II reported in the literature[45,46] we have considered both possibilities. The results are presented in Table 1. The second method is based on the observation of the crystallization kinetics. In this case, to estimate the content of each polymorph we have employed the Johnson–Mehl–Avrami–Kolmogorov (JMAK) model for the independent transformation

Table 1 Content of different polymorphic forms of fenofibrate in the material cold-crystallized under isothermal conditions

Method	Temperature (K)	Form I	Form II
DSC	293.15	0.97[a]	0.03[a]
		0.73[b]	0.27[b]
	303.15	0.97[a]	0.03[a]
		0.68[b]	0.32[b]
Avrami model	293.15	0.82	0.18
	303.15	0.81	0.19

[a] Reported by Di Martino.[45] [b] Reported by Gorniak.[46]

of the two phases.[47] This model is described using the following equation:

$$V = 1 - f\exp(-(k_1 t)^{n_1}) - (1 - f)\exp(-(k_2 t)^{n_2}) \quad (7)$$

where V is the relative degree of crystallinity calculated from eqn (6), f is a fraction content of the polymorph, t is the time, k_1 and k_2 are crystallization rates of form I and crystalline form II, respectively, and n_1 and n_2 are the corresponding Avrami exponents. The results of the fitting are presented in Fig. 2c as black solid lines. As can be seen in Table 1, the estimated content of form II at 293 K and 303 K is similar. However, the results vary between each other, depending on the chosen method. This is caused by a significant difference between the enthalpy of melting reported for form II (Di Martino *et al.* 10.3 ± 6.3 kJ mol^{-1}[45] and Gorniak *et al.* 0.9 kJ mol^{-1}[46]), and the fact that the adopted model of the crystallization kinetics assumes lack of the interaction between phases during crystallization. Nevertheless, by comparing the obtained results, it seems that the enthalpy of melting determined by Gorniak *et al.* appears to be more accurate. From a detailed analysis of the crystallization kinetic data using the Avrami equation, we have also estimated the temperature evolution of the Avrami parameter, the magnitude of activation energy for the nucleation and the overall crystallization process. These data will be presented in the further part of this paper.

3.2 X-ray diffraction studies of the crystallization kinetics

In Fig. 3a–c we show X-ray diffraction patterns recorded upon crystallization of fenofibrate at different temperatures. For crystalline fenofibrate, the two most intense diffraction peaks can be used as indicators of the crystallization process. The first one is located at a scattering angle 2θ of 8.12° and corresponds to Miller indices (hkl) $1\bar{1}\bar{3}$.[48] The second peak is observed at a 2θ of 6.00°. In fact, this is the sum of the two peaks located at 5.90° ($11\bar{1}$) and 6.08° ($1\bar{1}1$).[48] The diffraction pattern of amorphous fenofibrate (see the upper panels in Fig. 3a–c) looks like a typical diffraction pattern collected for amorphous organic compounds. It has broad diffuse peaks. More detailed analysis of the collected data reveals the existence of three diffuse peaks at 2θ = 6.00° ($s \approx 1.32$ Å^{-1}), 8.45° ($s \approx 1.66$ Å^{-1}) and 15.11° ($s \approx 2.95$ Å^{-1}), where s is the scattering vector expressed by the equation $s = \frac{4\pi}{\lambda}\sin\theta$ (Å^{-1}). The first two of them corresponded to the most intense peaks reported for the crystalline material.

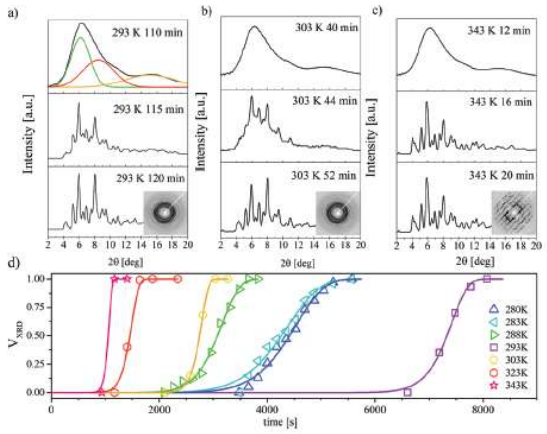

Fig. 3 X-ray diffraction patterns collected upon crystallization of fenofibrate at (a) 293 K, (b) 303 K and (c) 343 K. Insets present 2D diffraction patterns collected after crystallization processes at the given temperatures. (d) Changes in the degree of crystallinity as a function of time. Solid lines represent Avrami fits.

Their presence confirms the existence of the short-range ordering in the amorphous materials.[49] The third peak does not correspond to any strong peak in the diffraction pattern of the crystalline sample. The peak located at this value of the scattering vector is often observed for amorphous organic substances. And as believed, it has intramolecular origin.[50] Once crystallization proceeds, the sharp Bragg's peaks start to appear in the diffraction pattern of the amorphous material. Their intensity increases with the crystallization process, while the time of their appearance is strongly temperature dependent. With increasing temperature, the liquid–crystal phase transition is faster. Because of the low angle resolution and signal to noise ratio, it was impossible to distinguish between different polymorphic forms of fenofibrate. By comparing the XRD data for 'as received' crystalline materials and fully recrystallized samples we have not observed much differences. One of the possibilities is that both polymorphic forms have very similar XRD patterns. The other one is due to the difference in the thermal history of the samples measured using DSC and XRD technique fenofibrate crystallizes to only one form. In the first case, our thermal protocol has involved cooling of the melted sample to the glassy state and then re-heating it to the desired crystallization temperature. On the other hand, for XRD studies the melted sample was immediately quenched to the crystallization temperature. With increasing temperature, 2D diffraction patterns (insets of Fig. 3a–c) for crystalline materials show regions of higher and lower intensities (darker and brighter circles). For clarifications, in 2D diffractograms circles represent the scattering vectors. With increasing distance from the center the values of the scattering angle increase. At 343 K the regions with higher or lower intensity for different values of the scattering angle forms parallel lines. This observation is related to the fact that at higher temperatures the growing crystals are bigger. And when compared to the sample crystallized at lower temperatures we have a lower number of crystals in our sample. This peculiar effect can be mistakenly ascribed to the presence of diffuse X-ray scattering (disorder in the crystal which is connected with additional short range ordering[51]). However, additional diffraction studies using the single diffraction XRD technique have excluded such a possibility.

We have also performed more quantitative analysis of XRD diffraction patterns collected upon crystallization of supercooled fenofibrate at different temperatures. For this, we need to assume that the intensity of the diffraction signal is directly proportional to the content of phases in the studied system.[52] As mentioned above, metastable form II of fenofibrate was almost indistinguishable in the diffraction data recorded for the fully recrystallized material. Therefore, we have not taken it into account while calculating the degree of crystallinity given as

$$V_{\mathrm{XRD}} = \frac{A_{\mathrm{P}}}{A_{\mathrm{T}}} \tag{8}$$

where A_{P} and A_{T} are the areas of XRD peaks of partially crystalline and fully crystalline materials, respectively. Fig. 3d shows the time dependence of the degree of crystallization evaluated at various temperatures using eqn (8). Similarly, as for DSC data, we have also observed that upon lowering the temperature the crystallization rate slows down and the induction period increases. The induction time, t_0, specifies a period required to produce crystal nuclei of sufficient size to grow. To describe the curves of the time evolution of the degree of crystallinity we have used the JMAK equation, eqn (5). As can be seen, a good description of the fitted data was achieved using the Avrami model assuming only one polymorphic form. In the further part of this paper, the results obtained from the JMAK equation will be used to determine the energy of activation of the overall crystallization process, nucleation barrier and evolution of Avrami parameters with temperature. The obtained values will be compared with results determined from other experimental techniques.

3.3 Analysis of the crystal growth kinetics using optical microscopy

The crystallization process of fenofibrate was also monitored using optical microscopy. Fig. 4a–c displays the morphology of

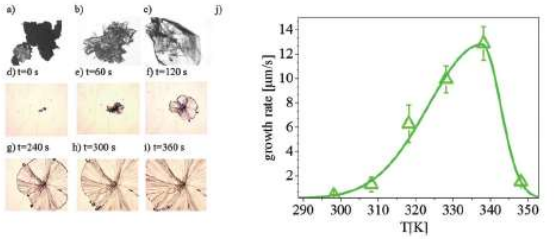

Fig. 4 Comparison of the morphology of fenofibrate crystals growing at different temperatures (a) 293 K, (b) 328 K and (c) 348 K. (d–i) Crystallization snapshots monitored under the microscope at 308 K. (j) The speed of the crystal growth for fenofibrate plotted as a function of temperature. Marked points (with error bars) represent the mean values measured at the same temperature. Green line is the asymmetric Gaussian function fit to the experimental data.

the crystals grown from drops at different temperatures. We have observed that the size and the average number of growing crystals change with increasing temperature. When crystallization is carried out at a higher temperature, the number of growing centers decreases. Moreover, the obtained crystals are bigger, block-like shape and slightly elongated in one direction. This is in agreement with 2D XRD data reported for fenofibrate crystallized at higher temperatures. A sequence of snapshots displayed in Fig. 4d–i shows the growth of a seeded crystal, between coverslips, in undercooled fenofibrate. By analyzing the speed of propagation of crystallization fronts at different temperatures we have determined the mean crystal growth rate obtained by measuring at each temperature a few crystals in various directions. The obtained results are presented in Fig. 4j. As can be seen, the temperature dependence of the crystal growth rate v forms an asymmetric curve with the maximum at 338 K, *i.e.* $T_m - T = 16$ K. Upon lowering the temperature, the rate of crystal growth increases due to the increase in the driving force towards crystallization. However, at higher undercooling rates it is inhibited because of the slowing down of the molecular motions in the viscous liquid. In the studied temperature range, the growth rates of fenofibrate change by approximately one order of magnitude. Recently, Amstad and co-workers[23] have reported crystal growth rates for fenofibrate studied within the temperature range 293–323 K using confocal microscopy. Here, we have significantly extended the temperature range, so that it covers almost the entire supercooled regime. By comparing the crystal growth rates determined using two different optical techniques we found quite good agreement, especially for data collected at lower temperatures. In both cases, with increasing temperature, the rates of crystal growth vary more, the same as the experimental uncertainty.

3.4 Crystallization kinetics followed using the dielectric technique

The principle idea of the dielectric measurements relies on the interactions of a studied material with an applied field. Thus, only molecules with the permanent dipole moment are able to reorientate in the electric field and contribute to the dielectric response of a given sample. Fenofibrate is a polar molecule (dipole moment $\mu = 3.9$ D), so we can surely follow its crystallization kinetics using the dielectric technique. The transformation from the liquid to the crystalline phase freezes the number of actively reorientating dipoles. Therefore, in the dielectric spectra we observe a gradual decrease of the dielectric permittivity increment and the amplitude of the α-relaxation (see Fig. 5a and b). By following these changes we are able to determine the evolution of the degree of crystallinity with time

$$V_{DS} = \varepsilon_n' = \frac{\varepsilon'(0) - \varepsilon'(t)}{\varepsilon'(0) - \varepsilon'(\infty)} \quad (9)$$

where ε_n' is the normalized dielectric permittivity, which corresponds to the crystalline volume fraction, $\varepsilon'(0)$ is the static dielectric permittivity at the beginning of the crystallization process, $\varepsilon'(\infty)$ is the value of dielectric permittivity after the crystallization process (at infinite time), and $\varepsilon'(t)$ is the value of

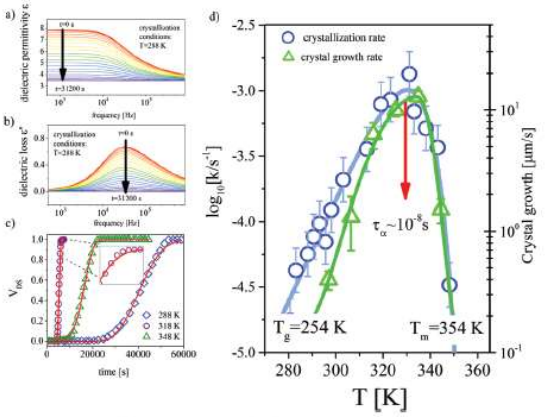

Fig. 5 The real (a) and imaginary (b) parts of complex dielectric permittivity recorded upon crystallization of fenofibrate at 288 K. Presented spectra were collected every 1200 seconds. Arrows indicate the direction of changes in the dielectric permittivity and loss spectra. (c) Evolution of the crystal volume fraction as determined from the analysis of time-dependent dielectric measurements at 288 K, 318 K and 348 K. Solid lines represent Avrami fits. Inset present the crystal volume fraction behavior in the range of 0.8 to 1.0 for the measurements at 318 K. (d) Temperature dependence of the overall crystallization determined for fenofibrate. Error bars are calculated as standard deviation. Blue line is a trend line, described using the relation, $\log(k) = Ae(-T/B) + CT + D$. Crystal growth rates are shown as well.

dielectric permittivity at a given time of crystallization. Fig. 5c shows ε_n' as a function of time at three selected crystallization temperatures. The obtained results were then fitted using the JMAK equation (eqn (5)). Similarly as for XRD data, only one set of Avrami parameters was needed to describe the $V_{DS}(t)$ dependence for fenofibrate. The thermal protocol in both cases was identical. From the analysis of time-dependent dielectric data measured at different temperatures we obtain the evolution of the overall crystallization rate in the entire supercooled liquid regime. The results are demonstrated in Fig. 5d. Comparison with the crystal growth data has revealed that the maxima of both curves are located in close proximity to each other. It is interesting to note that at the right-hand side of the curve (*i.e.* closer to the melting point) the temperature dependences of k and v are almost identical. In contrast, at higher undercooling rates, the overall crystallization rate curve is slightly broader than the crystal growth rate curve which is possibly due to the contribution coming from the nucleation process. By looking at the experimental data presented in Fig. 5d one can also clearly see that within the temperature range covering more than 70 K, k changes only within two decades. The same applies to $v(T)$ dependence. By utilizing the results of the previous dielectric relaxation studies, we get that at the maximum rate of crystallization the time scale of the cooperative reorientational motions is $\sim 10^{-8}$ s. We wish to note that this is accidentally very close to the onset of the cooperative mobility in supercooled liquids.[53]

Understanding the relationship between time scales of α-relaxation and crystallization is an important aspect for

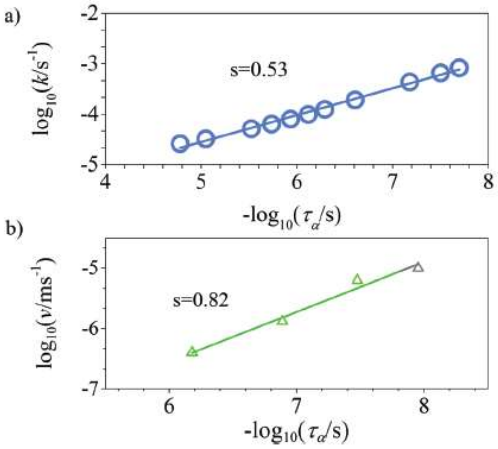

Fig. 6 The dependence of the (a) overall crystallization rate constant and (b) crystal growth rate (v) plotted *versus* α-relaxation time τ_α of fenofibrate. Solid lines denote a linear fit to the data.

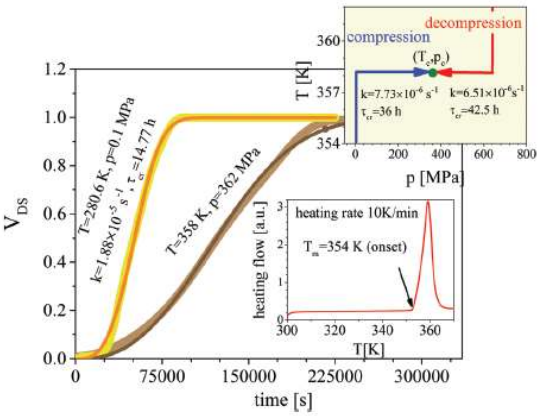

Fig. 7 Main plot: time-dependent changes in the degree of crystallinity V_{DS} observed for fenofibrate upon crystallization under different thermodynamic conditions but with approximately the same α-relaxation time. The upper panel shows a schematic illustration of two alternative routes of approaching desired crystallization conditions (T_c, p_c). The lower panel shows the DSC thermogram of fenofibrate crystallized under high pressure.

recognizing the kinetic contribution to the crystallization process of the glass-forming liquids.[54] Therefore, the next step of our analysis has involved comparison of the temperature dependence of the overall crystallization and crystal growth rates with the corresponding $\tau_\alpha(T)$ dependence. To do that the data taken from the same temperature range were plotted in a log–log plot. Dielectric relaxation times of fenofibrate were taken from our recent paper.[55] As can be seen in Fig. 6a the α-relaxation time changes approximately two times faster than the overall crystallization rate (slope = 0.53). On the other hand, a better correlation was found between the α-relaxation time and the crystal growth rate (slope = 0.82). This is in fair agreement with the results reported for indomethacin. In that case, the crystal growth rate was found to be coupled with the molecular motions responsible for self-diffusion (slope = 1),[56] whereas the α-relaxation time changes much faster with the temperature and the crystallization time.[14] In consequence, the molecular mobility associated with cooperative glassy dynamics cannot be used as a single parameter that controls the crystallization in the supercooled liquid.

Another important aspect of the present study was to understand the effect of pressure on the crystallization tendency of supercooled fenofibrate. As shown recently, we can move in T–p space along different iso-invariant lines such as isobars (p = const.), isotherms (T = const.), isochores (V = const.), isochrones (τ_α = const.) or even iso-$\Delta\mu$ (where $\Delta\mu$ is the thermodynamic driving force towards crystallization).[14] Each of these iso-invariant lines contributes to a better understanding of the crystallization tendency of glass-forming liquids under varying thermodynamic conditions. However, only by studying crystallization in iso-τ_α and iso-$\Delta\mu$ states, it is possible to recognize which of the two factors, kinetics or thermodynamics, contribute more to the overall crystallization behavior of a given system. Here, we have investigated the crystallization behavior of fenofibrate at different combinations of temperature and pressure while maintaining the same time scale of α-relaxation, $\log_{10}(\tau_\alpha/s = -4.44)$ s. This includes the following set of (T, p) pairs: T = 280.6 K, p = 0.1 MPa and T = 358 K, p = 362 MPa. As illustrated in Fig. 7 with increasing pressure the crystallization of fenofibrate slows down. The characteristic time scale of the crystallization process increases more than two times. Analogous behavior was also observed for other pharmaceutical substances with weak intermolecular interactions, *e.g.* ibuprofen[57] or ketoprofen.[58] However, we have also noted that the crystallization rate of fenofibrate depends on the thermodynamic pathways. In the upper inset of Fig. 7 we present an illustrative scheme of changing the temperature and pressure to achieve desired crystallization conditions. In the first case, we have set the starting conditions at 580 MPa and 368 K. Under these conditions, fenofibrate remains in a highly viscous liquid regime, slightly above the glass transition temperature. Next, the sample was cooled down to 358 K to form a glass. Then, we have lowered the pressure to 362 MPa and performed time-dependent dielectric measurements. In the second case, the sample was heated to 358 K (above T_m) at atmospheric pressure and next compressed to reach the desired pressure (362 MPa). Therefore, there is a large density difference between the two different starting conditions. The former one is surely denser than the latter one ($\log\tau_\alpha$ = 0.44 s^{-1} for T = 358 K and p = 580 MPa, $\log\tau_\alpha$ = −8.58 s^{-1} for T = 358 K and p = 0.1 MPa). As it turned out this plays a decisive role in the overall crystallization behavior of the investigated liquid under selected (T_c, p_c) conditions. Comparison of the crystallization times ($\tau_{cry} = 1/k$) has revealed that the rate of crystallization is clearly lower for a sample which approached desired thermodynamic conditions *via* decompression at a fixed temperature. Moving in the T–p space along various paths has resulted in approximately 6.5 h of difference in the total crystallization time. From that, it is evident that we can alter the crystallization behavior of the glass-forming liquid

not only by manipulating with (T, p) combinations but also the thermodynamic history of the sample.

As mentioned previously fenofibrate has two crystalline forms which differ not only in the stability but also the density (form I, 1.285 g cm^{-3},[48] and form II, 1.304 g cm^{-3} [59]). As a rule, at high pressures more dense crystalline phases are favored. Thus, it is highly interesting to verify if compression favors a more denser metastable form of fenofibrate. We could expect that from the Ostwald rule of stages.[60] For that purpose, we have performed DSC measurements of the crystalline material obtained upon crystallization at 362 MPa and 358 K. The experimental protocol has involved lowering the temperature to 293 K and then the release of pressure to atmospheric pressure conditions. The lower inset in Fig. 7 shows the DSC thermogram obtained upon heating fenofibrate crystallized under high pressure and (T_c, p_c) conditions. We have observed only one thermal event related to the melting temperature of polymorph I, but no signs of metastable form II. This result indicates that form I of fenofibrate is preferable more under increased pressure which is quite important information, especially in the context of pharmaceutical applications. It seems that crystallization of fenofibrate on increased pressure could be a useful strategy to get rid of the unwanted metastable polymorphic form.

3.5 Comparison of the crystallization kinetics results

As the last point, we have analyzed together crystallization results obtained for fenofibrate using different experimental techniques. In Fig. 8a and b we present the temperature evolution of the Avrami parameter n and the crystallization constant k which were determined from the fitting of calorimetric, X-ray diffraction and dielectric data. As can be seen, in the studied temperature range, the Avrami parameter varies within 2.6–3.3. The values of the Avrami parameter close to 3 suggest the spherical growth of crystals in three-dimensions. A comparison of the crystallization results has also revealed that k determined from the dielectric measurements is apparently lower than that obtained from the calorimetric and X-ray diffraction data, see Fig. 8b. This behavior is not surprising because many factors influence the initiation and the crystallization process, such as the sample preparation, thermal history, the presence of impurities, or geometry of the container.[61] The activation energy for the crystallization of fenofibrate is ~30–50 kJ mol^{-1}, depending on the experimental technique. In contrast, for pharmaceutical compounds such as sildenafil or nifedipine approximately 4–5 times higher values of activation energies were reported (for sildenafil, the obtained energies vary in the range 175–207 kJ mol^{-1} that is ±30 kJ mol^{-1}, depending on the selected method).[21,62] We have also analyzed changes in the induction period with temperature, as demonstrated in Fig. 8c. The induction time is frequently related to the nucleation event, by assuming its inverse proportionality to the nucleation rate.[63] Thus, from the slope of $\log t_{ind}$ *vs.* T^{-1} we were able to evaluate the activation energy of the nucleation process. As can be seen, the obtained values are very high and comparable (within the experimental uncertainty) to E_a for the overall crystallization. This indicates that the formation of crystal nuclei is the major bottleneck for the entire crystallization of supercooled fenofibrate.

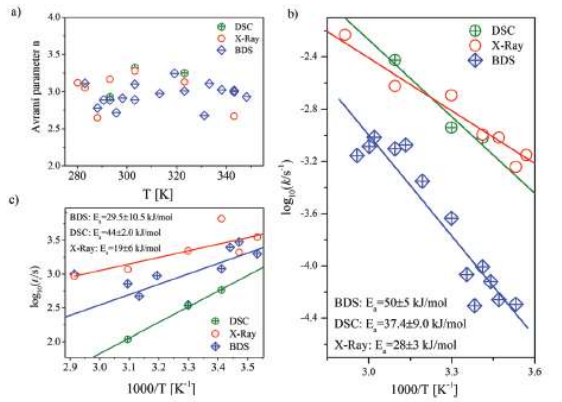

Fig. 8 Temperature dependence of the (a) Avrami parameter, (b) crystallization constant rate and (c) induction time obtained from the analysis of the dielectric, calorimetric and X-ray diffraction data for fenofibrate. Solid lines represent the Arrhenius fit to the experimental data.

4 Conclusions

We have performed a detailed investigation on the crystallization behavior of supercooled fenofibrate using different experimental techniques (DSC, X-ray diffraction, dielectric and optical microscopy). Each of these methods gives some valuable information about the crystallization tendency of the investigated compound. Since crystallization is a multivariate problem, only when combined, it is possible to provide a complete picture of the crystallization process. Additionally, dielectric measurements carried out under increased pressure enable exploring the influence of varying thermodynamic conditions on the crystallization process. The main conclusions of the present study are listed below:

- Cold-crystallization studies using DSC have confirmed the appearance of the second polymorphic form of fenofibrate. It accompanies stable form I and emerges only during crystallization at temperatures lower than approximately 303 K. On the other hand, at higher temperatures fenofibrate re-crystallizes only to stable form I.
- From the analysis of the 2D diffraction patterns it was concluded that the morphology/size of the growing crystals changes with temperature. Metastable form II of fenofibrate was almost indistinguishable in the dielectric and X-ray diffraction data.
- Evolution of the crystal growth rate with temperature shows a characteristic bell-shape with an asymmetric maximum located at $T = T_m - T = 16$ K. Since the nucleation process is a thermal dependent process and the probability of creating new nuclei decreases with increasing temperature, we have observed that close to T_m the growing crystals are larger.

• By following the crystallization kinetics using dielectric spectroscopy we have determined the evolution of the crystallization rate, k, in the temperature range between T_g and T_m. The maximum of the overall crystallization rate was found to be located in close vicinity to the maximum of the crystal growth rate. In this temperature region, the time scale of the cooperative reorientational motions is $\sim 10^{-8}$ s. This is very close to the onset of cooperative mobility in supercooled liquids.

• By comparing the temperature evolution of the crystal growth and overall crystallization rates with the α-relaxation time we show that τ_α correlates much better with v than with k. This leads to a conclusion that molecular dynamics has a significant influence on the crystallization process, but surely does not govern it alone.

• Crystallization of fenofibrate slows down with increasing pressure along isochrone. However, the thermodynamic history of reaching crystallization conditions (history of changing the temperature and pressure to approach a new thermodynamic state point) has an important impact on the reaction rate.

• We found that the activation energy for the crystallization in the temperature range of interest was rather low, $\sim$30–50 kJ mol^{-1}. Among that, a major contribution comes from the nucleation process.

Acknowledgements

The authors are grateful for the financial support from the National Science Centre within the framework of the Opus project (Grant No. DEC 2014/15/B/ST3/00364).

References

1 *Crystal Growth Processes Based on Capillarity: Czochralski, Floating Zone, Shaping and Crucible Techniques*, ed. T. Duffar, Wiley-Blackwell, 2010.
2 *Crystallization: Basic Concepts and Industrial Applications*, ed. W. Beckmann, Viley-VCH, 2013.
3 J. W. Mullin, *Crystallization*, Butterworth Heinemann, 4th edn, 2001.
4 A. Myerson, *Handbook of Industrial Crystallization*, Heinemann, Boston, USA, 2002.
5 *Engineering of Crystalline Materials Properties: State of the Art in Modeling, Design and Applications*, Edition Series: NATO Science for Peace and Security Series B: Physics and Biophysics, ed. D. Novoa, J. J. Braga and L. Addadi, Springer, Berlin, 2008.
6 D. Erdemir, A. Y. Lee and A. S. Meyerson, *Acc. Chem. Res.*, 2008, **42**, 621–629.
7 P. G. Debenedetti and F. H. Stillinger, *Nature*, 2001, **410**, 259–267.
8 L. Berthier and M. D. Ediger, *Phys. Today*, 2016, **69**, 40.
9 L. A. Yu, *Adv. Drug Delivery Rev.*, 2001, **48**, 27–42.
10 J. Kim, Z. Hong, G. Li, S. Tze-bin, J. Chey, Y. S. Lee, J. You, C. Chun-Chao, D. K. Sadana and Y. Yang, *Nat. Commun.*, 2015, **6**, 6391.
11 C. M. Roland, S. S. Hensel-Bielowka and M. Paluch, *Rep. Prog. Phys.*, 2005, **68**, 1405.
12 G. Floudas, M. Paluch, G. A. Grzybowski and K. Ngai, *Molecular Dynamics of Glass-Forming Systems: Effects of Pressure*, ed. F. Kremer, Springer-Verlag, Berlin, 2011.
13 K. Adrjanowicz, A. Grzybowski, K. Grzybowska, M. Pionteck and J. Paluch, *Cryst. Growth Des.*, 2014, **14**, 2097–2104.
14 K. Adrjanowicz, K. Koperwas, G. Szklarz, M. Tarnacka and M. Paluch, *Cryst. Growth Des.*, 2016, **16**, 7000–7010.
15 K. Adrjanowicz, K. Koperwas, M. Tarnacka, K. Grzybowska, K. Niss, J. Pionteck and M. Paluch, *Cryst. Growth Des.*, 2016, **16**, 6263–6268.
16 M. Sleutel, J. Lutsko, A. E. S. Van Driessche, M. A. Durán-Olivencia and D. Maes, *Nat. Commun.*, 2014, **5**, 5598.
17 E. R. Gasser, U. Weeks, A. Schofield, P. N. Pusey and D. A. Weitz, *Science*, 2001, **292**, 258–262.
18 O. Galkin and P. G. Vekilov, *J. Phys. Chem. B*, 1999, **103**, 10965–10971.
19 S. De Panfilis and A. Filipponi, *J. Appl. Phys.*, 2000, **88**, 562–570.
20 K. Jamie, J. K. Hobbs, O. E. Farrance and L. Kailas, *Polymer*, 2009, **50**, 4281–4292.
21 K. Kolodziejczyk, K. Grzybowska, Z. Wojnarowska, M. Dulski, L. Hawelek and M. Paluch, *Cryst. Growth Des.*, 2014, **14**, 3199–3209.
22 B. J. Bulkin, M. Lewin and J. Kim, *Macromolecules*, 1987, **20**, 830–835.
23 E. Amstad, F. Spaepena and D. A. Weitz, *Phys. Chem. Chem. Phys.*, 2015, **17**, 30158–30161.
24 *Disordered Pharmaceutical Materials*, ed. M. Descamps, Wiley-VCH, 2016.
25 M. J. Chapman, *Atherosclerosis*, 2003, **171**, 1–13.
26 S. Jamzad and R. Fassihi, *AAPS PharmSciTech*, 2006, **7**, E17–E22.
27 D. R. Guay, *Cardiovasc. Drug Rev.*, 2002, **20**, 281–302.
28 A. M. Babu, B. Rao and P. Sudhakar, *Int. J. Biol. Pharm. Res.*, 2012, **3**, 616–623.
29 L. Hu, H. Wu, F. Niu, C. Yan, X. Yang and Y. Jia, *Int. J. Pharm.*, 2011, **420**, 251–255.
30 K. Kawakami, S. Zhang, R. S. Chauhan, N. Ishizuka, M. Yamamoto, Y. Masaoka, M. Kataoka, S. Yamashita and S. Sakuma, *Int. J. Pharm.*, 2013, **450**, 123–128.
31 M. Vogt, K. Kunath and J. B. Dressman, *Eur. J. Pharm. Biopharm.*, 2008, **68**, 283–288.
32 S. Watterson, S. Hudson, M. Svard and Å. C. Rasmuson, *Fluid Phase Equilib.*, 2014, **367**, 143–150.
33 A. Kalivoda, M. Fischbach and P. Kleinebudde, *Int. J. Pharm.*, 2012, **429**, 58–68.
34 P. Di Martino, S. Palmieri and G. Martelli, *Chem. Pharm. Bull.*, 2000, **55**, 625–626.
35 D. Zhou, G. G. Z. Zhang, D. Law, D. J. W. Grant and E. A. Schmitt, *J. Pharm. Sci.*, 2002, **91**, 1863–1872.
36 A. Heinz, K. C. Gordon, T. McGoverin, C. M. Rades and C. Strachan, *Eur. J. Pharm. Biopharm.*, 2009, **71**, 100–108.
37 P. Tipduangta, K. Takieddin, L. Fábián, P. Belton and S. Qi, *Cryst. Growth Des.*, 2015, **15**, 5011–5020.

38 J. A. Baird, B. V. Eerdenbrugh and L. S. Taylor, *J. Pharm. Sci.*, 2010, **99**, 3787–3806.
39 U. Sailajaa, M. S. Thayyilb, N. K. Kumarc and G. Govindaraj, *J. Pharm. Anal.*, 2014, **6**, 165–170.
40 M. Avrami, *J. Chem. Phys.*, 1939, 7, 1103–1112.
41 M. Avrami, *J. Chem. Phys.*, 1940, **8**, 212–224.
42 W. Johnson and R. Mehl, *Am. Inst. Min. Metall. Eng.*, 1939, **135**, 416–458.
43 A. Kolmogorov, *Bull. Acad. Sci. USSR, Ser. Math.*, 1937, **3**, 355–359.
44 A. Burbelko, E. Fras and W. Kapturkiewicz, *Mater. Sci. Eng., A*, 2005, **413**, 429–434.
45 P. D. Martino, G. F. Palmieri and S. Martelli, *Pharmazie*, 2000, **55**, 625–626.
46 A. Gorniak, A. Wojakowska, B. Karolewicz and J. Pluta, *J. Therm. Anal. Calorim.*, 2011, **104**, 1195–1200.
47 J. Blàzquez, C. Conde and A. Conde, *Int. J. Therm. Sci.*, 2015, **88**, 1–6.
48 R. F. Henry, G. Z. Zhang, Y. Gao and I. S. Buckner, *Acta Crystallogr., Sect. E: Struct. Rep. Online*, 2003, **59**, 699–700.
49 A. Guinier, *X-Ray Diffraction: In crystals, imperfect crystals, and amorphous bodies*, W. H. Freeman and company, 1963.
50 S. E. Keinath, R. L. Miller and J. K. Rieke, *Order in the "amorphous" state of polymers*, Plenum Press, 1985.
51 J. Kusz, M. Zubko, A. Fitch and P. Gutlich, *Z. Kristallogr.*, 2011, **226**, 576–584.
52 K. Norrish and R. M. Taylor, *Clay Miner.*, 1962, **5**, 98–109.
53 W. Kob, C. Donati, S. Plimpton, S. Poole and P. Glotzer, *Phys. Rev. Lett.*, 1997, **79**, 2827–2830.
54 K. Grzybowska, S. Capaccioli and M. Paluch, *Adv. Drug Delivery Rev.*, 2016, **100**, 100–158.
55 G. Szklarz, K. Adrjanowicz, M. Dulski, J. Knapik and M. Paluch, *J. Phys. Chem. B*, 2016, **120**, 11298–11306.
56 S. F. Swallen and M. D. Ediger, *Soft Matter*, 2011, **7**, 10339.
57 K. Adrjanowicz, K. Kaminski, Z. Wojnarowska, M. Dulski, L. Hawelek, S. Pawlus and M. Paluch, *J. Phys. Chem. B*, 2010, **114**, 6579–6593.
58 K. Adrjanowicz, K. Kaminski, M. Paluch and K. Niss, *Cryst. Growth Des.*, 2015, **15**, 3257–3263.
59 G. K. Balendiran, N. Rath, A. Kotheimer, C. Miller, M. Zeller and N. P. Bath, *J. Pharm. Sci.*, 2012, **101**, 1555–1569.
60 W. Ostwald, *Z. Phys. Chem.*, 1987, 22, year.
61 M. H. Jensen, C. Alba-Simionesco, K. Niss and T. Hecksher, *J. Phys. Chem.*, 2015, **143**, 134501.
62 E. Kaminska, M. Tarnacka, P. Wlodarczyk, K. Jurkiewicz, K. Kolodziejczyk, M. Dulski, D. Haznar-Garbacz, L. Hawelek, K. Kaminski, A. Wlodarczyk and M. Paluch, *Mol. Pharmaceutics*, 2015, **12**, 3007–3019.
63 J. W. Mullin, *Crystallization*, Butterworth Heinemann, 4th edn, 2001.

Dr inż. Karolina Jurkiewicz
Instytut Fizyki, Uniwersytet Śląski w Katowicach
Zakład Biofizyki i Fizyki Molekularnej
ul. 75 Pułku Piechoty 1A
41-500 Chorzów

Chorzów, 17.07.2018 r.

OŚWIADCZENIE

Oświadczam, że w pracy:

1. G. Szklarz, K. Adrjanowicz, J. Knapik-Kowalczuk, K. Jurkiewicz and M. Paluch, *Crystallization of supercooled fenofibrate studied at ambient and elevated pressures*, Phys. Chem. Chem. Phys., 2017, 19, 9879–9888, DOI: 10.1039/C7CP00823F

mój wkład polegał na wykonaniu pomiarów rentgenowskiej dyfraktometrii proszkowej (XRPD) oraz analizy otrzymanych dyfraktogramów.

Karolina Jurkiewicz

1

A3. Confinement-induced changes in the glassy dynamics and crystallization behavior of supercooled fenofibrate

Autorzy: G. Szklarz, K. Adrjanowicz, M. Tarnacka, J.Pionteck, M. Paluch
Referencja: J. Phys. Chem. C 2018, 122, 1384–1395
Impact Factor czasopisma z roku opublikowania pracy: **4.536**
Liczba punktów ministerialnych MNiSW czasopisma (2016): **35**
DOI: 10.1021/acs.jpcc.7b10946

Mój udział w poniższym artykule polegał na przygotowaniu próbek do pomiarów, przeprowadzeniu pomiarów dielektrycznych, analizie i opracowaniu wyników pomiarów oraz na przygotowaniu manuskryptu. Wkład pozostałych współautorów zamieszczono w formie oświadczeń.

THE JOURNAL OF PHYSICAL CHEMISTRY C

Article

Cite This: J. Phys. Chem. C 2018, 122, 1384−1395

pubs.acs.org/JPCC

Confinement-Induced Changes in the Glassy Dynamics and Crystallization Behavior of Supercooled Fenofibrate

Grzegorz Szklarz,*[,†,‡] Karolina Adrjanowicz,*[,†,‡] Magdalena Tarnacka,[†,‡] Jurgen Pionteck,[§] and Marian Paluch[†,‡]

[†]Institute of Physics, University of Silesia, ulica 75 Pulku Piechoty 1, 41-500 Chorzow, Poland

[‡]Silesian Center for Education and Interdisciplinary Research (SMCEBI), ulica 75 Pulku Piechoty 1a, 41-500 Chorzow, Poland

[§]Leibniz Institute of Polymer Research Dresden, Hohe Str. 6, D-01069 Dresden, Germany

ABSTRACT: Here, we have studied the effect of spatial restrictions on the molecular dynamics and crystallization behavior of modeled lipophilic drug fenofibrate incorporated into nanoporous aluminum oxide membranes of different pore size. Our measurements demonstrate that, on subsequent cooling, dynamics of confined liquid split up into two distinct fractions, due to the presence of core and interfacial layers. At the temperature, at which vitrification of the interfacial layer takes place ($T_{g\_interface}$), departure from the bulk-like behavior occurs, and molecules in the center of the pores enter quasi-isochoric conditions. Depending on the thermal protocol and pore size, the volume fixed at $T_{g\_interface}$ might be a bit different so as the core liquid's dynamics. Interestingly, below that temperature, the nanoconfined liquid can still obey the fundamental density scaling relation ($1/TV^{\gamma}$), just like in the bulk phase, while not necessarily isochronal superposition. This is in contrast to a common observation that the validity of the density scaling in bulk glass-forming systems always goes together with isochronal superposition of the α-relaxation, and vice versa. Finally, our careful analysis of the crystallization kinetics as a function of lowering pore diameter indicates for systematic slowing down crystallization progress, the shift of the maximum crystallization rate toward higher undercooling and decrease in the dimensionality of growing crystals.

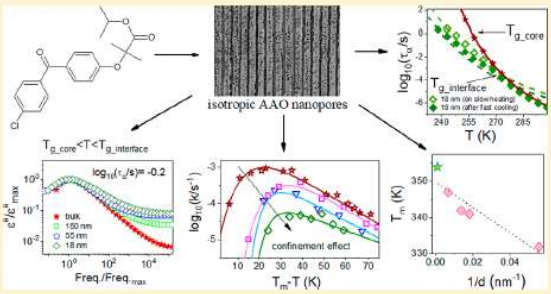

INTRODUCTION

Understanding the behavior of soft matter in hard confinement has a fundamental meaning in physics and numerous technological applications.[1−4] When spatial limitations reach a nanoscale level, we typically observe dramatic changes in the molecular dynamics and phase transition behavior. For molecular liquids confined to cylindrical nanopores, this is reflected in a downward shift of the glass transition and melting temperatures, as compared to the bulk.[5,6] In geometrical nanoconfinement, interfacial interactions in close vicinity of the hard pore walls start to play an extremely important role. This leads to the formation of a molecular layer with reduced mobility in comparison to molecules in the center of the pore. On subsequent cooling, these two fractions of molecules vitrify at different temperatures, roughly with a gap of 25−45 K depending on the pore diameter.[7,8] Recently, it was demonstrated that vitrification of the interfacial layer has a significant impact on the core dynamics leading to a pronounced departure from the bulk-like behavior of the α-relaxation time, which starts to follow quasi-isochoric dependences.[9,10] Such conditions when one fraction of the molecules becomes already immobilized while the other one can still relax/move on experimental time scale offer a unique opportunity to study an out-of-equilibrium glassy dynamics.[11] Here, in contrast to typical aging experiments carried out in bulk glasses, equilibrium recovery during the course of physical aging is probed via changes in the core dynamics, which in turn is strongly affected by already vitrified interfacial layer.

At first sight, dynamics of viscous liquid confined in nanopores seems to be much different from the bulk behavior. However, our recent experimental results[12] demonstrate that confined liquid, same as the bulk fluid, obeys the density scaling idea, which assumes that the dynamics in supercooled liquids can be described through a single scaling relation, $1/TV^{\gamma}$, where γ is a material constant.[13−15] Since the value of the scaling parameter seems to be insensitive to geometrical confinement, we can describe evolution of the α-relaxation time at varying thermodynamic conditions (T, p) for a bulk liquid phase based on its behavior at the nanoscale confinement, and vice versa.[12]

Geometrical nanoconfinement also affects the overall crystallization behavior of the molecular glass-formers and provides an opportunity to examine liquid−crystal phase transformations at the length scale corresponding to the critical nucleus size, where thermodynamic aspects related to the crystallization event may change dramatically, thus providing new approaches

Received: November 6, 2017
Revised: December 7, 2017
Published: December 7, 2017

DOI: 10.1021/acs.jpcc.7b10946
J. Phys. Chem. C 2018, 122, 1384−1395

to control polymorphism, crystallization tendency, or crystal properties.[16] The most characteristic confinement effect on crystallization in nanopores is a shift of the melting point, being either negative (more common) or positive in sign.[6,17] Such effect is often explained by taking into account interfacial interactions, specific surface energy, or varying pore geometry.[6] With lowering pore diameter, changes in the crystallization mechanism were also observed from predominantly a heterogeneous to the homogeneous one.[18,19] In addition to that, in highly ordered, non-cross-linking cylindrical nanopores, only specific crystal orientations are preferred instead of nuclei randomly growing in different directions. This might alter the crystalline structure and, in consequence, affect, e.g., ferroelectric properties of some copolymers.[20] All the above indicate that nonporous environment enables to change/control the crystallization outcome from the very early stages of the crystallization process.

In this work, we examine the effect of geometrical nanoconfinement provided by nanoporous alumina on the dynamics and crystallization tendency of molecular glass-former, fenofibrate, known mostly for its pharmaceutical activity (cholesterol reducing agent). For that purpose, a combination of dielectric and calorimetric techniques were employed. In line with our recent finding, we focus particular attention on testing the validity of the density scaling relation and isochronal superposition for nanoconfined liquid. We found that within the temperature range between vitrification of the interfacial layer ($T_{g\_interface}$) and molecules in the core (T_{g_core}) confined liquid might fulfill the density scaling relation, while not necessarily isochronal superposition for the α-relaxation. This stands in contradiction to theoretical expectations and experimental evidence reported for glass-forming liquids in the bulk phase, where these two features always go together.[21−23] Thus, if one fails, the other fails too. Since control over crystallization behavior of amorphous fenofibrate, but also many other amorphous pharmaceutical compounds, is of great interest in developing modern drug delivery systems,[24,25] we demonstrate fundamental changes in the overall crystallization kinetics of the investigated material incorporated to alumina nanopores of different pore sizes. In a broad sense, crystallization plays a critical role in science and technology.[26−28] Thus, a better knowledge of the crystallization habits of molecular glass-formers under geometrical confinement is essential to develop strategies allowing to produce new materials with tailored-made structure and properties. Hopefully, further information obtained from this study will be useful to understand better the effect of spatial restrictions on the nanometer scale on the crystallization progress of the molecular liquids.

■ EXPERIMENTAL SECTION

Materials. Fenofibrate ($C_{20}H_{21}ClO_4$, molar mass 360.831 g/mol) of 99% purity was purchased from Sigma-Aldrich as a white crystalline powder and used without further purification. The chemical structure of the investigated material can be found elsewhere.[29] The melting point of a stable crystalline form of fenofibrate (form I) is T_m = 354 K, while its glass transition temperature T_g = 254 K (based on calorimetric data).[30] As nanoporous templates, we used commercially available anodized aluminum oxide (AAO) membranes (Synkera Technologies, Inc.) composed of uniform arrays of unidirectional and non-cross-linking pores of different sizes (18, 55, 73, 100, and 150 nm). Before filling, the AAO membranes were dried in an oven at 423 K under vacuum to remove any volatile impurities from the nanochannels. Then, we have used them as confining matrices for fenofibrate. Filling of the nanopores proceeded by capillary action at 354 K under vacuum (10^{-2} bar) for more than 2 weeks. Every few days, infiltrated fenofibrate AAO templates were brought to ambient temperature, and their upper and bottom surfaces were carefully cleaned with Kimtech wipes and weighted. To ensure complete filling, the infiltration procedure was repeated until no changes in mass of the filled membranes were observed. Typically, we get a sample mass of ∼3.37 mg (150 nm), ∼1.67 mg (100 nm), ∼1.16 mg (73 nm), ∼1.45 mg (55 nm), and ∼1.65 mg (18 nm). By taking into account porosity of AAO templates (from 35% in 150 nm to 10% in 73 nm) and the density of the bulk material, this procedure ensures nanopore filling of more than 90%.

Methods. *Dielectric Measurements.* Complex dielectric permittivity was measured by using a Novocontrol Alpha-A and Beta analyzers. AAO templates filled with fenofibrate were placed between two circular electrodes and measured as a function of temperature in the frequency range of 10^{-2}−10^{6} Hz. Such nanoporous membranes are typically produced in the form of round discs (13 mm diameter, 50 μm thick). Each of such discs contains uniform non-cross-linking cylindrical pores that are aligned perpendicular to the surface of the material and penetrate its entire thickness. The pore channels are aligned parallel to each other. Upon dielectric measurements, such nanochannels with a liquid confined inside act as small capacitors connected parallel. Dielectric contribution coming from AAO membrane itself is negligibly small in comparison to dielectric permittivity response of the confined liquid. It gives almost a frequency- and temperature independent-flat line with no signs of any relaxation processes. The temperature was controlled with stability better than 0.1 K by a Quatro Cryosystem. To study dynamics of confined fenofibrate, we have employed two different thermal protocols: (i) fast cooling (∼10−12 K/min) of the confined material from the melting temperature down to the glassy state, followed then by slow heating with a rate of 0.5 K/min, or (ii) slow cooling of the confined material (0.5 K/min) all the way down from the melting temperature to the glassy state. For crystallization experiment, thermal protocol involved cooling (at a rate of 10 K/min) of the confined material from melting temperature down to the desired crystallization temperature. Then, time-dependent dielectric measurements were performed in the temperature range from 278 to 328 K. After crystallization, the temperature was slowly increased to detect the melting temperature of the sample confined at nanopores of different pore sizes.

DSC Measurements. Calorimetric measurements were carried out by Mettler-Toledo DSC apparatus equipped with a liquid nitrogen cooling accessory and an HSS8 ceramic sensor (heat flux sensor with 120 thermocouples). Temperature and enthalpy calibrations were performed by using indium and zinc standards. The sample was prepared in an open aluminum crucible (40 μL) outside the DSC apparatus. For that purpose, nanoporous membranes filled with investigated materials were crashed to powders. Samples were scanned at heating/cooling rates of 5 and 10 K/min over a temperature range from 175 to 363 K. Each measurement at a given temperature was repeated three times. T_g values were determined as the point corresponding to the midpoint inflection of the extrapolated onset and the end of the transition curve, while T_m as the onset point of the endothermic peak in DSC curve. To study the effect of density equilibration, time-dependent measurements were performed at temperatures located within $T_{g\_core} < T < T_{g\_interface}$.

DOI: 10.1021/acs.jpcc.7b10946
J. Phys. Chem. C 2018, 122, 1384−1395

In this case, confined to AAO nanopores, fenofibrate was quenched to 173 K ($T < T_{g\_core}$) and then heated up with the rate of 10 K/min to a given aging temperature (T_{aging} = 258 K for 150 nm, T_{aging} = 258 K for 73 nm, T_{aging} = 253 K for 18 nm). At this temperature, it was held for 3 h and then cooled back to 173 K and scanned with the rate of 10 K/min up to 363 K.

Volumetric Measurements. Pressure−volume−temperature (PVT) measurements were performed using a Gnomix dilatometer operating within the range of pressure from 10 to 200 MPa. The sample (~1.5 g) was embedded in a nickel foil and then immersed in mercury, which was used as a confining fluid. Measurements of the specific volume changes in the liquid state were performed upon cooling/heating runs (2.5 K/min) within the temperature range of 488 to 326 K at a fixed pressure ranging from 10 to 200 MPa with 10 MPa interval. Since some slight recrystallization signatures were observed upon heating at 60 and 180 MPa, only data recorded on downward runs were used in further analysis, i.e., to parametrize $V(T, p)$ behavior in the liquid phase of fenofibrate using the Tait equation of state. Please note that the PVT measurements were carried out far above the glass transition temperature of fenofibrate (T_g = 254 K at 0.1 MPa, T_g = 290.5 K at 200 MPa, based on dielectric data).[29]

RESULTS AND DISCUSSION

Effect of Confinement on Glassy Dynamics. In Figure 1a−c, we show representative thermograms obtained for fenofibrate confined in AAO nanopores of different pore sizes. Two endothermic peaks denote vitrification of the interfacial layer at $T_{g\_interface}$ and molecules in the core (at T_{g_core}), as commonly explained by the two-layer model.[8] Both events were found to show a characteristic signature of the glass-transition, i.e., cooling rate dependence. With increasing cooling rate, the glass-transition temperature typically shifts to a higher temperature.[31] In agreement with literature reports,[6,12,32,33] we also found that T_{g_core} decrease with decreasing pore diameter. However, $T_{g\_interface}$ shows much weaker pore size dependence. The difference between values of both glass transition temperatures changes from $\Delta T = T_{g\_interface} - T_{g\_core}$ = 25 K in 150 nm pores to ΔT = 37 K in 18 nm. Such scenario when $T_{g\_interface} > T_{g\_bulk}$ while $T_{g\_core} < T_{g\_bulk}$ is typically observed for non-hydrogen bonded liquids shows weak interaction with the pore walls. DSC thermograms recorded for bulk fenofibrate (T_g = 254 K) can be found elsewhere.[30]

The thickness of the interfacial layer can be calculated as $d[1 - (1 - \Delta C_{p,interface}/\Delta C_{p,total})^{1/2}/2]$ where d is pore diameter and the total heat capacity change is $\Delta C_{p,total} = \Delta C_{p,interface} + \Delta C_{p,core}$.[8] In Figure 1d, we plot it as a function of pore radius. As can be seen, the thickness of the interfacial layer increases almost linearly with increasing pore diameter and does not show any cooling rate dependence (cooling with 5 and 10 K/min results in the same thickness). Obtained values are comparable to those found for other glass-forming materials confined to AAO templates (e.g., PMMA,[7] salol,[9] or PPG[34]), but much higher than those obtained for small organic molecules confined to controlled pore glass (CPG), ~1.2−2.5 nm.[8,35] It is also worth to note that, while the thickness of the interfacial layer seems to be the same in CPG material of different pore sizes, in our case, it shows a clear pore size dependence.

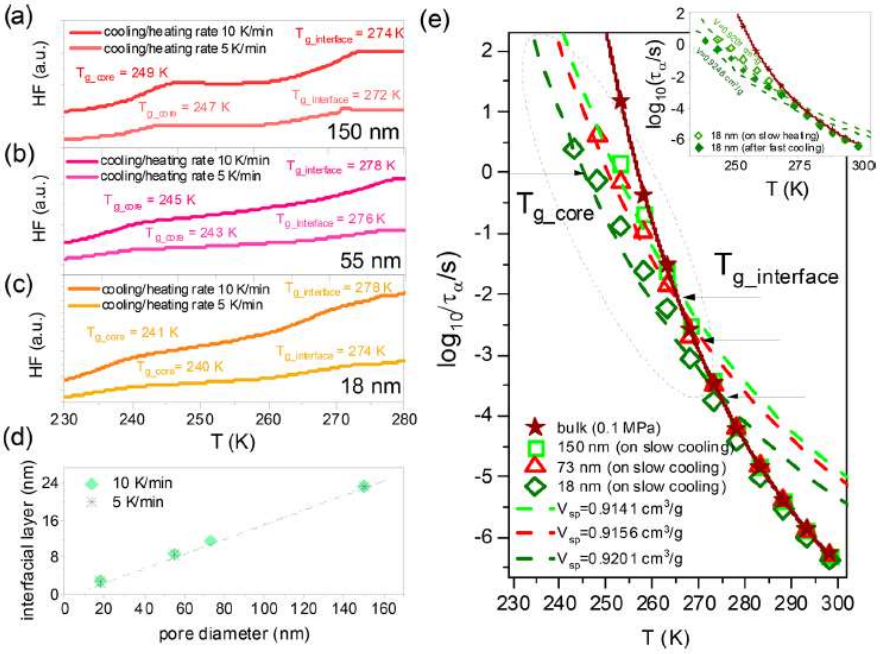

Figure 1. DSC thermograms obtained for fenofibrate confined to (a) 150, (b) 55, and (c) 18 nm AAO nanopores. (d) Change of the interfacial layer thickness as a function of pore diameter. (e) Temperature evolution of α-relaxation times for fenofibrate in bulk and confined to nanopores of different pore sizes. Dielectric data were recorded on slow cooling (1 K/min). The solid line denotes the VFT fit of the α-relaxation time for the bulk liquid, whereas dashed lines are isochoric dependences of α-relaxation times determined based on the high-pressure dielectric relaxation and PVT data. The inset shows a comparison of $\tau_\alpha(T)$ dependences obtained for fenofibrate in 18 nm pores depending on the thermal protocol. The two different protocols are either slow cooling with the rate of 1 K/min or fast cooling with 10−12 K/min well below the glass transition (measured on reheating). For both samples, the α-relaxation times measured within T_{g_core} and $T_{g\_interface}$ are described by slightly different isochores.

DOI: 10.1021/acs.jpcc.7b10946
J. Phys. Chem. C 2018, 122, 1384−1395

However, the calculated ratio between the pore diameter and its interfacial layer thickness is almost the same (150 nm, −6.4; 55 nm, −6.2; 18 nm, −6.4). A very similar finding was also found for salol in AAO nanopores.[9] So, although the thickness of interfacial layer decreases with decreasing pore diameter, it remains practically the same in comparison to the pore diameter. Taking into account the above results, it becomes evident that the strength of the interactions between pore walls and molecules in its close vicinity determines the thickness of the interfacial layer. These two seem to be completely different in AAO and CPG nanopore environments.

In Figure 1e, we show the temperature dependence of the α-relaxation time for fenofibrate confined within AAO nanopores. For the sake of clarity, dielectric results obtained at 150, 73, and 18 nm pores are only presented. As can be seen, the temperature dependence of τ_α in AAO nanopores follows bulk-like behavior at high temperatures. However, as temperature and pore size decreases, dynamics of the nanoconfined liquid becomes progressively faster compared to the bulk and departs from the VFT law. Similar results were also observed for a number of glass-forming materials confined to nanopores.[36,37] Based on previous results,[9,10,12] we associate the temperature at which a characteristic deviation from the bulk-like dynamics occurs to vitrification of the interfacial layer. The liquid in the center of the pores vitrifies at much lower temperature. Here, in order to avoid extrapolation of the $\tau_\alpha(T)$ dependence to 100 s, we set T_{g_core} to be the temperature at which τ_α = 1 s. The inset in Figure 1e demonstrates that the temperature dependence of α-relaxation time measured within T_{g_core} and $T_{g\_interface}$ depends on the thermal protocol. Slow cooling with the rate of 1 K/min results in vitrification of the interfacial layer at slightly lower temperature, compared to sample being previously cooled down from the melting temperature with the rate of 10−12 K/min. Recently, we have demonstrated that at $T_{g\_interface}$ the volume of the confined liquid becomes frozen, and starting from that temperature, the α-relaxation dynamics of the core molecules enters the isochoric conditions (V = const.).[10,12] Thus, each $\tau_\alpha(T)$ dependence measured in AAO nanopores within T_{g_core} and $T_{g\_interface}$ represent certain isochore. This picture will not qualitatively change if we start to vary with the thermal history of the confined material. In such case, the volume fixed at $T_{g\_interface}$ will be slightly different, but still, the behavior of $\tau_\alpha(T)$ below that temperature will follow isochoric dependences (though not identical).

To explore this aspect, we show in Figure 1e (as dashed lines) isochores that were used to describe the temperature dependences of α-relaxation time for confined fenofibrate. Such procedure takes the advantages of utilizing high-pressure results obtained for bulk fenofibrate and will be described in more details just below. For that, dielectric relaxation studies at varying (T, p) conditions[29] as well as PVT measurements are needed. In Figure 2a, we show representative changes of the specific volume for investigated liquid as a function of temperature and pressure. To parametrize obtained $V_{sp}(T, p)$ dependence, the Tait equation of state was employed[38]

$$V(T,p) = (V_0 + V_1T + V_2T^2)\left[1 - 0.0894\ln\left(1 + \frac{p}{b_0\exp(-b_1T)}\right)\right] \quad (1)$$

where T is temperature in Celsius degrees and p is a pressure in megapascals. Simultaneous fitting analysis of all cooling isobars yields the following set of parameters: V_0 = 0.91858 cm^3/g, V_1 = 6.2885 × 10^{-4} cm^3/(°C g), V_2 = 4.07295 × 10^{-7} cm^3/(°C^2 g), b_0 = 245.37905 MPa, and b_1 = 0.00519 °C^{-1}. Having PVT data parametrized, we can convert experimentally measured $\tau_\alpha(T, p)$ dependences to $\tau_\alpha(T, V)$ ones. In the next step, to describe evolution of τ_α in a T−V plane, the modified temperature−volume version of the Avramov model was used[39]

$$\log\tau(T,V) = A + \left(\frac{B}{TV^\gamma}\right)^D \quad (2)$$

where A, B, D, and γ are fitting parameters. The two-dimensional surface described with the set of following fitting parameters γ = 4.33363, D = 5.19385, B = 256.53745, and A = −8.24192 is presented for fenofibrate in Figure 2b. From that, one can easily determine isochoric relaxation times for bulk liquid. Then, by extrapolating obtained dependences from the positive range of pressure to the negative pressure domain, it is possible to describe the behavior of α-relaxation times in confined geometry.

As can be seen in Figure 1e, with decreasing pore diameter the volume fixed at $T_{g\_interface}$ increases (so paradoxically, the density of confined material decreases with increasing confinement). It is also worth to note that, depending on the thermal protocol, $\tau_\alpha(T)$ dependences measured within T_{g_core} and $T_{g\_interface}$ are described by slightly different isochoric curves (see again the inset in Figure 1e). This is due to the fact glass transition event is in general a kinetic phenomenon. Thus, depending on the cooling rate, the liquid volume corresponding to $T_{g\_interface}$ will change too. Slow cooling results in lowering both $T_{g\_interface}$ and the value of the specific volume that becomes fixed below that temperature, whereas upon fast quenching the interfacial layer vitrifies at a slightly higher temperature and somewhat higher volume. For fenofibrate confined in 18 nm pores, the density difference at $T_{g\_interface}$, generated either by slow cooling or fast quenching, is approximately 0.5%. Except for cooling rate dependence, confined liquid in AAO nanopores shows just below $T < T_{g\_interface}$, direct evidence of the physical aging phenomenon, considered as another characteristic signature of out-of-equilibrium glassy dynamics. We will discuss this effect later on.

The next step of our study involves testing the density scaling idea for fenofibrate confined to AAO nanopores. Herein, it is worth to note that superimposing the dynamic properties (viscosity, α-relaxation time, or diffusion coefficient) onto one single curve when plotted as a function of $1/TV^\gamma$ is considered as one of the most significant achievements in the high-pressure studies of glass-forming materials.[13,14,25,26,40] In agreement with our recent finding,[12] the universal character of such scaling relation can be extended from the bulk phase to 2D nanoconfinement, while the unchanged value of the material constant γ provide a link between the dynamics of glass-forming liquid at the macro- and nanoscales. The validity of the density scaling, for fenofibrate, is presented in Figure 2c, showing that all isobaric and isothermal dependences measured on increased pressure as well as those in AAO nanopores collapse when the scaling parameter is adjusted to γ = 4.3. Since investigated material lacks any strong intermolecular hydrogen bond, the quality of the density scaling as well as the value of γ parameter are similar to that reported for van der Waals liquids like OTP (4), methyl ketoprofen (4.7),[41] or dimethyl phthalate (3.9). Thus, our results serve as another evidence that the density scaling idea can, indeed, apply to nanoconfined liquid the same as for bulk material. Qualitatively, changes in the thermal protocol, e.g., quench of the liquid in the pores instead of its

DOI: 10.1021/acs.jpcc.7b10946
J. Phys. Chem. C 2018, 122, 1384−1395

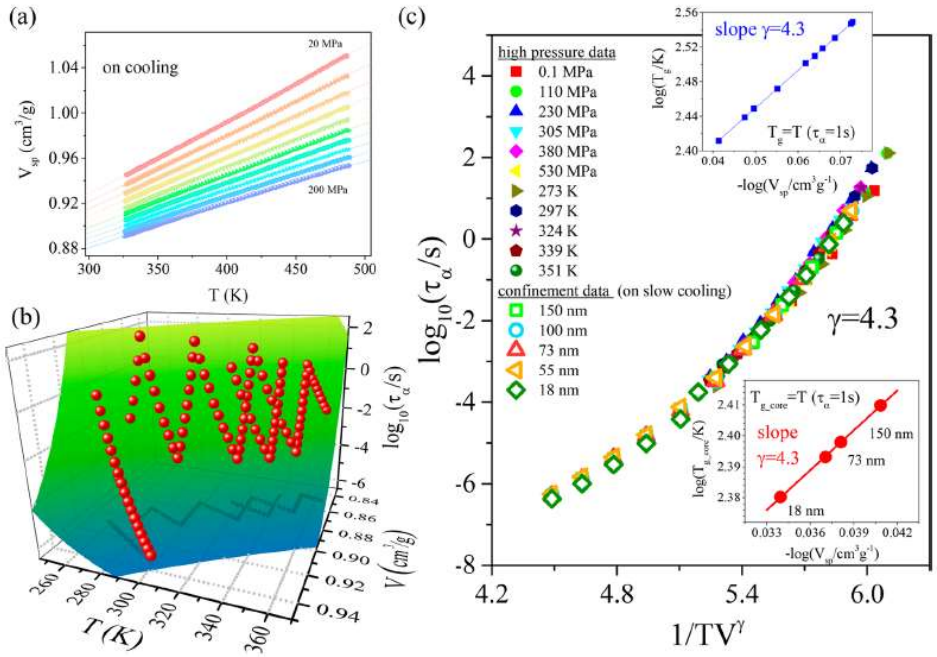

Figure 2. (a) Temperature dependence of specific volume for various isobars measured in the liquid state of fenofibrate in the pressure range of 20−200 MPa (with the step of 20 MPa). Solid lines represent the best fits to the Tait eq (eq 1). (b) α-relaxation time plotted as a function of temperature and volume. The two-dimensional surface was determined using the modified Avramov equation. (c) Density scaling of α-relaxation time for fenofibrate that includes isobaric and isothermal data taken from high-pressure studies as well as those measured in the nanoconfinement. The single scaling parameter γ = 4.3 is able to superimpose the relaxation time measured at various thermodynamic conditions. For fenofibrate confined in AAO nanopores, dielectric data included in the scaling plot are only those measured in the temperature range between T_{g_core} and $T_{g\_interface}$. The lower inset shows dependence of the glass-transition temperature T_{g_core} vs specific volume fixed at that temperature in double-logarithmic scale. A similar plot presented in the upper inset refers to high pressure data. The slope of $\log_{10}$ T_g ($\log_{10}$ V_g) dependence provides an alternative strategy to obtain the scaling parameter γ.

slow cooling, will not affect the density scaling in nanopores. In such case, the $\tau_\alpha(T)$ dependences obtained below $T_{g\_interface}$ will still become isochoric, but the system will adopt a bit different (isochoric) state.

For glass-forming liquids, which obeyed the density scaling, γ exponent can be determined from the linear regression of $\log(T_g)$ vs $\log(V_g)$ dependence, where T_g and V_g are glass transition temperature and volume, respectively.[42] Insets in Figure 2c show such plots separately for high-pressure and confinement data. It can be seen that obtained data are consistent and that both give a straight line with the slope 4.3. To avoid extrapolation, T_g values for compressed and confined fenofibrate were defined for temperatures at which τ_α = 1 s. Both R^2 values are 0.99994.

After validating the density scaling for the investigated sample, we move on to isochronal superposition. Isochronal superposition is a characteristic property of various glass-forming systems (excluded hydrogen bonded liquids), which implies that the shape of the relaxation function depends only on the average relaxation time and remains $T-p$ invariant along so-called isochrones.[25,26,43,44] In agreement with numerous high-pressure results, isochronal superposition and density scaling apply to a large class of liquids. Both features always go together and were explained in terms of the isomorph theory,[24,45] which predicts dynamic invariance along lines (isomorphs) in phase diagram for those systems that show strong potential energy−virial correlations. However, more recent evidence indicates that strong virial potential−energy correlations are not the necessary conditions to see in the phase diagram lines of invariant dynamics.[46]

In Figure 3, we have compared the shape of the α-relaxation spectrum at various isochronal states that were composed of dielectric data collected at different combinations of (T, p) or in nanopores of different pore sizes. Figure 3a demonstrates that below $T_{g\_interface}$ the distribution of the α-relaxation time in 18 nm pores depends on the thermal history. We found that the shape of the α-relaxation on the low-frequency side is much broader for the quenched sample. This effect becomes even more pronounced with lowering the temperature. The distribution of the relaxation time, while keeping the same peak maximum, $\log_{10}(\tau_\alpha/s) = -0.2$, also becomes systematically broader with lowering the pore diameter (see Figure 3b). This result provides clear evidence that isochronal superposition does not apply in this case, and what's more, it indicates increased local scale heterogeneity of the liquid dynamics in nanopores (especially low-frequency modes). This behavior can be explained by dynamic exchange the molecules between core molecules and interfacial molecules[47] or by exchange the relaxing molecules between unevenly relaxing clusters.[48] However, above $T_{g\_interface}$, i.e., in the bulk-like dynamic region, the shape of the α-relaxation peak is essentially invariant to confinement effect (see Figure 3c). Such divergence in the dynamics of fenofibrate confined in nanopores is very surprising finding that it raises very fundamental questions whether satisfying the density scaling law by a glass also entails the fulfilment of the isochronal superposition, and

DOI: 10.1021/acs.jpcc.7b10946
J. Phys. Chem. C 2018, 122, 1384−1395

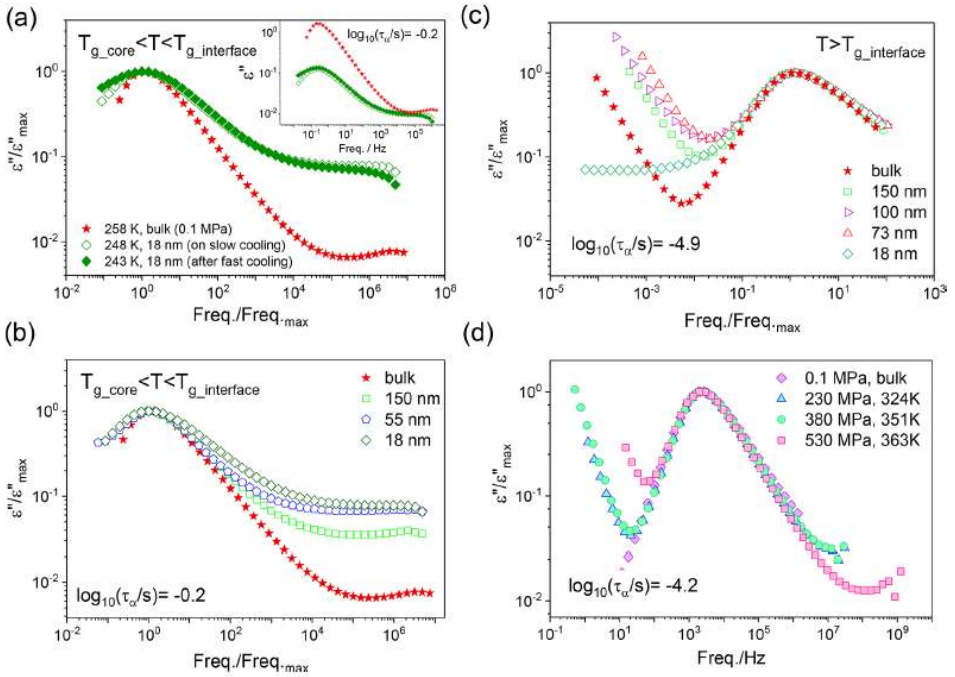

Figure 3. Comparison of the shape of the α-relaxation under isochronal conditions for fenofibrate confined in AAO templates (a) of 18 nm pore diameter depending on the thermal history of the sample. The inset shows raw dielectric data measured in the bulk and nanopores (within $T_{g\_core} < T < T_{g\_interface}$). Peak positions roughly match the same relaxation time, $\log_{10}(\tau_\alpha/s) = -0.2$. Confined in AAO nanopores (b) within temperatures $T_{g\_core} < T < T_{g\_interface}$ (isochrone $\log_{10}(\tau_\alpha/s) = -0.2$) and (c) $T > T_{g\_interface}$ (isochrone $\log_{10}(\tau_\alpha/s) = -4.9$) as obtained upon slow cooling (1−2 K/min) of the sample. Panel (d) shows dielectric spectra obtained for a bulk liquid at different combinations of temperature and pressure. All chosen spectra have approximately the same α-relaxation time, $\log_{10}(\tau_\alpha/s) = -4.2$.

vice versa; do these two always go together? To the best of authors knowledge, there are no single experimental data on glass-forming liquid for which the density scaling holds while the isochronal superposition does not, and vice versa. This, apparently, seems to be true only in case of bulk liquids. Fenofibrate, in general, follows quite nicely both rules as demonstrated in Figures 1e and 3d, respectively. However, when confined to nanometer pores, its dynamics obey within $T_{g\_core} < T < T_{g\_interface}$, the density scaling law, while not the isochronal superposition for the α-relaxation. Clearly, to have a better overlook of this finding, theoretical studies on dynamics of soft matter in the presence of geometrical confinement would be a great advantage.

As already noted, except of cooling rate dependence, another universal evidence of the glass transition is physical aging, which takes place below T_g. Upon this process, an out-of-equilibrium glass changes gradually its material properties (e.g., density, enthalpy, Young modulus, etc.), to reach an equilibrium configuration. For bulk liquids, when the glass-transition temperature is approached, the α-relaxation is far too slow to be directly probed in the dielectric experiment. Thus, typically, physical aging is followed by monitoring time-dependent changes in the dc-conductivity or secondary relaxation, which are believed to mimic the structural relaxation and sense volume changes that accompany equilibration process.[49,50] However, for the nanoconfined system, we can directly follow changes in the α-relaxation dynamics upon physical aging in an experimentally accessible frequency window. This is due to the fact that molecules in the interfacial layer vitrify at a much higher temperature as those located in the center of the pores. Here, we take advantage of the connection between both fractions of the molecules, as the freezing of the interfacial layer has still a significant impact on the core dynamics below $T_{g\_interface}$.

This we can observe in Figure 4a where time-dependent changes in the dielectric spectra of the fast quenched fenofibrate confined in the 18 nm pore at fixed temperature $T = 253$ K (i.e., $T < T_{g\_interface}$) are presented. Upon annealing, the α-relaxation peak shifts toward lower frequencies and approaches the position characteristic for the slowly cooled sample. In agreement with the results presented in the inset of Figure 1e, such equilibration process must be accompanied by densification of the confined material (when we approach the vitrification temperature of the interfacial layer via fast quench, the volume fixed at $T_{g\_interface}$ is higher than that on slow cooling). A similar finding was also reported for van der Waals liquids DC704 and 5PPE (see ref 12 and Supporting Materials therein). In addition to that, we would like to draw the reader's attention to the breadth of the α-relaxation peak which narrows with the aging time, indicating the approach of more homogeneous dynamics upon such process.

In analogy to dielectric aging experiments, we have also performed calorimetric studies upon which the sample was quenched with the rate of 10 K/min to $T < T_{g\_core}$ and then heated up and annealed for 3 h at a given temperature located within T_{g_core} and $T_{g\_interface}$. Comparison DSC thermograms recorded before and after annealing of fenofibrate confined to 150 nm AAO nanopores can be found in Figure 4b. As can be seen,

DOI: 10.1021/acs.jpcc.7b10946
J. Phys. Chem. C 2018, 122, 1384−1395

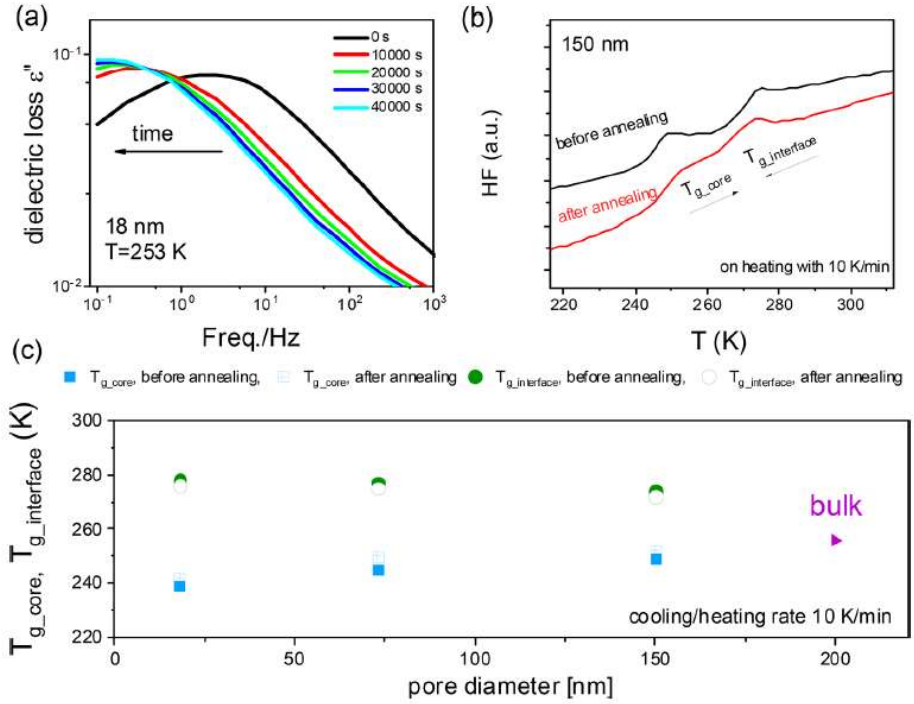

Figure 4. (a) Shift of the α-relaxation peak upon time-dependent measurements carried out at 253 K ($T_{g\_core} < T < T_{g\_interface}$) for quenched sample confined in 18 nm pores. (b) DSC thermograms recorded before and after 3 h annealing of fenofibrate incorporated to 150 nm pores at T = 258 K. (c) Changes in the glass transition temperatures for core and interfacial layers before (filled symbols) and after (open symbols) annealing of fenofibrate in nanopores of different pore diameters. In each case, annealing was carried out at temperatures located within $T_{g\_core} < T < T_{g\_interfac}$ (T = 253 K in 18 nm, 258 K in 73 nm, and 258 K in 150 nm). T_g value for bulk liquid serves as a reference.

calorimetric evidence of the equilibration process in nanoconfinement is the shift of T_{g_core} and $T_{g\_interface}$ toward higher and lower temperatures, respectively. Irrespective of the pore diameter, T_{g_core} increases roughly 3−4 K within 3 h of annealing; meanwhile, $T_{g\_interface}$ decreases by 2−3 K. A kind of similar shift (5−6 K in T_{g_core} and 1−2 K in $T_{g\_interface}$) was observed for triphenyl phosphite confined in alumina nanopores.[51] The results presented in Figure 4b,c demonstrate that the glassy dynamics related to the two fractions of the molecules in the nanopores approach each other on annealing. From that, we can make an even more surprising guess that the confinement effects observed below $T_{g\_interface}$ seems to be only a matter of time scale. So, infinitely long cooling rate or equilibration time might shift confined liquid dynamics back to the bulk-like behavior. The results obtained for fenofibrate are in line with our recent finding reported for van der Waals liquid, dimethyl pthathale, confined to alumina membranes, which prior to crystallization at $T < T_{g\_interface}$ show a pronounced shift of the α-relaxation time toward equilibrium/bulk behavior characteristic for a given temperature.[52] In this case, the initial value of the α-relaxation time for confined liquid does not exceed more than a few seconds, while the time needed to approach equilibrium takes days. In contrast, Li and co-workers have observed for PMMA confined in AAO nanopores that $T_{g,interface}$ increases and T_{g_core} decreases gradually with increasing annealing time, which was related to the transfer of the polymer chains from core volume to the interfacial layer.[7] Based on calorimetric data, the authors have also concluded that the distribution of relaxation times in the interfacial layer becomes broader during annealing and that the change in the dynamics of one fraction of the molecules in nanopores causes the variation of the other one. The latter finding that the interplay between core-interfacial structure determines the behavior of glass-forming liquids in confined geometry has also been disclosed from the present study.

Effect of Confinement on Crystallization. In the next step, we have studied the influence of two-dimensional nanoconfinement provided by AAO nanoporous membranes on the crystallization tendency of fenofibrate. In the bulk phase, fenofibrate reveals two polymorphs among which form I (T_m = 254 K) is the most stable one, while form II (T_m = 347 K) shows up only upon recrystallization of the glassy material.[53] The second polymorphic form is highly unstable and unwanted in pharmaceutical formulations. Thus, to avoid the formation of metastable form II, in this study, our thermal protocol has involved cooling of the confined liquid from the melting temperature to the desired crystallization temperature without approaching the glassy state. Crystallization kinetics of fenofibrate confined to AAO templates (pore sizes from 150 to 18 nm) was studied in a wide temperature range with the use of dielectric spectroscopy. Representative changes in the dielectric spectra and real and imaginary parts of complex dielectric permittivity, which accompany crystallization of fenofibrate in nanopores at 298 K, are given in Figure 5a,b, respectively. An observed drop of the strength of the α-relaxation upon time-dependent measurements signifies a systematic decrease of the liquid fraction. As the polarization response of the liquid phase comes mostly from the reorientational movements of the

DOI: 10.1021/acs.jpcc.7b10946
J. Phys. Chem. C 2018, 122, 1384−1395

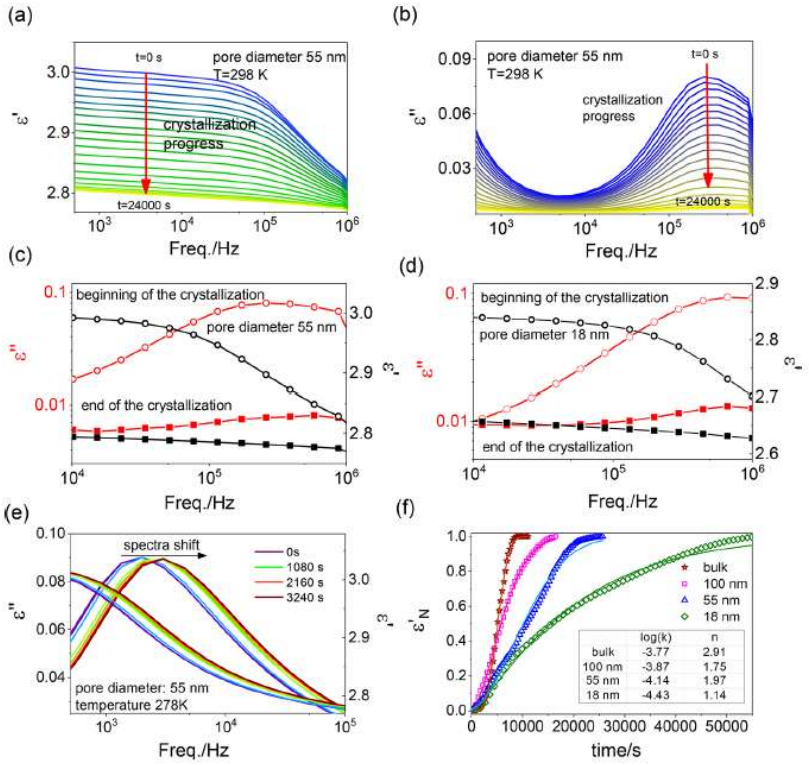

Figure 5. Frequency dependence of the (a) real and (b) imaginary parts of the complex dielectric permittivity ε^* collected upon crystallization of fenofibrate confined in 18 nm AAO pores at 298 K. Frequency dependent real (black) and imaginary (red) parts of the complex dielectric permittivity recorded at 298 K at the initial (open symbols) and final stages of the crystallization (filled symbols) of fenofibrate confined to (c) 55 nm and (d) 18 nm membranes. (e) Changes in the dielectric spectra recorded for fenofibrate confined in 55 nm pores before crystallization at 278 K. (f) Time evolution of normalized dielectric permittivity (ε'_N) for fenofibrate confined to nanoporous alumina of different pore diameter at 298 K. Solid lines denote fits of the experimental data to the Avrami equation.

molecules and the number of such actively reorientating dipolar species decreases with crystallization progress, we can follow the crystallization kinetics of the investigated sample via monitoring variation in the dielectric permittivity with time. From the analysis of the dielectric spectra recorded at the initial and final stages of the transformation process (see Figure 5c,d) we found that when crystallization of fenofibrate is carried out in nanochannels provided by AAO templates, it never ends up reaching 100% crystallinity (the α-relaxation is still detectable in the dielectric spectra even at the very final stages of crystallization process). Depending on the pore diameter, the residual liquid volume fraction varies from 2% in 150 nm pore to 10% in 18 nm pores. However, at the same temperature, bulk fenofibrate recrystallizes completely. We attribute the observed finding to spatial restrictions provided by nanoporous matrices, which hamper the crystallization of the investigated material. The other, very characteristic effect that accompanies crystallization of fenofibrate in AAO nanopores (but not in the bulk[30]) is the initial shift of the α-relaxation peak toward higher frequencies, as demonstrated in Figure 5e. We have noted that only after such equilibration process is completed, the actual crystallization of confined fenofibrate takes place. Recently, similar speeding up of the molecular motions before crystallization was observed for van der Waals liquid, dimethyl phthalate confined to nanoporous alumina.[52]

To get insight into the crystallization kinetics of fenofibrate incorporated to AAO nanopores, we have conducted time-dependent studies under isothermal conditions, covering a broad temperature range, from low to high undercoolings. Crystallization progress was monitored by following changes in the static dielectric permittivity for the selected frequency (but always within the low-frequency region), which were then normalized according to the following formula

$$\varepsilon'_N(t) = \frac{\varepsilon'(t=0) - \varepsilon'(t)}{\varepsilon'(t=0) - \varepsilon'(t=\infty)} \quad (3)$$

where $\varepsilon'(t)$ is the value of the static dielectric permittivity for the selected frequency at a given time t, $\varepsilon'(t=0)$ is the value of the static dielectric permittivity for the same selected frequency at the beginning of the crystallization, and $\varepsilon'(t=\infty)$ is the long-time limiting value. The lower (=0) and upper (=1) limits of the normalized dielectric permittivity signifies no crystallinity and completed crystallization, respectively. As the initial value of the static permittivity at a given temperature, we use ε' for the fully equilibrated sample (i.e., after the α-peak shift). Due to incomplete crystallization in nanopores, we estimate $\varepsilon'(t=\infty)$ by using the value of ε' from the high-frequency region at the final transformation time. Representative crystallization kinetic curves obtained for fenofibrate crystallizing at 298 K inside AAO nanopores are depicted in Figure 5f. It is evident that with

DOI: 10.1021/acs.jpcc.7b10946
J. Phys. Chem. C 2018, 122, 1384−1395

lowering the pore diameter crystallization progress at a fixed temperature significantly slows down. In 18 nm nanopores, crystallization time is more than five-fold longer than in bulk. Further analysis is based on the Avrami equation,[54,55] which describes the transformed crystalline volume fraction via

$$V \equiv \varepsilon'_N(t) = 1 - \exp(-kt^n) \quad (4)$$

where k is the rate constant and n is the Avrami parameter. Crystallization rate k contains combined information on the rates of nucleation N and crystal growth G, as $k = NG^{n-1}$, whereas the Avrami parameter provides information on both the dimensionality of growing crystals (growth in one, two or three dimensions) and time dependence of the nucleation process (nucleation event can be instantaneous or sporadic with the number of nuclei linearly increasing with time). As can be seen in Figure 5f, the Avrami equation provides quite a good description of the experimental data. From the fitting parameters, we get that confinement of fenofibrate in AAO nanopores slows down crystallization time and reduces the Avrami exponent relative to the bulk.

To have a better overlook on this finding, we have carried out crystallization kinetics studies not only as a function of lowering pore diameter but also the temperature, covering more than 70 K in the supercooled liquid regime. Figure 6a demonstrates changes in the crystallization rate for bulk and confined fenofibrate. As can be seen, when crystallization rate is plotted versus temperature, it shows a maximum (obviously being an outcome of the nucleation and crystal growth rates maxima). The location of the maximum crystallization rate shifts toward lower temperature with lowering the pore size, and its intensity decreases considerably. Since the melting temperature also changes with the pore diameter, a more qualitative comparison of obtained crystallization data is given in Figure 6b,c, where the variation of k and n is plotted versus reduced temperature, $T_m - T$. Now, it is more evident that with lowering the pore size the maximum of the crystallization rate shifts toward high undercoolings, i.e., away from the melting temperature. We also note that k seems to have much weaker temperature dependence as the pore sizes decrease. Inside 18 nm pores, k varies at most 0.5 decades over 50 K change in temperature, whereas in the bulk the same variation in the temperature affects the crystallization rate by more than two decades. Confinement effect is also responsible for a pronounced drop of the Avrami parameter from the value close to 3, which is characteristic for fenofibrate crystallizing from the bulk liquid phase to $n \cong 1$ when confined in 18 nm pores. The value of the Avrami parameter close to 3 suggests that the spherical crystals grow in three-dimensions. In turn, when n approaches 1, crystallites most likely will adopt a rod-like morphology (alongside the pore walls) and grow from instantaneous nuclei. This effect seems to be a common feature for all glass-forming materials crystallizing inside cylindrical shape nanopores[19,52,56] and indicates that under 2D-nanoconfinement the crystal growth is drastically hampered by the spatial constraints. By looking at the results presented in Figure 6c, we also note that the value of the Avrami parameter is determined in principle by the pore size, while it does not show a pronounced temperature dependence.

The two most pronounced confinement effects on crystallization, i.e., the shift of the crystallization maximum toward lower temperatures (higher undercooling) and reduced value of the Avrami parameter, signify fundamental changes in the nucleation mechanism. As suggested in the literature, with lowering pore diameter, nucleation is predominantly homogeneous.[19,56−58] Such a change in the nucleation character from heterogeneous to homogeneous results in nuclei of sufficiently small size that can be estimated from the following equation:[59]

$$r_c = \frac{2\sigma T_m}{\Delta H_m \rho_c \Delta T} \quad (5)$$

where ΔH_m is latent heat of fusion, T_m is the equilibrium melting temperature, ρ_c is the crystal density (= 1.18 g/cm^3 for fenofibrate), σ is the surface energy ($\cong$ 15 mJ/m^2 for fenofibrate[60]), and ΔT is undercooling ($T_m - T$). Figure 6d illustrates the variation in critical nuclei radius as a function of undercooling. Obtained data seems to be quite consistent with results reported by Amstad and co-workers who get that at room temperature (ΔT = 61 K) $r_c \cong$ 1.8 nm and contains

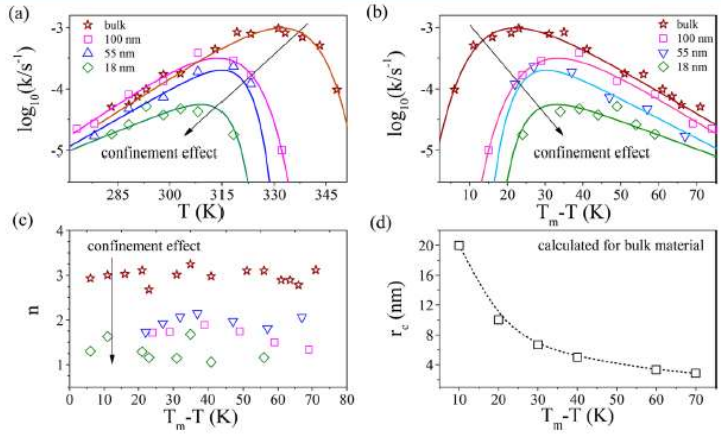

Figure 6. Variation of (a) the crystallization rate k as a function of temperature for fenofibrate confined to AAO porous membranes of different pore sizes. Panel (b) shows the same crystallization data but plotted versus degree of undercooling, $T_m - T$, where T_m denotes melting temperature of fenofibrate in nanopores of a particular pore diameter. Solid lines denote the fit of the experimental data with the use of an exponential function plus a linear term. (c) Temperature dependence of the Avrami exponent n obtained for fenofibrate crystallizing in AAO nanopores. Bulk crystallization data are shown as a reference. (d) Radius of critical nuclei plotted versus undercooling ($T_m - T$) as estimated for bulk fenofibrate by using eq 5.

DOI: 10.1021/acs.jpcc.7b10946
J. Phys. Chem. C 2018, 122, 1384−1395

approximately 26 fenofibrate molecules.[60] We note that at ΔT = 20 K, which corresponds to the maximum of the crystallization rate for bulk fenofibrate, r_c is approximately 10 nm. Then, for higher degree of undercooling r_c systematically decreases. At the temperature corresponding to the maximum of $k(T)$ in 18 nm pores, critical nuclei is $r_c \cong 6$ nm. Since the value of $2r_c$ is still smaller than the pore diameter, it explains why fenofibrate inside 18 nm AAO nanopores is still able to nucleate. In contrast, Dwyer and co-workers obtained nanocrystalline fenofibrate in controlled pore glass (CPG) only when pore sizes were greater than 20 nm.[61] This suggests that the differences in the surface interactions between the guest molecules and host environment (silica or alumina membranes) might also contribute to the crystallization of the molecular systems under 2d-nanoconfinement.

As a final step, we have studied the effect of confinement on the melting behavior of fenofibrate. Figure 7a demonstrates changes in the real part of complex dielectric permittivity upon heating of the crystalline material confined inside AAO nanopores. A sharp increase in ε' signifies melting temperature upon which reorientational movements of the dipolar molecules are freed again. However, on DSC thermograms, the melting event shows up as an exothermic peak, which broadens with lowering the pore diameter (see Figure 7b). In contrast to common belief, the heat of fusion in nanopores is not constant, but strongly decreases with confinement. The inset in Figure 7b demonstrates an almost linear decrease in ΔH_m with the inverse of the pore diameter. Herein, the bulk value was added as a reference and plotted assuming that d = 1000 nm. For fenofibrate confined in CPG, ΔH_m was also reported to decrease linearly as a function of $1/d$.[61] The reason for the reduction of ΔH_m in nanopores is a very intriguing problem. Assuming that a drop of ΔH_m is because of the confinement effect, which reduces the overall degree of crystallinity, one can expect that the number of molecules participating in the melting event is reduced in nanopores. However, as pointed out by Jackson and McKenna,[62] this is not in line with a continuous decrease of T_m observed at the same time when pore sizes decrease. This phenomenon can be explained by capillary effects and associated with the change of the interfacial energies between the substrate and solid or liquid phase of the substance. Furthermore, taking into consideration other interactions of substance and substrate, we can explain a drop of ΔH_m along with reducing the diameter of nanopores.

Figure 7c demonstrates depression of the melting temperature as a function of the reciprocal of pore diameter. Due to the fact that the melting event smears out as the pore diameter decrease, obtained from calorimetric (the onset of the melting endotherm) and dielectric measurements, T_m in 18 nm pores are probably so much different. The lowered melting temperature under geometrical nanoconfinement is frequently ascribed to the limitation in the crystal size and can be portrayed with the use of Gibbs−Thomson equation[63]

$$T_m(p_0) - T_m(d) = \frac{4\sigma T_m(p_0)}{d\Delta H_m \rho_c} \tag{6}$$

where d is pore diameter. The above equation requires the assumption that ρ, σ, and ΔH_m are independent of pore size and refer to bulk values. With the above requirements, plotting T_m versus inverse of pore diameter should give a linear relationship. Experimental data presented in Figure 7c does not follow perfectly a linear trend, not surprising because ΔH_m varies with pore size. Nevertheless, to some extent the Gibbs−Thomson relation is able to provide a rough estimate of the melting depression in the nanopores.

As a final point, we have also considered a relationship between melting temperature and glass transition temperature. Both quantities are typically linked via 2/3 ratio (T_g/T_m = 0.67).[64] However, in the case of fenofibrate, a value of 0.71 seems to describe better T_m/T_g dependency at both, ambient and elevated pressures (see Figure 7d). In contrast, when going

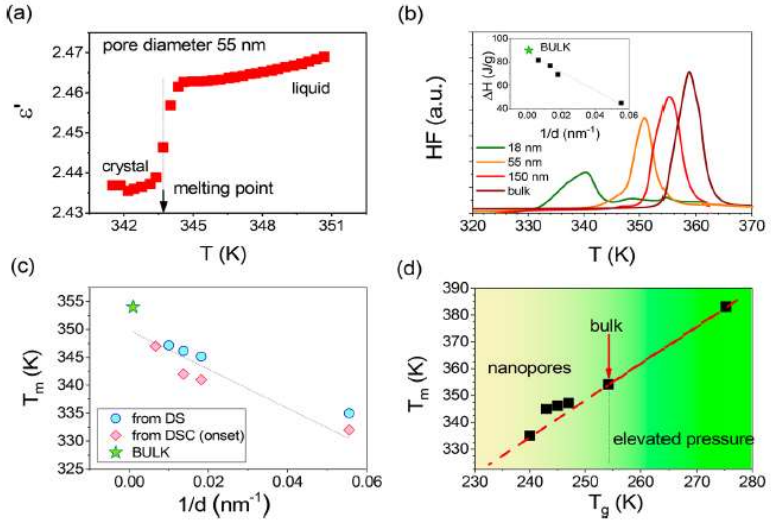

Figure 7. Representative changes in the dielectric permittivity recorded upon heating of crystalline fenofibrate confined to 18 nm pores at frequency $f = 10^5$ Hz. (b) DSC traces versus temperature showing melting endotherms for fenofibrate in AAO nanopores. The inset shows heat of fusion plotted as a function of inverse pore diameter. (c) Shift in the melting temperature as a function inverse pore diameter. The behavior of the bulk material is shown as well. (d) Melting temperature plotted as a function of the glass transition temperature (T_g = T at which τ_α = 10 s). Presented data cover high pressure and confinement regions.

DOI: 10.1021/acs.jpcc.7b10946
J. Phys. Chem. C 2018, 122, 1384−1395

from the bulk to nanoconfinement, a clear change in the slope of T_m (T_g) takes place. A similar finding that the melting temperature plotted as a function of the corresponding glass transition temperature shows weaker changes in the nanopores was also reported recently for dimethyl phthalate confined in AAO nanopores.[52] Herein, for consistency with previous results,[29] we have defined T_g (or T_{g_core}) as a temperature at which the α-relaxation time is equal to 10 s.

CONCLUSIONS

In this work, we have carefully investigated the impact of the 2D nanoconfinement on glassy dynamics and crystallization process of the supercooled fenofibrate. As shown, due to the presence of the two glass transition temperatures in nanopores, we can distinguish two fractions of the molecules: interfacial, which interact with the pore walls, and core, which is deprived of this effect. The existence of these two layers affects molecular dynamics of the nanoconfined system. It is responsible for deviation from VFT-law behavior at higher undercooling and a broadening of the α-relaxation peak. Despite that, surprisingly, the nanoconfined liquid can still satisfy the density scaling relation ($1/TV^{\gamma}$), just like the bulk fluid. However, this does not go together with the isochronal superposition.

Next, we showed the influence of geometric constraints on the crystallization process. As expected, in nanopores, crystallization of fenofibrate slows down significantly in comparison to bulk. As we found, the crystallization rate constant (k) seems to have much weaker temperature dependence as the pore sizes decrease. Together with the shift of the maximum crystallization rate toward higher undercooling and a pronounced decrease of the Avrami parameter, this serves as strong evidence that homogeneous nucleation becomes more favored than heterogeneous with decreasing pore size. A very specific crystallization of molecular liquids in AAO nanopores is a kind of the equilibration process that takes place before crystallization begins, and it is reflected in a shift of the α-relaxation toward faster dynamics. Lastly, we have also examined the influence of nanoconfinement on the melting behavior of fenofibrate. In a result of that, a drop of T_m, ΔH_m, and smearing out of the melting event with a reduction of the pores diameter are reported. We have also considered a relationship between melting temperature and glass transition temperature showing a pronounced change in the slope of T_m (T_g) dependence when crossing from bulk to nanoconfinement.

AUTHOR INFORMATION

Corresponding Authors

*E-mail: gszklarz@us.edu.pl.

*E-mail: kadrjano@us.edu.pl.

ORCID

Grzegorz Szklarz: 0000-0002-9657-8055

Karolina Adrjanowicz: 0000-0003-0212-5010

Magdalena Tarnacka: 0000-0002-9444-3114

Notes

The authors declare no competing financial interest.

ACKNOWLEDGMENTS

This work is funded by Polish Ministry of Science and Higher Education within the "Iuventus Plus" project (0001/IP3/2016/74). G.S. and M.P. are grateful for financial support from the National Science Centre within the framework of the Opus project (Grant No. DEC 2014/15/B/ST3/00364).

REFERENCES

(1) Losic, D.; Santos, A., Eds. *Nanoporous Alumina: Fabrication, Structure, Properties and Applications*; Springer International Publishing: Switzerland, 2015.

(2) Richert, R. Dynamics of Nanoconfined Supercooled Liquid. *Annu. Rev. Phys. Chem.* **2011**, *62*, 65−84.

(3) Chayen, N. E.; Saridakis, E.; Sear, R. P. Experiment and Theory for Heterogeneous Nucleation of Protein Crystals in a Porous Medium. *Proc. Natl. Acad. Sci. U. S. A.* **2006**, *103* (3), 597−601.

(4) Park, S. S.; Santha Moorthy, M.; Ha, C.-S. Periodic Mesoporous Organosilicas for Advanced Applications. *NPG Asia Mater.* **2014**, *6*, e96.

(5) Jackson, C. L.; McKenna, G. B. Vitrification and Crystallization of Organic Liquids Confined to Nanoscale Pores. *Chem. Mater.* **1996**, *8*, 2128−2137.

(6) Alcoutlabi, M.; McKenna, G. B. Effects of Confinement on Material Behaviour at the Nanometre Size Scale. *J. Phys.: Condens. Matter* **2005**, *17* (15), R461.

(7) Li, L.; Zhou, D.; Huang, D.; Xue, G. Double Glass Transition Temperatures of Poly(methyl Methacrylate) Confined in Alumina Nanotube Templates. *Macromolecules* **2014**, *47* (1), 297−303.

(8) Park, J.-Y.; McKenna, G. B. Size and Confinement Effects on the Glass Transition Behavior of Polystyrene/O-terphenyl Polymer Solutions. *Phys. Rev. B: Condens. Matter Mater. Phys.* **2000**, *61*, 6667−6676.

(9) Adrjanowicz, K.; Kolodziejczyk, K.; Kipnusu, W. K.; Tarnacka, M.; Mapesa, E. U.; Kaminska, E.; Pawlus, S.; Kaminski, K.; Paluch, M. Decoupling Between the Interfacial and Core Molecular Dynamics of Salol in 2D Confinement. *J. Phys. Chem. C* **2015**, *119* (25), 14366−14374.

(10) Adrjanowicz, K.; Kaminski, K.; Koperwas, K.; Paluch, M. Negative Pressure Vitrification of the Isochorically Confined Liquid in Nanopores. *Phys. Rev. Lett.* **2015**, *115*, 265702.

(11) Tarnacka, M.; Madejczyk, O.; Kaminski, K.; Paluch, M. Time and Temperature as Key Parameters Controlling Dynamics and Properties of Spatially Restricted Polymers. *Macromolecules* **2017**, *50* (13), 5188−5193.

(12) Adrjanowicz, K.; Kaminski, K.; Tarnacka, M.; Szklarz, G.; Paluch, M. Predicting Nanoscale Dynamics of a Glass-Forming Liquid from its Macroscopic Bulk Behavior and Vice Versa. *J. Phys. Chem. Lett.* **2017**, *8* (3), 696−702.

(13) Alba-Simionesco, C.; Cailliaux, A.; Alegria, A.; Tarjus, G. Scaling out the Density Dependence of the α-relaxation in Glass-Forming Polymers. *Europhys. Lett.* **2004**, *68*, 58−64.

(14) Dreyfus, C.; Le Grand, A.; Gapinski, J.; Steffen, W.; Patkowski, A. Scaling the α-relaxation Time of Supercooled Fragile Organic Liquids. *Eur. Phys. J. B* **2004**, *42*, 309−319.

(15) Casalini, R.; Roland, C. M. Thermodynamical Scaling of the Glass Transition Dynamics. *Phys. Rev. E* **2004**, *69*, 062501.

(16) Jiang, Q.; Ward, M. D. Crystallization Under Nanoscale Confinement. *Chem. Soc. Rev.* **2014**, *43*, 2066−2079.

(17) Alba-Simionesco, C.; Dosseh, G.; Dumont, E.; Frick, B.; Geil, B.; Morineau, D.; Teboul, V.; Xia, Y. Confinement of Molecular Liquids: Consequences on Thermodynamic, Static and Dynamical Properties of Benzene and Toluene. *Eur. Phys. J. E: Soft Matter Biol. Phys.* **2003**, *12*, 19−28.

(18) Duran, H.; Steinhart, M.; Butt, H.-J.; Floudas, G. From Heterogeneous to Homogeneous Nucleation of Isotactic Poly(propylene) Confined to Nanoporous Alumina. *Nano Lett.* **2011**, *11* (4), 1671−1675.

(19) Suzuki, Y.; Duran, H.; Akram, W.; Steinhart, M.; Floudas, G.; Butt, H.-J. Multiple Nucleation Events and Local Dynamics of Poly(e-caprolactone) (PCL) Confined to Nanoporous Alumina. *Soft Matter* **2013**, *9*, 9189−9198.

(20) Garcia-Gutierrez, M.-C.; Linares, A.; Hernandez, J. J.; Rueda, D. F.; Ezquerra, T. A.; Poza, P.; Davies, R. J. Confinement-Induced One-Dimensional Ferroelectric Polymer Arrays. *Nano Lett.* **2010**, *10* (4), 1472−1476.

DOI: 10.1021/acs.jpcc.7b10946
J. Phys. Chem. C 2018, 122, 1384−1395

(21) Pedersen, U. R.; Gnan, N.; Bailey, N. P.; Schrøder, T. B.; Dyre, J. C. Strongly Correlating Liquids and Their Isomorphs. *J. Non-Cryst. Solids* **2011**, *357*, 320−328.
(22) Roland, C. M.; Hensel-Bielowka, S.; Paluch, M.; Casalini, R. Supercooled Dynamics of Glass-Forming Liquids and Polymers Under Hydrostatic Pressure. *Rep. Prog. Phys.* **2005**, *68*, 1405−1478.
(23) Floudas, G.; Paluch, M.; Ngai, K. L., Eds. *Molecular Dynamics of Glass-Forming Systems: Effects of Pressure*; Springer-Verlag: Berlin, Germany, 2011.
(24) Yu, L. Amorphous Pharmaceutical Solids: Preparation, Characterization and Stabilization. *Adv. Drug Delivery Rev.* **2001**, *48* (1), 27−42.
(25) Baird, J. A.; Van Eerdenbrugh, B.; Taylor, L. S. A Classification System to Assess the Crystallization Tendency of Organic Molecules from Undercooled Melts. *J. Pharm. Sci.* **2010**, *99* (9), 3787−3806.
(26) Novoa, J. J.; Braga, D.; Addadi, L. *Engineering of Crystalline Materials Properties: State of the Art in Modeling, Design and Applications*; Springer: Berlin, Germany, 2008.
(27) Myerson, A. *Handbook of Industrial Crystallization*; Butterworth-Heinemann: Boston, MA, 2002.
(28) Beiner, M.; Rengarajan, G. T.; Pankaj, S.; Enke, D.; Steinhart, M. Manipulating the Crystalline State of Pharmaceuticals by Nanoconfinement. *Nano Lett.* **2007**, *7*, 1381−1385.
(29) Szklarz, G.; Adrjanowicz, K.; Dulski, M.; Knapik, J.; Paluch, M. Dielectric Relaxation Study at Ambient and Elevated Pressure of the Modeled Lipophilic Drug Fenofibrate. *J. Phys. Chem. B* **2016**, *120*, 11298−11306.
(30) Szklarz, G.; Adrjanowicz, K.; Knapik-Kowalczuk, J.; Jurkiewicz, K.; Paluch, M. Crystallization of Supercooled Fenofibrate Studied at Ambient and Elevated Pressures. *Phys. Chem. Chem. Phys.* **2017**, *19* (15), 9879−9888.
(31) Debenedetti, P. G.; Stillinger, F. H. Supercooled Liquids and the Glass Transition. *Nature* **2001**, *410*, 259−267.
(32) Simon, S. L.; Park, J. Y.; McKenna, G. B. Enthalpy Recovery of a Glass-Forming Liquid Constrained in a Nanoporous Matrix: Negative Pressure Effects. *Eur. Phys. J. E: Soft Matter Biol. Phys.* **2002**, *8*, 209−216.
(33) Jackson, C. L.; McKenna, G. B. The Glass Transition of Organic Liquids Confined to Small Pores. *J. Non-Cryst. Solids* **1991**, *131*−*133*, 221−224.
(34) Tarnacka, M.; Kaminski, K.; Mapesa, E. U.; Kaminska, E.; Paluch, M. Studies on the Temperature and Time Induced Variation in the Segmental and Chain Dynamics in Poly(propylene glycol) Confined at the Nanoscale. *Macromolecules* **2016**, *49*, 6678−6686.
(35) Koh, Y. P.; Simon, S. L. Trimerization of Monocyanate Ester in Nanopores. *J. Phys. Chem. B* **2010**, *114*, 7727−7734.
(36) Arndt, M.; Stannarius, R.; Groothues, H.; Hempel, E.; Kremer, F. Length Scale of Cooperativity in the Dynamic Glass Transition. *Phys. Rev. Lett.* **1997**, *79*, 2077−2080.
(37) Patkowski, A.; Ruths, T.; Fischer, E. W. Dynamics of Supercooled Liquids Confined to the Pores of Sol-Gel Glass: A Dynamic Light Scattering Study. *Phys. Rev. E: Stat. Phys., Plasmas, Fluids, Relat. Interdiscip. Top.* **2003**, *67*, 021501.
(38) Tait, P. G. *Physics and Chemistry of the Voyage of H. M. S. Challenger*; HMSO: London, England, 1888; Vol. 2, Part 4.
(39) Casalini, R.; Mohanty, U.; Roland, C. M. Thermodynamic Interpretation of the Scaling of the Dynamics of Supercooled Liquids. *J. Chem. Phys.* **2006**, *125*, 014505.
(40) Gundermann, G.; Pedersen, U. R.; Hecksher, T.; Bailey, N. P.; Jakobsen, B.; Christensen, T.; Olsen, N. B.; Schrøder, T. B.; Fragiadakis, D.; Casalini, R.; et al. Predicting the Density Scaling Exponent from Prigogine-Defay Ratio Measurements. *Nat. Phys.* **2011**, *7*, 816−821.
(41) Adrjanowicz, K.; Pionteck, J.; Paluch, M. Isochronal Superposition and Density Scaling of the Intermolecular Dynamics in Glass-Forming Liquids With Varying Hydrogen Bonding Propensity. *RSC Adv.* **2016**, *6*, 49370.
(42) Paluch, M.; Grzybowska, K.; Grzybowski, A. Effect of High Pressure on the Relaxation Dynamics of Glass-forming Liquids. *J. Phys.: Condens. Matter* **2007**, *19*, 205117.
(43) Roland, C. M.; Casalini, R.; Paluch, M. Isochronal Temperature-Pressure Superpositioning of the α-relaxation in Type-A Glass Formers. *Chem. Phys. Lett.* **2003**, *367*, 259.
(44) Roed, L. A.; Gundermann, D.; Dyre, J. C.; Niss, K. Communication: Two Measures of Isochronal Superposition. *J. Chem. Phys.* **2013**, *139* (10), 101101.
(45) Pedersen, U. R.; Bailey, N.; Schrøder, T. B.; Dyre, J. C. Strong Pressure-Energy Correlations in van der Waals Liquids. *Phys. Rev. Lett.* **2008**, *100*, 015701.
(46) Olsen, A. E.; Dyre, J. C.; Schrøder, T. B. Pseudoisomorphs in Liquids With Intramolecular Degrees of Freedom. *J. Chem. Phys.* **2016**, *145*, 241103.
(47) Pissis, P.; Kyritsis, A.; Daoukaki, D.; Barut, G.; Pelster, R.; Nimtz, G. Dielectric Studies of Glass Transition in Confined Propylene Glycol. *J. Phys.: Condens. Matter* **1998**, *10*, 6205−6227.
(48) Dendzik, Z.; Gorny, K.; Kośmider, M.; Żurek, S. Confinement Size Effect in Dipolar Relaxation of Glycerol Molecules Cluster Encapsulated Inside Carbon Nanotubes-Computer Simulation Study. *Rev. Adv. Mater. Sci.* **2010**, *23*, 42−51.
(49) Struik, L. C. E. *Physical Aging in Amorphous Polymers and Other Materials*; Elsevier: Amsterdam, Holland, 1978.
(50) Lunkenheimer, P.; Wehn, R.; Schneider, U.; Loidl, A. Glassy Aging Dynamics. *Phys. Rev. Lett.* **2005**, *95* (5), 055702.
(51) Tarnacka, M.; Kaminska, E.; Kaminski, K.; Roland, C. M.; Paluch, M. Interplay Between Core and Interfacial Mobility and Its Impact on the Measured Glass Transition: Dielectric and Calorimetric Studies. *J. Phys. Chem. C* **2016**, *120*, 7373.
(52) Adrjanowicz, K.; Szklarz, G.; Koperwas, K.; Paluch, M. Comparison of High Pressure and Nanoscale Confinement Effects on Crystallization of the Molecular Glass-Forming Liquid, Dimethyl Phthalate. *Phys. Chem. Chem. Phys.* **2017**, *19*, 14366−14375.
(53) Martino, P. D.; Palmieri, G. F.; Martelli, S. Evidence of a Metastable Form of Fenofibrate. *Pharmazie* **2000**, *55*, 625−626.
(54) Avrami, M. Kinetics of Phase Change. II Transformation-Time Relations for Random Distribution of Nuclei. *J. Chem. Phys.* **1940**, *8*, 212−224.
(55) Avrami, M. Kinetics of Phase Change. I General Theory. *J. Chem. Phys.* **1939**, *7*, 1103−1112.
(56) Suzuki, Y.; Duran, H.; Steinhart, M.; Kappl, M.; Butt, H.-J.; Floudas, G. Homogeneous Nucleation in Predominantly Cubic Ice Confined in Nanoporous Alumina. *Nano Lett.* **2015**, *15* (3), 1987−1992.
(57) Yao, Y.; Sakai, T.; Steinhart, M.; Butt, H.-J.; Floudas, G. Effect of Poly(ethylene oxide) Architecture on the Bulk and Confined Crystallization Within Nanoporous Alumina. *Macromolecules* **2016**, *49*, 5945−5954.
(58) Suzuki, Y.; Duran, H.; Steinhart, M.; Butt, H.-J.; Floudas, G. Homogeneous Crystallization and Local Dynamics of Poly(ethylene oxide) (PEO) Confined to Nanoporous Alumina. *Soft Matter* **2013**, *9*, 2621.
(59) Mullin, J. W. *Crystallization*, 4th ed.; Butterworth-Heinemann: Oxford, 2001.
(60) Amstad, E.; Spaepen, F.; Weitz, D. A. Crystallization of Undercooled Liquid Fenofibrate. *Phys. Chem. Chem. Phys.* **2015**, *17*, 30158−30161.
(61) Dwyer, L. M.; Michaelis, V. K.; O'Mahony, M.; Griffin, R. G.; Myerson, A. S. Confined Crystallization of Fenofibrate in Nanoporous Silica. *CrystEngComm* **2015**, *17* (41), 7922−7929.
(62) Jackson, C. L.; McKenna, G. B. The Melting Behavior of Organic Materials Confined in Porous Solids. *J. Chem. Phys.* **1990**, *93*, 9002.
(63) Defay, R.; Prigogine, I.; Bellemans, A.; Everett, D. H. *Surface Tension and Adsorption*; Wiley: New York, 1966.
(64) Kauzmann, W. The Nature of the Glassy State and the Behavior of Liquids at Low Temperatures. *Chem. Rev.* **1948**, *43* (2), 219−256.

DOI: 10.1021/acs.jpcc.7b10946
J. Phys. Chem. C 2018, 122, 1384−1395

Dr Magdalena Tarnacka
Instytut Fizyki, Uniwersytet Śląski w Katowicach
Zakład Biofizyki i Fizyki Molekularnej
ul. 75 Pułku Piechoty 1A
41-500 Chorzów

Chorzów, 5.07.2018 r.

OŚWIADCZENIE

Oświadczam, że w pracy:

1. G. Szklarz, K. Adrjanowicz, M. Tarnacka, J. Pionteck, M. Paluch, *Confinement-induced changes in the glassy dynamics and crystallization behavior of supercooled fenofibrate*, J. Phys. Chem. C, 2018, 122, 1384–1395, DOI: 10.1021/acs.jpcc.7b10946

mój wkład polegał na wykonaniu pomiarów przy pomocy skaningowej kalorymetrii różnicowej (DSC).

Magdalena Tarnacka

Leibniz-Institut
für Polymerforschung
Dresden

Institut
Makromolekulare Chemie
Abt. Funktionale
Nanokomposite und Blends

Abteilungsleiterin
Dr.
Petra Pötschke

Bearbeiter
Dr.
Jürgen Pionteck
wiss. Mitarbeiter
T - 393 **F** - 98299
pionteck@ipfdd.de

Sekretariat
Beate Marchlewski
T - 299 **F** -98299
marchlewski-beate@ipfdd.de

Datum:
06.07.2018

Ihre Zeichen:

DECLARATION

I declare that my contribution in the paper

1. G. Szklarz, K. Adrjanowicz, M. Tarnacka, J. Pionteck, M. Paluch, *Confinement-induced changes in the glassy dynamics and crystallization behavior of supercooled fenofibrate*, J. Phys. Chem. C, 2018, 122, 1384–1395, DOI: 10.1021/acs.jpcc.7b10946

was the realization of the Pressure–Volume–Temperature (PVT) measurements for determination of the pressure and temperature dependency of the specific volume of fenofibrate.

Sincerely yours

Jürgen Pionteck

DRESDEN concept

Leibniz Gemeinschaft

A4. Cooling-rate versus compression-rate dependence of the crystallization in the glass-forming liquid, propylene carbonate

Autorzy: G. Szklarz, K. Adrjanowicz, M. Paluch
Referencja: Cryst. Growth Des. 2018, 18, 2538–2544
Impact Factor czasopisma z roku opublikowania pracy: **4.055**
Liczba punktów ministerialnych MNiSW czasopisma z roku opublikowania pracy: **35**
DOI: 10.1021/acs.cgd.8b00123

Mój udział w poniższym artykule polegał na wykonaniu pomiarów dielektrycznych, analizie i interpretacji wyników pomiarów oraz na przygotowaniu manuskryptu. Wkład pozostałych współautorów zamieszczono w formie oświadczeń.

CRYSTAL GROWTH & DESIGN

Article

Cite This: Cryst. Growth Des. 2018, 18, 2538−2544

pubs.acs.org/crystal

Cooling-Rate versus Compression-Rate Dependence of the Crystallization in the Glass-Forming Liquid, Propylene Carbonate

Grzegorz Szklarz,*[,†,‡] Karolina Adrjanowicz,*[,†,‡] and Marian Paluch[†,‡]

[†]Institute of Physics, University of Silesia, 75 Pulku Piechoty 1, 41-500 Chorzow, Poland

[‡]Silesian Center for Education and Interdisciplinary Research (SMCEBI), 75 Pulku Piechoty 1a, 41-500 Chorzow, Poland

ABSTRACT: The effect of cooling and compression rates on the tendency to crystallize/vitrify the canonical glass-forming liquid, propylene carbonate (PC), was studied by using dielectric spectroscopy. Based on constructed time−temperature transformation (TTT) and continuous heating transformation (CHT) diagrams, we have determined the critical scanning rates that allow avoiding crystallization on cooling from the liquid state and reheating of the glassy sample, respectively. In a similar way to isobaric temperature-dependent studies, we have also carried out isothermal high-pressure measurements upon which the crystallization tendency of PC was examined as a function of varying compression and decompression rates (pressures up to 1.3 GPa). We propose time−pressure transformation (TPT) and continuous decompression transformation (CDT) diagrams as the pressure analogs of the TTT and CHT diagrams. Obtained results demonstrate that, qualitatively, one gets the same picture when pressure (instead of the temperature) is used as the principal adjustable thermodynamic parameter. In agreement with this finding, a careful comparison of the time-dependent crystallization results collected under isobaric and isothermal conditions has revealed that within the considered $T-p$ range the maximal crystallization rate and dimensionality of the growing crystals do not depend significantly on whether we vary with the temperature at a fixed pressure or pressure at a constant temperature.

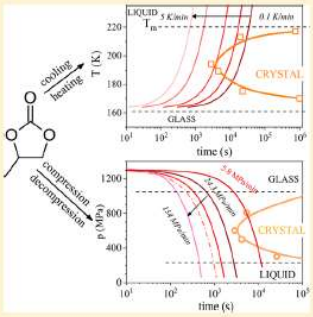

INTRODUCTION

Glass formation plays an important role in several research disciplines (including physics, chemistry, biology, or material science) as well as numerous technological applications (e.g., amorphous semiconductors, solid-state electrolytes, optical fibers, energy, and waste storage).[1−6] Because of the above reasons, understanding the conditions that may favor vitrification on cooling, rather than crystallization, have great scientific and practical meaning. This, however, remains a long-standing scientific problem. Over the past decades, numerous attempts to provide universal criteria enabling to predict/quantify the glass-forming tendency of various materials were proposed, e.g., based on the molecular architecture,[7−9] the strength of the intermolecular attractions,[10,11] and values of T_b/T_m or T_g/T_m ratios (where T_g is the glass transition temperature, T_m is the melting temperature, and T_b is the absolute boiling temperature).[12−16] Unfortunately, none of the proposed measures provide a convincing prediction of the glass-forming tendency that applies to a broad spectrum of different systems.

Vitrification takes place when the rate of cooling is fast enough so that there is no time for nuclei to form and grow. The two essential constituents of the crystallization process, i.e., nucleation and crystal growth, are determined by the interplay between thermodynamic and kinetic factors. With increasing undercooling, the free energy barrier between liquid and crystalline states decreases, driving the system toward crystallization. However, the concurrent slowing down of the molecular movement needed at the liquid−crystal interface impede the crystallization process. This results in a characteristic bell-shaped curves of the nucleation and crystal growth rates maxima,[17−19] as demonstrated in Scheme 1a. Depending on the intensity and the extent of overlap, avoiding crystallization on cooling requires different efforts. For example, when the maxima of nucleation and crystal growth rates are located near to each other, a liquid would be prone to crystallize rather than vitrify on cooling. In such case, the smaller the liquid volume and higher the cooling rate, the lower probability of crystallization.[7] However, when the optimal temperature regions for nucleation and crystal growth do not superimpose, a liquid can be quenched and forms a glass. However, on subsequent heating of such sample, it is susceptible to crystallization after passing through the nucleation and then the crystal growth zones in the right and noninterchangeable order.[20]

For practical reasons, understanding the conditions that must be fulfilled to bypass crystallization on cooling a liquid from the melt are expressed in terms of the time−temperature transformation (TTT) diagrams. TTT diagram demonstrates changes in the crystallization rate below T_m as a characteristic "C-shaped" curve in the time−temperature coordinates. The "nose" in TTT diagram defines, via temperature at which the

Received: January 22, 2018
Revised: February 18, 2018
Published: February 26, 2018

DOI: 10.1021/acs.cgd.8b00123
Cryst. Growth Des. 2018, 18, 2538−2544

Scheme 1. Schematic Evolution of the Temperature (a) and Pressure (b) Dependences of the Nucleation N and Crystal Growth G Rates[a]

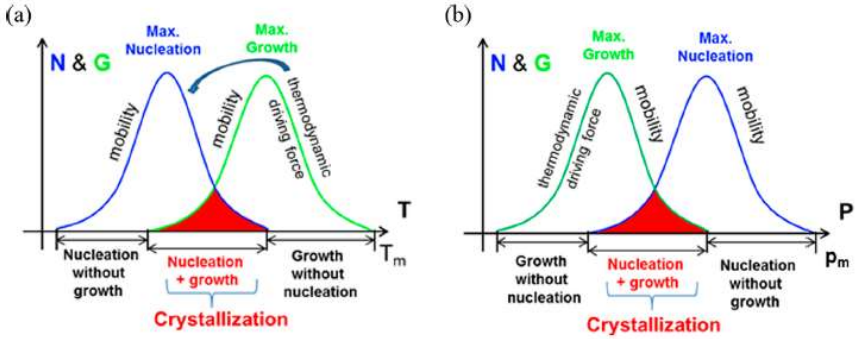

[a]The overlap zone of these two processes and their absolute magnitudes determine the overall crystallization behavior of a material upon upward and downward T/p scans.

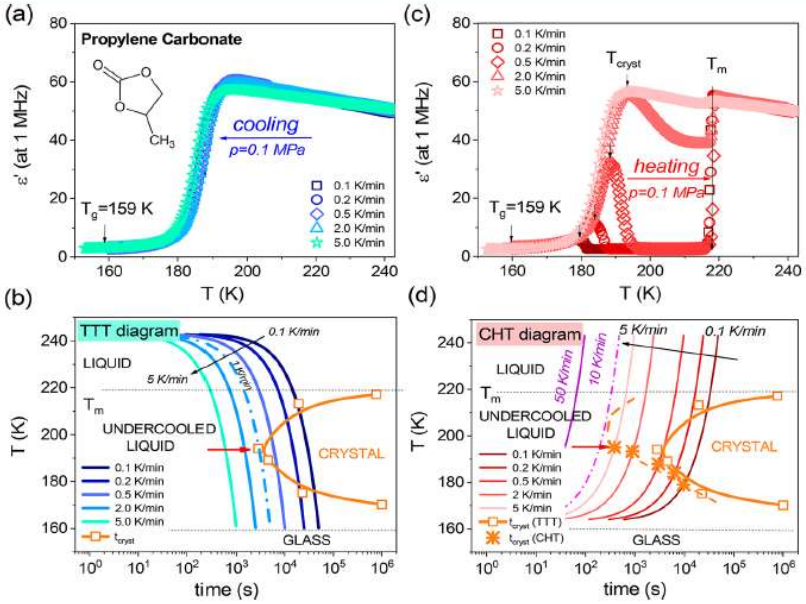

Figure 1. Evolution of the dielectric constant ε' at 1 MHz as measured for PC at 0.1 MPa upon (a) cooling and (c) heating with different scanning rates. (b) TTT diagram constructed based on isothermal crystallization data recorded at 0.1 MPa. The minimal scanning rate, which allows avoiding crystallization on cooling, is that for which the cooling line does not intersect with the "nose" of the TTT curve. (d) CHT diagram demonstrating crystallization tendency of PC at 0.1 MPa upon reheating of the glassy sample with different heating rates.

crystallization rate reaches its maximum value, the critical cooling rate needed to avoid crystallization when cooling a liquid from T_m. When the transformation kinetics takes place under nonisothermal conditions, just like in the industrial processing, continuous cooling transformation (CCT) diagrams are more useful. CCT diagrams provide information on the initial and final transformation temperatures as well as the final product obtained during continuous cooling at various constant cooling rates. However, the heating analog of the TTT diagram is the continuous heating transformation (CHT) diagram, which reports on time and temperature required to reach a certain phase transformation during the course of continuous heating with various constant heating rates. TTT, CCT, and CHT diagrams allow developing the time–temperature conditions essential for the glass-formation/crystallization of organic- and inorganic-based substances.[21−24]

Without any doubts, the temperature is a fundamental thermodynamic variable controlling vitrification. However, the results collected over the past years have demonstrated that only in combination with high-pressure studies one gets a complete description of the crystallization and glass formation phenomena.[25−30] Pressurization of liquid at a fixed temperature can be also used to produce glasses.[31] Scheme 1b demonstrates a very schematic overview on the pressure profile of the nucleation and the crystal growth rates. Upon compression at fixed temperature and above the melting point, a liquid overpasses first via the optimal zone for the crystal growth (located at lower pressures) and afterward the region where the

DOI: 10.1021/acs.cgd.8b00123
Cryst. Growth Des. 2018, 18, 2538−2544

nucleation process is favorable. However, it is completely unknown if both thermodynamic parameters, i.e., temperature and pressure, affect location/separation of the nucleation and the crystal growth rates maxima with respect to each other in exactly the same way. Herein, one should remember that temperature and pressure are not equivalent thermodynamic variables. While temperature affects the kinetic energy of the molecules, pressure acts mostly on the intermolecular distances between them. Thus, understanding the response of the glass-forming liquids to both variables, temperature and pressure, is essential to take full advantage of the two-dimensional $T-p$ phase space and produce materials with desired properties and structure.

In this article, we wish to compare the effect of temperature and pressure on the glass-forming tendency of the van der Waals liquid, propylene carbonate (PC). We show that crystallization behavior of the investigation sample can be controlled not only by changing the rate of cooling/heating but also the compression/decompression rate. Based on the obtained results we have constructed time−pressure transformation (TPT) and continuous decompression transformation (CDT) diagrams as the pressure analogs of the TTT and CHT diagrams. In both cases, avoiding crystallization on reheating/decompression from the glassy state was found to be far more challenging than cooling/pressurizing a liquid from T_m. Surprisingly, we found that within the studied $T-p$ range the crystallization rate and dimensionality of the growing crystals do not depend significantly on whether temperature or pressure is used as the controlling thermodynamic variable. This means that to some of the extent the increasing pressure mimics the crystallization behavior of the investigated sample as on lowering the temperature, and thus, can be used interchangeably.

EXPERIMENTAL SECTION

Materials. Propylene carbonate (MW = 102.09 g·mol^{-1}) of purity >99% was purchased from Sigma-Aldrich and used as received. The chemical structure of PC (T_g = 159 K at 0.1 MPa) can be found in Figure 1a as an inset.

Methods. The real part of complex dielectric permittivity (ε') was measured with the use of Novocontrol GMBH Alpha dielectric spectrometer. For studies carried out at atmospheric pressure, the temperature was controlled by Quattro Novocontrol system with a stability better than 0.1 K. The liquid sample was placed between two stainless steel electrodes separated by a gap of 0.05 mm provided by a Teflon spacer. Measurements of the dielectric permittivity at 1 MHz frequency were performed under nitrogen atmosphere within the temperature range from 250 to 150 K using various scanning rates. For high-pressure studies, we have used Unipress high-pressure equipment (Institute of High-Pressure Physics, Warsaw, Poland). The high-pressure setup consists of a MP5 micropump with a two-pulse step motor, control unit allowing to regulate the speed of compression by changing the frequency of the motor movements (and therefore also the piston position), stainless-steel vessel (shown elsewhere),[32] and hydraulic ram for monostat LC20T, which replaces the laboratory hydraulic press LCP20. The latter one is supplied with pressure generated by a MP5 micropump. A ram piston via the pusher transfers the force to the monostat and generates the pressure in it. The ratio of the ram's piston diameter to the monostat's piston diameter provides appropriate multiplication factor and allows to obtain desired pressure in the LC20T monostat (high-pressure vessel).[33] A high-pressure plug with a dielectric cell (for details, see ref 34) filled with the investigated sample (~3 mL volume) was placed into Teflon bellow mounted in the high-pressure vessel. The temperature in the pressure vessel was controlled by a Tenney Junior environmental chamber. Routinely, we have also measured the temperature inside the high-pressure vessel by a Pt100 sensor located about 2.5 cm away from the sample. For thermally equilibrated systems, the sample and high-pressure cylinder temperature are almost the same (±2 K).

We have also carried out time-dependent isobaric (p = 0.1 MPa) and isothermal (T = 243 and 253 K) dielectric studies to determine the temperature and pressure evolution of the crystallization rate and Avrami parameter. By following changes in the dielectric response of the sample upon crystallization progress, it is possible to study the crystallization kinetics at the real-time of the measurements. To do that, obtained data were expressed in terms of the normalized permittivity $\varepsilon'_N(t) = (\varepsilon'_{initial} - \varepsilon'(t))/(\varepsilon'_{initial} - \varepsilon'_{final})$ and then fitted with the use of Avrami equation,[35,36] $\varepsilon'_N(t) = 1 - \exp(-kt^n)$ where n is the Avrami parameter and k is the crystallization rate. Changes in the static dielectric permittivity were recorded every 300 s. Prior, the sample was cooled down (with the rate of ~5 K/min) or compressed from the liquid state (compression rate ≈ 40 MPa/min) to the desired crystallization conditions (T, p), so without approaching the glassy state. The crystallization tendency of PC during cooling/heating with different scanning rates, as predicted by TTT and CHT diagrams, was verified with the use of dielectric and calorimetric techniques.

RESULTS AND DISCUSSION

Figure 1a demonstrates changes in the real part of complex dielectric permittivity (at 1 MHz frequency) recorded for PC upon cooling with different scanning rates at 0.1 MPa. A characteristic step of ε' when lowering the temperature is due to the dielectric dispersion. For glass-forming liquids, it signifies that the dielectric α-relaxation systematically slows down and eventually moves out of the experimental window as the glass transition temperature, T_g, is approached. Since $\varepsilon'(T)$ dependences collected upon scanning with different cooling rates are almost identical, one can suppose that the glassy state can be reached easily, even if a very slow cooling rate is applied. However, from such a naive picture one cannot evaluate whether cooling of the investigated liquid down to $T < T_g$ with varying cooling rates always results in obtaining completely amorphous material, or rather crystallization event might also happen in the meantime. If the crystallinity fraction is very small, it can be hardly detectable in the dielectric response of the bulk viscous liquid, thus giving an impression that the liquid/crystal phase transition is avoided. For that reason, more useful information allowing to evaluate crystallization tendency of the glass-forming systems on cooling with different scanning rates provides TTT diagrams.

We have investigated crystallization tendency of PC at few temperatures located within T_g and T_m, under atmospheric pressure conditions. Time-dependent changes in the dielectric spectra accompanying crystallization progress were used to describe the kinetics of the liquid/crystal phase transition. Obtained in this way, evolution of the crystallization time as a function of temperature is presented in Figure 1b. Its maximum forms a characteristic nose of the TTT curve. By plotting obtained results in this way, one can easily note that the cooling rates from 0.1 to 0.5 K/min are, as a matter of fact, too slow and might result in a partial crystallization of the sample. In turn, above the critical rate of 1 K/min, only the glassy state should be reached on cooling, as the cooling lines do not intersect anymore with the crystallization zone.

On heating from the glassy state, the crystallization tendency of PC changes dramatically. We can explain it by the fact that the nuclei formed at lower temperature start to grow as the temperature increases, once reaching the optimal temperature range. Figure 1c demonstrates a crystallization event as a sudden drop of the dielectric permittivity, whose onset shifts toward higher temperature with increasing the scanning rate.

DOI: 10.1021/acs.cgd.8b00123
Cryst. Growth Des. 2018, 18, 2538−2544

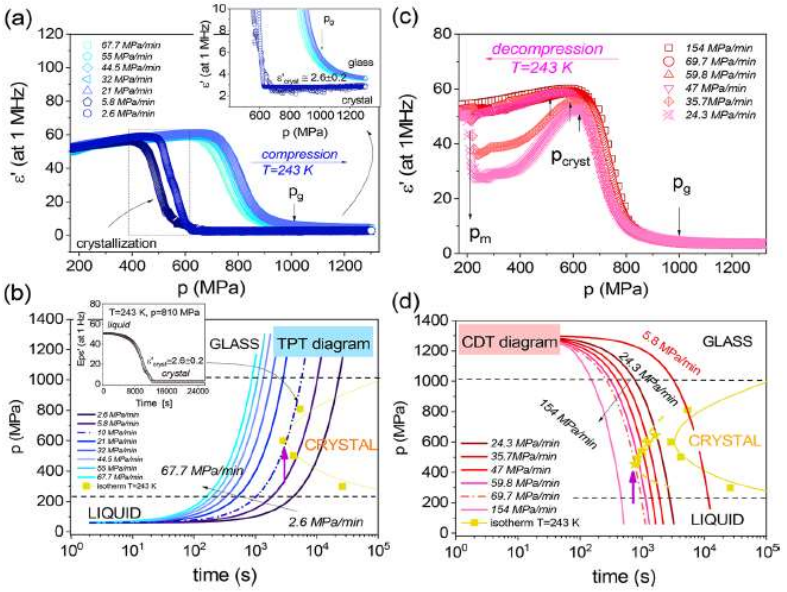

Figure 2. Evolution of the dielectric permittivity ε' at 1 MHz as measured for PC at 243 K upon (a) compression and (c) decompression with different scanning rates. Inset in panel (a) enlarges values of ε' at the very final stages of the compression process. (b) TPT diagram constructed based on the time-dependent crystallization data recorded at various pressures along isotherm T = 243 K. Above the compression rate greater than 10 MPa/min, it is possible to completely avoid crystallization. The inset demonstrates changes in the real part of the dielectric permittivity (at 1 Hz) upon time-dependent crystallization studies carried out at p = 810 MPa and T = 243 K. (d) CDT diagram is demonstrating crystallization tendency of PC at 243 K upon decompression of the sample from the glassy to the liquid state with the use of different scanning rates.

Each time the obtained crystalline material melts at T_m = 218 K, meaning that only one polymorph is formed.

When the time needed for the crystal growth takes longer than the heating rate, a crystallization event does not take place. For PC, above the scanning rates of 10 K/min crystallization, signatures were not detected neither in the dielectric nor calorimetric data. In analogy with TTT diagram, we have also constructed a CHT diagram, which portrays crystallization tendency of the investigated liquid in the course of continuous heating with a constant rate in time and temperature coordinates. For PC, such CHT diagram is given in Figure 1d. In this case, we were able to capture only the low-temperature side of the crystallization curve, as the crystallization rates recorded on heating are almost one decade faster than on cooling. From that, one can see that even for the same material TTT and CHT diagrams might not essentially look the same.

Having analyzed crystallization tendency of PC at 0.1 MPa, we can now move on to high-pressure studies. From now on, pressure instead of temperature will be used as the thermodynamic observable of interest. The increase in pressure at fixed temperature is the same as lowering the temperature at fixed pressure, which slows down the molecular motions and might bring the system either to the glassy or the crystalline states. Figure 2a demonstrates changes in ε' (at 1 MHz) recorded upon pressurization of PC at 243 K with different compression rates. In analogy to temperature scans, we have also observed a characteristic dielectric dispersion curve signifying moving down the α-relaxation process in the experimental window. While keeping isothermal conditions, T = 243 K, the glass-transition event takes place at p_g = 1.01 GPa.[37,38] When starting from the same initial point (243 K, 0.1 MPa), vitrification of PC at atmospheric pressure requires a drop of the temperature by more than 80 K.

It can be seen in Figure 2a that the dielectric data recorded upon isothermal pressurization of PC with very low compression rates (2.6 and 5.8 MPa/min) indicates at least partial crystallization of the investigated samples as their ε'(p) dependences clearly do not match with the other ones. Moreover, in the inset of Figure 2a we show that the final values of ε' reported for PC at 243 K after compression to 1.3 GPa with the rates of 2.6 and 5.8 MPa/min are a bit lower than that obtained for other glassy samples. However, they coincide perfectly well with that reported for the crystalline material obtained upon time-dependent crystallization studies carried out at 243 K and 810 MPa (see inset in Figure 2b). To describe the crystallization tendency of PC along isotherm T = 243 K, we have performed crystallization kinetic measurements at various pressures, located within p_g and p_m, i.e., pressures corresponding to the glass transition and melting events at 243 K, respectively. The former one can be easily detected in the dielectric loss spectra of the compressed glass-forming liquid as a pressure at which τ_α reaches 100 s. However, the latter one corresponds to pressure at which we observe a sharp increase in ε' on heating, which is due to freeing of the orientational motions of the dipolar species as the crystal/liquid phase transformation takes place (see e.g., Figure 2c).

Pressure evolution of the isothermal crystallization time determined based on the dielectric data is presented in Figure 2b. The maximum of the crystallization rate at 243 K is located at around 600 MPa and forms a characteristic nose of the time−pressure transformation (TPT) diagram. We have termed it in this way to mark clearly that it represents the pressure analogue of the TTT diagram. Constructed TPT

DOI: 10.1021/acs.cgd.8b00123
Cryst. Growth Des. 2018, 18, 2538−2544

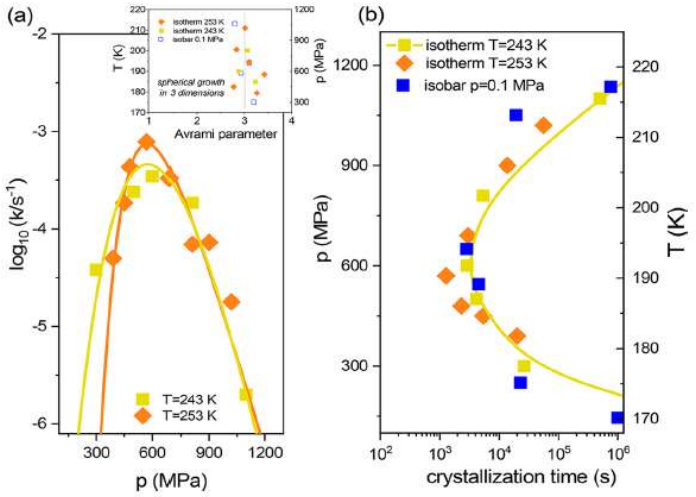

Figure 3. (a) Crystallization rate for PC plotted as a function of pressure as determined along two different isotherms, T = 243 and 253 K. The inset shows the evolution of the Avrami parameter either as a function of pressure (for isothermal data) or temperature (atmospheric pressure isobar). (b) Comparison of the crystallization times (t_{cryst}) considered either in pressure or temperature coordinates. The solid line represents the fit to the data with the use of the exponential linear combination function.

diagram for PC was also supplemented by continuous lines corresponding to various compression rates. In agreement with the results presented in Figure 2a, compression rates 2.6 and 5.8 MPa/min are indeed too slow to form a glassy state, as they intersect with the crystallization curve. In turn, when the rate of compression is greater than 10 MPa/min, crystallization is avoided, and only the glassy state is expected to form on squeezing of the liquid PC.

Decompression from the glassy state, just like glass reheating, produces significant changes in the crystallization tendency of the investigated sample, see Figure 2c. Likewise, crystallization is far more difficult to avoid, in particular, when using similar scanning rates as that obtained on the upstroke. This serves as a strong evidence that the maximum of the nucleation rate considered either in temperature or pressure coordinates must be located in a close vicinity of the glass-transition. When going out of the glassy state, either by increasing temperature or lowering pressure, we overpass again via the zone where the crystal growth is favorable, and crystallization takes place much faster. As the values of ε' does not drop down completely to that characteristic for the crystalline sample (for PC ε'_{cryst} = 2.55 at 0.1 MPa), we can suppose that there is still some significant amount of the liquid fraction in the depressurized material. During decompression of PC under isothermal conditions with different scanning rates, we observe only one melting event (seen in the dielectric spectra as a rather sharp increase of the dielectric permittivity). For that reason, we believe that PC has only one polymorphic form during isothermal crystallization. This should be however verified in the future by performing additional high-pressure X-ray diffraction studies. In contrast, Bauer and co-workers have demonstrated that isothermal compression and decompression with different paces can induce elusive polymorphic transformation of ice.[39,40]

The melting temperature of the investigated material increases by ~12.5 K per each 100 MPa (dT_m/dp). Then, using famous "2/3 ratio" between T_m and T_g, this gives the pressure coefficient of the glass transition temperature (dT_g/dp ≅ 8 K/100 MPa), which agrees very well with the value reported in the literature based on experimental study (i.e., >7 K/100 MPa).[38] In the dielectric response of amorphous PC decompressed with the rate of 154 MPa/min, we have not observed crystallization traces, meaning that at such high compression-rates there is no ample time for the crystal to grow. Therefore, by varying with compression/decompression rates, we can actually control the crystallization/glass formation propensity of the molecular systems, just like when using the temperature.

At this point, it is worth mentioning that compression and decompression processes are always accompanied by the local temperature gradients as the energy stored in the system is released or retrieved as the volume occupied by the molecules is changed. For rapid changes in pressure, this local temperature variation can be very great, resulting in the process of compression/decompression to proceed under conditions being far from isothermal. Based on experimental observation, we suppose that the heating effect generated during compression (rated from 2.3 to 154 MPa/min) should result in the local temperature changes no greater than 5 K. Thus, it should not affect significantly the overall picture of the crystallization behavior of PC as extracted from this study.

In Figure 3a, we present the evolution of the crystallization rate k and Avrami parameter n as determined for PC along two isotherms T = 243 K and T = 253 K. With increasing temperature, we do not observe significant changes in the position of the overall crystallization rate curve, although its intensity at the maximum slightly increases. We suppose that this effect can be related somehow to increase in the magnitude and overlap of the $N(p)$ and $G(p)$ dependences as the temperature increase. In analogy, the ease of crystallization with increasing temperature seems to produce a similar effect as increasing pressure. Recently, based on the predictions of the classical theory of nucleation and crystal growth models, we have demonstrated that the overlapping of the $N(T)$ and $G(T)$ dependences is expected to expand with increasing pressure.

DOI: 10.1021/acs.cgd.8b00123
Cryst. Growth Des. 2018, 18, 2538−2544

Thus, accelerating the crystallization progress of the compressed glass-forming liquid.[41]

In the next step, we have compared the temperature and pressure dependences of the crystallization time ($t_{cryst} = 1/k$) obtained along isobar 0.1 MPa and isotherms 243 and 253 K, as illustrated in Figure 3b. It is very interesting that obtained dependences considered either in T or p coordinates look very similar. Similarly, we found that n is very weakly temperature- and pressure-dependent as demonstrated in the inset of Figure 3a. In both cases, the Avrami parameter fluctuates around 3, which indicates the spherical character of the crystallization process. Finding n to remain almost temperature and pressure invariant within the considered $T-p$ range, covering more than 50 K change in temperature or 1 GPa in pressure, indicates that the density of the parental phase does not affect in any way the morphology of the newly formed crystalline phase.

The results obtained above for the modeled glass-forming liquid PC suggests that when it comes to crystallization phenomenon, increasing pressure results, to some extent, in the same effect as lowering the temperature. Thus, the classical formalism used so far to describe the glass-forming tendency of the different materials as a function of temperature can be transferred to those research in which pressure is the principle control variable. Since the overall picture of the crystallization behavior of investigated compound obtained from either TTT/CHT and TPT/CDT diagrams are consistent, it seems that it does not really matter which thermodynamic observable we choose to invoke changes in the crystallization/glass-forming tendency of PC.

■ CONCLUSIONS

A number of the natural phenomena as well as industrial processes that take advantage of glass-formation require fast processing, very often taking place under either nonisothermal or nonisobaric conditions. Understanding the phase transformation that might take place in the meantime is critical for a number of applications, as the degree of crystallinity or crystallization behavior determines a number of the most important physicochemical features. A very useful approach allowing to understand better transition taking place under such conditions and its impact of the properties of the outcome material represent time−temperature/continuous cooling or heating transformation diagrams, known very well in the metallic glasses or alloys community.

Herein, we have confirmed the applicability of such transformation diagrams in studying the crystallization tendency of the canonical molecular glass-former, propylene carbonate. We have determined the critical scanning rates allowing to avoid crystallization, demonstrating that the overall crystallization rate curve recorded on heating is shifted almost one decade toward shorter crystallization times with respect to that obtained on cooling. In addition to that for the first time, we have extended such approach for high-pressure research, i.e., when pressure instead of temperature is used as the thermodynamic parameter of interest. Thus, in analogy to TTT and CHT diagrams in which temperature is the key variable, we have constructed their pressure analogues, termed here as time−pressure transformation (TPT) and continuous−decompression transformation (CDT) diagrams. Just like when heating a glassy sample at a fixed pressure, avoiding crystallization upon depressurization from the glassy state at constant temperature were found to be far more challenging and require higher scanning rates. Nevertheless, by varying with the rates of compression and decompression one can suppress/induce crystallization of PC in exactly the same way as on cooling from the melt or glass reheating. Comparison of the isothermal and isobaric crystallization results has led to a surprising finding that within the considered $T-p$ range temperature and pressure dependences the overall crystallization rate and dimensionality of the growing crystals mimic each other. This means that, qualitatively, one can end up with the same overall picture of the crystallization behavior of the investigated compound irrespective of the chosen observable. So, both thermodynamic variables, temperature and pressure, can be used interchangeably to tune/modify glass-formation and crystallization behavior of the molecular systems. Therefore, our experimental results might provide clues for developing/modeling various processes related to crystallization and glass formation in academic and industrial applications.

■ AUTHOR INFORMATION

Corresponding Authors

*E-mail: kadrjano@us.edu.pl.

*E-mail: gszklarz@us.edu.pl.

ORCID

Grzegorz Szklarz: 0000-0002-9657-8055

Karolina Adrjanowicz: 0000-0003-0212-5010

Notes

The authors declare no competing financial interest.

■ ACKNOWLEDGMENTS

K.A. acknowledges financial support from the Ministry of Science and Higher Education within "Iuventus Plus" project (0001/IP3/2016/74). M.P. and G.S. are grateful for the financial support from the National Science Centre within the framework of the Opus project (Grant No. DEC 2014/15/B/ST3/00364).

■ REFERENCES

(1) Anderson, P. W. Through the glass lightly. *Science* **1995**, *267*, 1610.

(2) Angell, C. A. Formation of glasses from liquids and biopolymers. *Science* **1995**, *267*, 1924−1935.

(3) Lin, L.; Xu, X.; Chu, Ch.; Majeed, M. K.; Yang, J. Mesoporous amorphous silicon: A simple synthesis of a high-rate and long-life anode material for lithium-ion batteries. *Angew. Chem., Int. Ed.* **2016**, *55*, 14063−14066.

(4) Levine, H. *Amorphous Food and Pharmaceutical Systems*; Royal Society of Chemistry: Cambridge, U.K., 2002.

(5) Seife, C. So much more to know. *Science* **2005**, *309*, 78−102.

(6) Berthier, L.; Ediger, M. D. Facets of glass physics. *Phys. Today* **2016**, *69*, 40.

(7) Turnbull, D. Under what conditions can a glass be formed? *Contemp. Phys.* **1969**, *10*, 473−488.

(8) Ping, W.; Paraska, D.; Baker, R.; Harrowell, P.; Angell, C. A Molecular engineering of the glass transition: glass-forming ability across a homologous series of cyclic stilbenes. *J. Phys. Chem. B* **2011**, *115*, 4696−4702.

(9) Alba-Simionesco, C.; Fan, J.; Angell, C. A. Thermodynamic aspects of the glass transition phenomenon. II. molecular liquids with variable interactions. *J. Chem. Phys.* **1999**, *110*, 5262.

(10) Koperwas, K.; Adrjanowicz, K.; Wojnarowska, Z.; Jedrzejowska, A.; Knapik, J.; Paluch, M. Glass-forming tendency of molecular liquids and the strength of the intermolecular attractions. *Sci. Rep.* **2016**, *6*, 36934.

DOI: 10.1021/acs.cgd.8b00123
Cryst. Growth Des. 2018, 18, 2538−2544

(11) Zhang, K.; Wang, M.; Papanikolaou, S.; Liu, Y.; Schroers, J.; Shattuck, M. D.; O'Hern, C. S. Computational studies of the glass-forming ability of model bulk metallic glasses. *J. Chem. Phys.* **2015**, *139*, 124503.
(12) Uhlmann, D. R. A kinetic treatment of glass formation. *J. Non-Cryst. Solids* **1972**, *7*, 337−348.
(13) Thomas, D. G.; Staveley, L. A. K. A study of the supercooling of drops of some molecular liquids. *J. Chem. Soc.* **1952**, 4569−4577.
(14) Kauzmann, W. The nature of the glassy state and the behavior of liquids at low temperatures. *Chem. Rev.* **1948**, *43*, 219.
(15) Turnbull, D.; Cohen, M. H. Concerning reconstructive transformation and formation of glass. *J. Chem. Phys.* **1958**, *29*, 1049.
(16) Uhlmann, D. R. Crystallization and Melting in Glass-Forming Systems. In *Materials Science Research, Vol. 4, Kinetics of Reactions in Ionic Systems*; Plenum Press: New York, 1969.
(17) Wunderlich, B. *Macromolecular Physics, Vol. 2 Crystal Nucleation, Growth, Annealing*; Academic Press: New York, 1976.
(18) Mullin, J. W. *Crystallization*, 4th ed.; Butterworth Heinemann: Oxford, U.K., 2001.
(19) Shelby, J. E. *Introduction to Glass Science and Technology*; Royal Society of Chemistry: Cambridge, U.K., 1997.
(20) Baird, J. A.; van Eerdenbrugh, B.; Taylor, L. S. A classification system to assess the crystallization tendency of organic molecules from undercooled melts. *J. Pharm. Sci.* **2010**, *99*, 3787−3806.
(21) Rupp, J. L. M.; Scherrer, B.; Schäuble, N.; Gauckler, L. J. Time-Temperature-Transformation (TTT) diagrams for crystallization of metal oxide thin films. *Adv. Funct. Mater.* **2010**, *20*, 2807−2814.
(22) Pizzi, A.; Zhao, C.; Kamoun, C.; Heinrich, H. TTT and CHT curing diagrams of water-borne polycondensation resins on lignocellulosic substrates. *J. Appl. Polym. Sci.* **2001**, *80*, 2128−2139.
(23) Sutton, R. L. Critical cooling rates to avoid ice crystallization in aqueous cryoprotectant solutions containing polymers. *J. Chem. Soc., Faraday Trans.* **1991**, *87*, 3747−3751.
(24) Sommer, J.-U.; Reiter, G. *Polymer Crystallization Observations, Concepts and Interpretations*; Springer: Berlin, Germany, 2003.
(25) Gutzow, I.; Durschang, B.; Russel, C. Crystallization of glassforming melts under hydrostatic pressure and shear stress: Part I Crystallization catalysis under hydrostatic pressure: possibilities and limitations. *J. Mater. Sci.* **1997**, *32*, 5389−5403.
(26) Adrjanowicz, K.; Koperwas, K.; Tarnacka, M.; Grzybowska, K.; Niss, K.; Pionteck, J.; Paluch, M. Changing the tendency of glass-forming liquid to crystallize by moving along different isolines in the *T-p* phase diagram. *Cryst. Growth Des.* **2016**, *16*, 6263−6268.
(27) Adrjanowicz, K.; Grzybowski, A.; Grzybowska, K.; Pionteck, J.; Paluch, M. Toward better understanding crystallization of supercooled liquids under compression. Isochronal crystallization kinetics approach. *Cryst. Growth Des.* **2013**, *13*, 4648−4654.
(28) Adrjanowicz, K.; Koperwas, K.; Paluch, M. Isobaric cooling or isothermal compression? Unveiling the effect of path dependence on crystallization. *Cryst. Growth Des.* **2017**, *17*, 2950−2954.
(29) Aziz, M. J.; Nygren, E.; Hays, J. F.; Turnbull, D. Crystal growth kinetics of boron oxide under pressure. *J. Appl. Phys.* **1985**, *57*, 2233.
(30) Devaud, G.; Aziz, M. J.; Turnbull, D. High pressure crystallization of As_2S_3. *J. Non-Cryst. Solids* **1989**, *109*, 121−128.
(31) Floudas, G.; Paluch, M.; Grzybowski, A.; Ngai, K. L. *Molecular Dynamics of Glass-Forming Systems: Effects of Pressure*; Springer-Verlag: Berlin, Germany, 2011.
(32) Adrjanowicz, K.; Grzybowski, A.; Grzybowska, K.; Pionteck, J.; Paluch, M. Effect of high pressure on crystallization kinetics of van der Waals liquid: An experimental and theoretical study. *Cryst. Growth Des.* **2014**, *14*, 2097−2104.
(33) Unipress. *Manual for Hydraulic Ram for LC20T Manostat*, 2014.
(34) Mierzwa, M.; Pawlus, S.; Paluch, M.; Zioło, J.; Szulc. Note: New feedthrough insulation method for the dielectric spectroscopy under ultrahigh pressure conditions. *Rev. Sci. Instrum.* **2010**, *81*, 066101.
(35) Avrami, M. Kinetics of phase change. I General theory. *J. Chem. Phys.* **1939**, *7*, 1103.
(36) Avrami, M. Kinetics of phase change. II Transformation-time relations for random distribution of nuclei. *J. Chem. Phys.* **1940**, *8*, 212−224.
(37) Pawlus, S.; Casalini, R.; Roland, C. M.; Paluch, M.; Rzoska, S. J.; Ziolo, J. Temperature and volume effects on the change of dynamics in propylene carbonate. *Phys. Rev. E* **2004**, *70*, 061501.
(38) Hensel-Bielowka, S.; Pawlus, S.; Roland, C. M.; Zioło, J.; Paluch, M. Effect of large hydrostatic pressure on the dielectric loss spectrum of type-A glass formers. *Phys. Rev. E* **2004**, *69*, 050501.
(39) Bauer, M.; Elsaesser, M. S.; Winkel, K.; Mayer, E.; Loerting, T. Compression-rate dependence of the phase transition from hexagonal ice to ice II and/or ice III. *Phys. Rev. B: Condens. Matter Mater. Phys.* **2008**, *77*, 220105.
(40) Bauer, M.; Winkel, K.; Toebbens, D. M.; Mayer, E.; Loerting, T. Hexagonal ice transforms at high pressures and compression rates directly into "doubly metastable" ice phases. *J. Chem. Phys.* **2009**, *131*, 224514.
(41) Adrjanowicz, K.; Koperwas, K.; Szklarz, G.; Tarnacka, M.; Paluch, M. Exploring the crystallization tendency of glass-forming liquid indomethacin in the *T−p* plane by finding different iso-invariant points. *Cryst. Growth Des.* **2016**, *16*, 7000−7010.

DOI: 10.1021/acs.cgd.8b00123
Cryst. Growth Des. 2018, 18, 2538−2544

5. PODSUMOWANIE

W powyższej pracy doktorskiej przedstawiono wyniki kompleksowych badań dynamiki molekularnej oraz procesu krystalizacji prowadzonych w zmiennych warunkach termodynamicznych (temperatura, ciśnienie, ograniczenie przestrzenne) na przykładzie dwóch substancji formujących stan szklisty *(i)* węglanu propylenu oraz *(ii)* fenofibratu. Zastosowane podejście pozwoliło na spojrzenie na badane zjawiska nie tylko przez pryzmat zmian temperatury/energii termicznej, lecz również gęstości upakowania molekuł. Spośród wszystkich badań jakie wykonano można wyróżnić te standardowe, które to są niezbędne dla zrozumienia podstawowych zjawisk zachodzących w substancjach formujących szkło, jak i te pionierskie, które rzucają zupełnie nowe światło na mechanizmy w nich zachodzące, a w szczególności na ich tendencję do krystalizacji. Pozwoliło to nie tylko na szczegółowe przeanalizowanie badanych zjawisk, lecz również na sprawdzenie wielu przewidywań teoretycznych związanych z dynamiką przejścia szklistego oraz procesem krystalizacji.

W pracy pokazano po raz pierwszy w sposób eksperymentalny (!), że tempem kompresji/dekompresji, analogicznie jak jest to w przypadku tempa chłodzenia/grzania, można sterować procesem formowania stanu szklistego oraz tendencją do krystalizacji. W rezultacie przeprowadzonych pomiarów zaproponowano diagramy Time-Pressure-Transformation/Time-Decompression-Transformation do opisu krzywych kompresji/dekompresji jako analogii do diagramów Time-Temperature-Transformation/Continious-Heating-Transformation używanych w literaturze dla krzywych chłodzenia/grzania. Ponadto, przeprowadzone pomiary krystalizacji dla warunków izobarycznych (p=0.1 MPa) jak i izotermicznych (T=243 K, T=253 K) wykazały, że zależność czasu krystalizacji w funkcji temperatury (dla p=0.1 MPa) i ciśnienia (dla T=243 K, czy też =253 K) są niemalże identyczne, i co również warto odnotować wartość parametru Avramiego jest praktycznie stała i oscyluje wokół 3. Prowadzić to może do zaskakującej konkluzji, że niezależnie od tego której zmiennej termodynamicznej użyjemy w celu modyfikacji tendencji do formowania stanu szklistego/krystalizacji badanej substancji to nie będzie miało to znaczącego wpływu na ogólny obraz jaki uzyskamy.

Badania dielektryczne prowadzone w warunkach podwyższonego ciśnienia dla fenofibratu także dostarczyły niezwykle ważnych i ciekawych informacji na temat dynamiki przejścia szklistego, a także jego tendencji krystalizacji w różnych warunkach (T, p). Wyniki badań pokazały, że fenofibrat jest substancją wrażliwą na ciśnienie, spełniającą regułę izochronicznej

superpozycji. Ponadto zauważono, że wraz z wzrostem ciśnienia parametr izobarycznej kruchości maleje, co informuje o tym, że im wyższe ciśnienie tym zachowanie czasów relaksacji ma charakter coraz bardziej arrheniusowski. Przy wykorzystaniu badań ciśnieniowych potwierdzono obecność β-relaksacji typu Johari-Goldstein, która to była oczekiwana na podstawie przewidywań modelu sprzężeniowego Ngai'a. Podczas przeprowadzonych badań zauważono także zaskakujące zachowanie przewodnictwa stałoprądowego. Otóż, wraz z wzrostem ciśnienia obserwowano dość znaczące zjawisko rozprężania pomiędzy ruchem reorientacyjnym molekuł a ruchami translacyjnymi cząstek obdarzonych ładunkiem, co świadczy że ruchy reorientacyjne molekuł podążają za zmianami temperaturowymi znacznie wolniej niż ruchy translacyjne cząsteczek naładowanych. W dalszej części prac badawczych zbadano wpływ temperatury i ciśnienia na proces krystalizacji fenofibratu. Badania przeprowadzone pod ciśnieniem atmosferycznym wykazały, że w zależności od temperatury fenofibrat krystalizuje do jednej lub dwóch form polimorficznych. Jednakże w trakcie procesu krystalizacji w warunkach podwyższonego ciśnienia zaobserwowano, że badana substancja krystalizuje wyłącznie do jednej, bardziej stabilnej, formy polimorficznej. Co więcej, zauważono również, że wybór odpowiedniej ścieżki termodynamicznej wpływa bezpośrednio na przebieg procesu krystalizacji. Wyniki te świadczą o tym, że kontrolując w odpowiedni sposób parametry termodynamiczne, a także poprzez wybór odpowiedniej ścieżki termodynamicznej można wpłynąć bezpośrednio na przebieg krystalizacji i uzyskiwany produkt, co może mieć potencjalnie duże zastosowanie aplikacyjne.

Równie ciekawych wyników eksperymentalnych dostarczyły badania wpływu dwuwymiarowych ograniczeń przestrzennych na dynamikę przejścia szklistego oraz przebieg procesu krystalizacji. Podążając za najnowszymi doniesieniami literaturowymi pokazano, że ciecz przechłodzona w nanoporach podlega idei skalowania gęstościowego i izochronicznej superpozycji, jednakże otrzymane rezultaty sugerują, że nie jest konieczne spełnienie zasady izochronicznej superpozycji, aby otrzymane dane podlegały skalowaniu gęstościowemu i na odwrót. W przypadku badania kinetyki krystalizacji zaobserwowano silną zmianę tendencji do krystalizacji oraz parametrów opisujących ten proces w zależności od rozmiaru porów jakich użyto. Pierwszą zauważalną zmianą była zmiana kształtu krzywej krystalizacji z sigmoidalnego na eksponencjalny. Oprócz tego zaobserwowano, zmianę kształtu krzywej krystalizacji, zmniejszenie wartości stałej krystalizacji i wartości parametrów Avramiego, a także przesunięcia maksimum krystalizacji w stronę niższych temperatur/wyższych stopni przechłodzenia. Co więcej

zaobserwowano, że fenofibrat w obecności dwuwymiarowych nanoograniczeń krystalizuje wyłącznie do jednej formy polimorficznej, co świadczy o tym, że stosując ograniczenia przestrzenne można, tak samo jak w przypadku podwyższonego ciśnienia, kontrolować przebieg procesu krystalizacji, a także mieć wpływ na otrzymywane formy polimorficzne.

Uzyskane wyniki mają niewątpliwie dużą wartość poznawczą, co niekoniecznie oznacza że podjętą tematykę całkowicie wyczerpują. Wręcz przeciwnie, nakreśliły nowe problemy badawcze, którymi mam nadzieję zająć się w przyszłości. Pierwszym z nich, wymagającym dalszej uwagi jest badanie wpływu ścieżki termodynamicznej na proces krystalizacji. Wymagać to będzie przeprowadzenia bardziej szczegółowych pomiarów wpływu różnego sposobu dochodzenia do wybranych warunków (T_c, p_c) na sam proces krystalizacji, w jak najszerszym zakresie temperatur i ciśnień. Drugim zagadnieniem, wartym szczegółowej uwagi jest zrozumienie, jaki wpływ na zjawiska obserwowane w nanoporach odgrywają efekty przyściankowe, a więc interakcje próbka/ścianka. W tym celu konieczna będzie modyfikacja ścianek porów, np. poprzez silanizację czy też stosując odpowiednie pokrycia tlenkami z użyciem techniki ALD**.** W sytuacji, gdy idea skalowania termodynamicznego została potwierdzona w obecności dwuwymiarowego ograniczenia przestrzennego, kolejnym ważnym krokiem musi być zweryfikowanie jej słuszności w układach ograniczonych jednowymiarowo. Pozwoliłoby to na uzyskanie spójnego obrazu/stworzenie uniwersalnego modelu łączącego obserwowane zjawiska w świecie nanoskopowym ze zjawiskami obserwowanymi w świecie makroskopowym.

6. BIBLIOGRAFIA

[1] McNaught, A. D.; Wilkinson, A. (Eds) *IUPAC Compendium of Chemical Terminology, 2nd ed. (the "Gold Book").* Blackwell Scientific Publications, 1997.

[2] Gibbs, J.H.; Di Marzio, E. A. Nature of the Glass Transition and the Glassy State. *The Journal of Chemical Physics*, **1958**, *28(3)*, 373–383.

[3] Chang, K. The Nature of Glass Remains Anything but Clear Anything but Clear. *New York Times*, July 29, 2008, 1–4.

[4] Anderson, P. W. Through the Glass Lightly. *Science*, **1995**, *267(5204)*, 1615–1616.

[5] Debenedetti, P. *Metastable Liquids: Concepts and Principles.* Princeton University Press, New Jersey, 1996.

[6] Bridgman, P. W. *Collected Experimental Papers.* Harvard University Press, Cambridge, 1964.

[7] Gilchrist, A.; Earley, J. E.; Cole, R. H. Effect of Pressure on Dielectric Properties and Volume of 1-Propanol and Glycerol. *The Journal of Chemical Physics*. **1957**, *26*, 196–200.

[8] Floudas, G.; Paluch, M.; Grzybowski, A.; Ngai, K. *Molecular Dynamics of Glass-Forming Systems: Effects of Pressure*. Springer-Verlag, Berlin, 2011

[9] Debenedetti, P.; Stillinger, F. Supercooled Liquids and the Glass Transition. *Nature*, **2001**, *410(6825)*, 259–267.

[10] Woodcock. L. V. Hard-Sphere Fluid Equation of State. *Journal of the Chemical Society*, *Faraday Transactions 2*, **1976**, *72*, 731–735.

[11] Cohen, M. H.; Grest, G. S. Liquid-Glass Transition, a Free-Volume Approach. *Physical Review B*, **1979**, *20(3)*, 1077–1098, 1979.

[12] Ediger, M. D.; Angell, C. A.; Nagel, S. R. Supercooled Liquids and Glasses. *Journal of Physical Chemistry*, **1996**, *100(31)*, 13200–13212.

[13] Angell, C. A.; Ngai, K. L.; McKenna, G. B.; McMillan, P. F.; Martin, S. W. Relaxation in Glassforming Liquids and Amorphous Solids. *Journal of Applied Physics*, **2000**, *88(6)*, 3113–3157.

[14] Kauzmann, W. The Nature of the Glassy State and the Behavior of Liquids at Low Temperatures. *Chemical Reviews*, **1948**, *43(2)*, 219–256.

[15] Schmelzer**,** J**.** W. P.**;** Abyzov, A. S.; Fokin V. M.; Schick, C. Kauzmann paradox and the crystallization of glass-forming melts, *Journal of Non-Crystalline Solids***, 2017**, in press.

[16] Stillinger, F. H.; Debenedetti, P. G.; Truskett, T. M. The Kauzmann Paradox Revisited, *Journal of Physical Chemistry B*, **2001**, *105*, 11809–11816

[17] Zallen, R. *The Physics of Amorphous Solids*. Wiley-VCH Verlag GmbH & Co., Weinheim, 2007.

[18] Chen, H.S.; Turnbull, D. Formation, Stability and Structure of Palladium-Silicon Based Alloy Glasses. *Acta Metallurgica*, **1969**, *17(8)*, 1021–1031.

[19] Yu, L. Amorphous Pharmaceutical Solids: Preparation, Characterization and Stabilization. *Advanced Drug Delivery Reviews*, **2001**, *48(1)*, 27–42.

[20] Turnbull, D. Under What Conditions can a Glass be Formed? *Contemporary Physics*, **1969**, *10(5)*, 473–488.

[21] Uhlmann, D. R. *Crystallization and Melting in Glass-Forming Systems*. in: Gray, T.J.; Fréchette, V.D. (eds) *Kinetics of Reactions in Ionic Systems. Materials Science Research.* Springer, Boston, MA, 1969.

[22] The Nobel Prize in Chemistry 2017.

[23] Klement, W.; Willens, R. H.; Duwez, P. Non-crystalline Structure in Solidified Gold–Silicon Alloys, *Nature*, **1960**, *187(4740)*, 869–870.

[24] Schick, C.; Mathot V. (Eds), *Fast Scanning Calorimetry*, Springer International Publishing, Switzerland, 2016.

[25] Sesták, J.; Mares, J. J.; Hubík, P. (Eds.) *Glassy, Amorphous and Nano-Crystalline Materials Thermal Physics, Analysis, Structure and Properties Glassy, Amorphous and Nano-Crystalline Materials*. Springer Science & Business Media, 2011.

[26] Rams-Baron, M.; Jachowicz, R.; Boldyreva, E.; Zhou, D.; Jamroz,W.; Paluch, M. *Amorphous Drugs: Benefits and Challenges*. Springer International Publishing, Berlin 2018.

[27] Demetriou, M. D.; Launey, M. E.; Garrett, G.; Schramm, J. P.; Hofmann, D. C.; Johnson, W. L.; Ritchie, R. O. A damage-tolerant Glass. *Nature Materials*, **2011***, 10(2)*, 123–128.

[28] Miller, J. S.; Stevens, K. R.; Yang, M. T.; Baker, B. M.; Nguyen, D.-H. T.; Cohen, D. M.; Toro, E.; Chen, A. A.; Galie, P. A.; Yu, X.; Chaturvedi, R.; Bhatia, S. N.; Chen, C. S. Rapid Casting of Patterned Vascular Networks for Perfusable Engineered Three-Dimensional Tissues, *Nature Materials*, 2012, *11(9)*, 768–774.

[29] Shintani, H.; Tanaka, H. Frustration on the Way to Crystallization in Glass, *Nature Physics*, **2006**, *2(3)*, 200–206.

[30] Russo, J.; Tanaka, H. The Microscopic Pathway to Crystallization in Supercooled Liquids, *Scientific Reports*, **2012**, *2*, 505.

[31] Jang, J.; Oh, J. Y.; Kim, S. K.; Choi, Y. J.; Yoon S. Y.; Kim, C. O. Electric-Field-Enhanced Crystallization of Amorphous Silicon, *Nature*, **1998**, *395(6701)*, 481–483.

[32] Adrjanowicz, K.; Paluch, M.; Richert, R. Formation of New Polymorphs and Control of Crystallization in Molecular Glass-Formers by Electric Field, *Physical Chemistry Chemical Physics*, **2018**, *20*, 925–931.

[33] Rengarajan, G. T.; Enke, D.; Steinhart M.; Beiner, M. Stabilization of the Amorphous State of Pharmaceuticals in Nanopores, *Journal of Materials Chemistry*, **2008**, *18(22)*, 2537–2539.

[34] Roland, C. M.; Hensel-Bielowka, S.; Paluch, M.; Casalini, R. Supercooled Dynamics of Glass-Forming Liquids and Polymers Under Hydrostatic Pressure, *Reports on Progress in Physics*, **2005**, *68(6)*, 1405–1478.

[35] Tarjus, G.; Kivelson, D.; Mossa, S.; Alba-Simionesco C. Disentangling Density and Temperature Eeffects in the Viscous Slowing Down of Glassforming Liquids, *Journal of Chemical Physics*, **2004**, *120(13)*, 6135–6141.

[36] Pawlus, S.; Casalini, R.; Roland, C. M.; Paluch, M.; Rzoska, S. J.; Ziolo, J. Temperature and Volume Effects on the Change of Dynamics in Propylene Carbonate, *Physical Review E*, **2004**, *70(6 Pt 1)*, 061501.

[37] Ostwald, W. Studien Uber die Bildung und Umwandlung Fester Korper. *Zeitschrift für Physikalische Chemie*, **1897**, *22*, 289–302.

[38] Mullin, J. W. *Crystallization (4th Edition)*. Butterworth-Heineman, Oxford, UK, 2001.

[39] Gutzow, I.; Schmelzer**,** J**.** W. P. *The Vitreous State: Thermodynamics, Structure, Rheology, and Crystallization*. Springer-Verlag, Berlin, 1995.

[40] Guo, C.; Wang, J.; Li, J.; Wang, Z.; Tang, S. Kinetic Pathways and Mechanisms of Two-Step Nucleation in Crystallization, *Physical Chemistry Letters*, **2016**, *7(24)*, 5008–5014.

[41] Erdemin, D.; Lee, A. Y.; Meyerson, A. S. Nucleation of Crystals From Solution: Classical and Two-Step Models, *Accounts of Chemical Research*, **2009**, *42(5),* 621–629.

[42] Gutzow, I.; Durschang, D.; Rüssel, C. J. Crystallization of Glass Forming Melts Under Hydrostatic Pressure and Shear Stress. Part I Crystallization Catalysis Under Hydrostatic Pressure: Possibilities and Limitations, *Journal of Materials Science*, **1997**, *32(20)*, 5389–5403.

[43] Schmelzer, J. W. P.; Abyzov, A. S. Pressure Induced Crystallization of Liquids: Maxima of Nucleation, Growth, and Overall Crystallization Rates, *International Journal of Applied Glass Science*, **2018**, *9(2)*, 198–207.

[44] Köncke U. Zachmann, H. G.; Baltá-Calleja, F. J. New Aspects Concerning the Structure and Degree of Crystallinity in High-Pressure-Crystallized Poly(ethylene terephthalate), *Macromolecules*, **1996**, *29(18)*, 6019–6022.

[45] Adrjanowicz, K.; Koperwas, K.; Tarnacka, M.; Grzybowska, K.; Niss, K.; Pionteck, J.; Paluch, M. Changing the Tendency of Glass-Forming Liquid to Crystallize by Moving Along Different Isolines in the T-p Phase Diagram., *Crystal Growth & Design*, **2016**, *16(11)*, 6263–6268.

[46] Schmelzer, J.; Möller, J.; Gutzow, I. Ostwald's Rule of Stages: The Effect of Elastic Strains and External Pressure, *Zeitschrift Für Physikalische Chemie*, **1998**, *204*, 171–181.

[47] Jiang Q.; Ward, M. D. Crystallization Under Nanoscale Confinement, *Chemical Society Reviews*, **2014**, *43(7)*, 2066–2079.

[48] F. Kremer (Ed*.), Series: Advances in Dielectrics, Dynamics in Geometrical Confinement*. Springer International Publishing, Switzerland, 2014.

[49] Koperwas, K.; Adrjanowicz, K.; Wojnarowska, Z.; Jedrzejowska, A.; Knapik, J.; Paluch, M. Glass-Forming Tendency of Molecular Liquids and the Strength of the Intermolecular Attractions, *Scientific Reports*, **2016**, *6*, 36934.

[50] He, H.; Yang, R.; Tang, X. In Vitro and In Vivo Evaluation of Fenofibrate Solid Dispersion Prepared by Hot-Melt Extrusion, *Drug Development and Industrial Pharmacy*, **2010**, *36(6)*, 681–687.

[51] Zhang, M.; Li, H.; Lang, B.; O'Donnell, K.; Zhang, H.; Wang, Z.; Dong, Y.; Wu, C.; Williams, R. O. Formulation and Delivery of Improved Amorphous Fenofibrate solid Dispersions Prepared by Thin Film Freezing, *European Journal of Pharmaceutics and Biopharmaceutics*, **2012**, *82(3)*, 534–544.

[52] Di Martino, P.; Palmieri, G. F.; Martelli, S. Evidence of a Metastable Form of Fenofibrate, *Pharmazie*, **2000**, *55(8)*, 625–626.

[53] Amstad, E.; Spaepen, F.; Weitz, D. A.; Crystallization of Undercooled Liquid Fenofibrate, *Physical Chemistry Chemical Physics*, **2015**, *17(44)*, 30158–30161.

[54] Tipduangta, P.; Takieddin, K.; Fábián, L.; Belton, P.; Qi, S. A. New Low Melting-Point Polymorph of Fenfibrate Prepared via Talc Induced Heterogeneous Nucleation, Crystal Growth & Design, **2015**, 15, 5011–5020

[55] Avramov, I.; Grzybowski, A.; Paluch, M. A New Approach to Description of the Pressure Dependence of Viscosity, *Journal of Non-Crystalline Solids*, **2009**, *355(10-12)*, 733–736.

[56] Adrjanowicz, K.; Kaminski, K;. Koperwas, K.; Paluch M. Negative Pressure Vitrification of the Isochorically Confined Liquid in Nanopores. *Physical Review Letters*, **2015**, *115(26)*, 265702.

[57] Ngai, K. L.; Rendell, R. W. *Chapter 4. Basic Physics of the Coupling Model: Direct Experimental Evidences* in Fourkas, J. T.; Kivelson, D.; Mohanty, U.; Nelson, K. (Eds.) *Supercooled Liquids: Advances and Novel Application (ACS Symposium Series Vol. 676).* American Chemical Society, Washington, DC, 1997.

[58] Heinz, A.; Gordon, K. C.; McGoverin, C. M., Rades, T.; Strachan, C. J. Understanding the Solid-State Forms of Fenofibrate – A Spectroscopic and Computational Study, *European Journal of Pharmaceutics and Biopharmaceutics*, **2009**, *71*, 100–108.

[59] Napolitano, S.; Glynos, E.; Tito, N. B. Glass Transition of Polymers in Bulk, Confined Geometries, and Near Interfaces, *Reports on Progress in Physics*, **2017**, *80(3)*, 036602.

[60] Adrjanowicz, K.; Kaminski, K.; Tarnacka, M.; Szklarz, G.; Paluch, M. Predicting Nanoscale Dynamics of a Glass-Forming Liquid From its Macroscopic Bulk Behavior and Vice Versa, *The Journal of Physical Chemistry Letters*, **2017**, *8(3)*, 696–702.

[61] Roed, L. A.; Gundermann, D.; Dyre, J. C.; Niss, K. Two Measures of Isochronal Superposition, *Journal of Chemical Physics*, **2013**, *139(10)*, 101101.

[62] Descamps, M.; Willart, J-F. Scaling Laws and Size Effects for Amorphous Crystallization Kinetics: Constraints Imposed by Nucleation and Growth Specificities, *International Journal of Pharmaceutics*, **2018**, *542(1-2)*, 186–195.